DEVELOPMENT AND APPLICATION OF AN ADVANCED SWITCHED RELUCTANCE GENERATOR DRIVE

A Dissertation

by

PEYMAN ASADI

Submitted to the Office of Graduate Studies of
Texas A&M University
in partial fulfillment of the requirements for the degree of

DOCTOR OF PHILOSOPHY

December 2006

Major Subject: Electrical Engineering

DEVELOPMENT AND APPLICATION OF AN ADVANCED SWITCHED RELUCTANCE GENERATOR DRIVE

A Dissertation

by

PEYMAN ASADI

Submitted to the Office of Graduate Studies of
Texas A&M University
in partial fulfillment of the requirements for the degree of

DOCTOR OF PHILOSOPHY

Approved by:

Chair of Committee,	Mehrdad Ehsani
Committee Members,	Karen L. Butler-Purry
	Shankar P. Bhattacharyya
	Mark T. Holtzapple
Head of Department,	Costas N. Georghiades

December 2006

Major Subject: Electrical Engineering

ABSTRACT

Development and Application of an Advanced Switched Reluctance Generator Drive.

(December 2006)

Peyman Asadi, B.S., Iran University of Science and Technology, Tehran, Iran;

M.S., University of Tehran, Tehran, Iran

Chair of Advisory Committee: Dr. Mehrdad Ehsani

This dissertation contains the results of research conducted on the design and control characterization of a Switched Reluctance Generator (SRG) for maximum output power. The SRG is an attractive solution to the increasing worldwide demand of electrical energy. It is low cost with a rugged structure, operates with high efficiency over a wide speed range, and is fault tolerant. In many applications, size and weight are the main criteria in selecting the generator. Hence, in design and control of the generator, system designers always strive for increasing power density, or in other words, maximizing the output power for a given size. Despite the extensive research on the motoring operation of the Switched Reluctance Machine, only a few publications have investigated the generating mode of operation of this machine. Results and algorithms from this research can be referenced for better utilizing the SRG in many applications.

As the first stage to output power maximization, design parameters and control variables affecting the average output power of the SRG are identified through a systematic approach. The optimal values for maximizing the output power are found through an analytical approach and iterative simulations. The results are then verified experimentally.

After finding the optimal values for control variables, a controller is designed. This controller is model dependent. If the model used for design is not accurate or the machine parameters are deviated from the designed values, the machine will not generate the maximum output power. Therefore, a self-tuning algorithm, based on a local search method, is proposed and experimentally tested. It works effectively and does not need extra hardware or rigorous calculations.

The attempts to benefit from the SRG may look tantalizing, but it poses a challenge as well. Output power maximization can lead to an oversized SRG converter and its output filter, which will reduce the overall power density of the motor drive. The last piece of this dissertation analyzes the effect of a commutation algorithm on the output filter, reducing its size with active control of phase currents, and proposing a novel control algorithm that was investigated through experiments over all of the speed range.

To my Parents

ACKNOWLEDGMENTS

I would like to express my appreciation to Dr. M. Ehsani for his inspiring guidance, constant encouragement and advice throughout the process of this work. I also would like to express my gratitude to Dr. B. Fahimi for his novel ideas and valuable advice. The cooperation and discussions with my colleagues at the Power Electronics and Motor Drive Lab were greatly helpful and enlightening during this course of research. I would like to thank all my current and former lab members, especially Dr. F. Rajaei, Dr. T. Kim, Mr. S. Welch, Mr. M. Azadpour, Mr. B. Nikbakhtian, Mr. H. Mena, and Mr. A. Schorcz. I thank the members of my advisory committee for their valuable comments and interest in this research work.

I would like to thank Miss Melly Suryani and Dr. Arta Sadrzadeh for all of their great support, help and kindness. Last, but not the least, I would like to express my gratitude to my family for all their support, help and advice during my studies. Their patience, abundant love and prayers were a high source of motivation at every step of my research.

TABLE OF CONTENTS

TABLE OF CONTENTS (Continued)

TABLE OF CONTENTS (Continued)

LIST OF TABLES

LIST OF FIGURES

LIST OF FIGURES (Continued)

LIST OF FIGURES (Continued)

FIGURE Page

LIST OF FIGURES (Continued)

LIST OF FIGURES (Continued)

LIST OF FIGURES (Continued)

CHAPTER I

INTRODUCTION

Electric generators are the main provider of increasing demand for electrical energy. Due to sporadic energy shortages and energy prices that are prone to unexpected spikes, many industries are seeking new ways to generate more power. While meeting the extensive energy needs of such facilities is possible with the current technology such as diesel-fired generators, there are many regulatory obstacles and environmental concerns that force industries to conduct research for new type of generators. Moreover, new applications such as traction drives for hybrid electric vehicles have special operating requirements that cannot be met by conventional generators, thus research on the new type of generators is inevitable. Research is challenged by demands to create energy-efficient generators that also are affordable and durable.

A Switched Reluctance Generator (SRG) is an attractive candidate for many applications. It is low cost with a rugged structure, operates with high efficiency over a wide speed range, and it is fault tolerant. However, due to its operating nature, it requires power switches and a controller. Just recently, inventions of low-cost power semiconductors and digital controllers have made the use of this generator practical. However, just a few applications have been reported; such as starter/generator for gas

---

This dissertation follows the style and format of *IEEE Transactions on Industry Applications.*

vehicles [8–11]. Optimal design and control of Switched Reluctance Machine is the key point for better utilizing SRG for more applications.

A. Current Status and Requirements of Electric Power Generation

According to the International Energy Outlook 2005 (IEO2005) report [12], world net electricity consumption will nearly double by 2025. Over the forecast period, the world electricity demand is projected to grow at an average rate of 2.6 percent per year, from 14,275 billion kWh in 2002 to 21,400 billion kWh in 2025 (Fig. 1) [13].

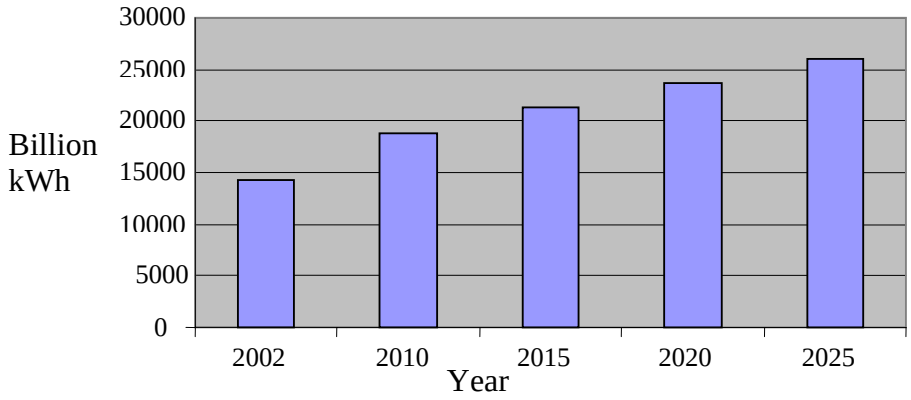

Fig. 1. World net electricity consumption, 2002-2025.

To meet the world's projected electricity demand over the 2002 to 2005 forecast period, an extensive expansion of installed generating capacity will be required. The mix of primary fuels used to generate electricity has changed a great deal over the past three decades on a worldwide basis. There is a continued increase in the use of natural gas for electricity generation. However, coal is projected to continue to retain the largest

market share for electricity generation. The role of nuclear power in the world's electricity market is projected to lessen. According to IEO2005 reference case, generation from hydropower and other renewable energy sources is projected to grow by 54 percent over the next 23 years, but despite solid achievements of renewable energy sources, their share of total electricity generation is projected to remain near the current level of 18 percent. Three challenges for using environmental friendly energy sources are (1) development of renewable technology, (2) its adoption by the utility sector (which itself is undergoing major change), and (3) governmental policies with regard to renewable energy sources. The technology development for many energy conversion systems depends on development of low-cost, reliable, and efficient electric generators [14].

Electric generators provide much of the electric energy for the world's industrial production. Electric generators are more efficient and cheaper than other sources of electric energy like solar cells and thermoelectric generators. Typically, manufacturers purchase motors and generators for use in a wide range of products. According to the U.S. Census Bureau in late 2003, the industry shipments of motors and generators were valued at US$8.0 billion where the share of generators was nearly US$3 billion [15].

In general, an electric generator should meet the following requirements:

- Reliable
- Stable with fast transient
- Fault tolerant
- Low maintenance

- Efficient
- Low cost
- Compact size

Alternating current synchronous generators are the most commonly used electric generators in the industry. With advanced power electronics and digital control, other types of generators like switched reluctance generators and brushless dc generators have become competitors, especially for small power plants. The ac synchronous generator is usually operated at constant speed and voltage. Environmental and safety constraints, as well as more demanding control requirements, are leading to variable-speed generators in many applications such as windmill generators. Variable-speed generators have several benefits in terms of stability and control, with higher efficiency in hydro power plants and high-speed combined cycle gas turbines. Variable-speed generators may provide more flexibility to the power system at a lower cost, with lower harmonic pollution. It has been reported that permanent-magnet synchronous generators give higher efficiencies over ac synchronous generators as a stand-alone diesel engine or gas turbine gensets [16]. Some energy-storage technologies, such as the flywheel, rely on variable-speed electromechanical energy conversion.

In the automotive industry, the demand for more electric energy has been increasing very rapidly in recent years. The average peak electric power required by the passenger vehicle has experienced a steady increase for over 90 years and it is projected to continuously increase in the future [17]. As shown in Fig. 2, the electric power on-board the vehicle was only a couple of hundred watts in 1930s. The growth rate of the

electric power was 2% per year from 1940 to 1970, while the rate became 6% per year from 1970 to 1990. With the introduction of hybrid electric vehicle and fuel cell vehicle propulsion, vehicle electric power grows with a rate of 8% per year while the electric power on the vehicles without electric propulsion may increase steadily from 1990 to 2020. With increased electric power requirements, the output power and the efficiency of the alternator have become more and more important in the vehicle. The reason is that the performance of a large alternator plays a big role on the vehicle performance and fuel consumption, compared to small alternator's effects. However, in automotive applications, performance and reliability can never be sacrificed in the quest for higher fuel economy at an affordable cost.

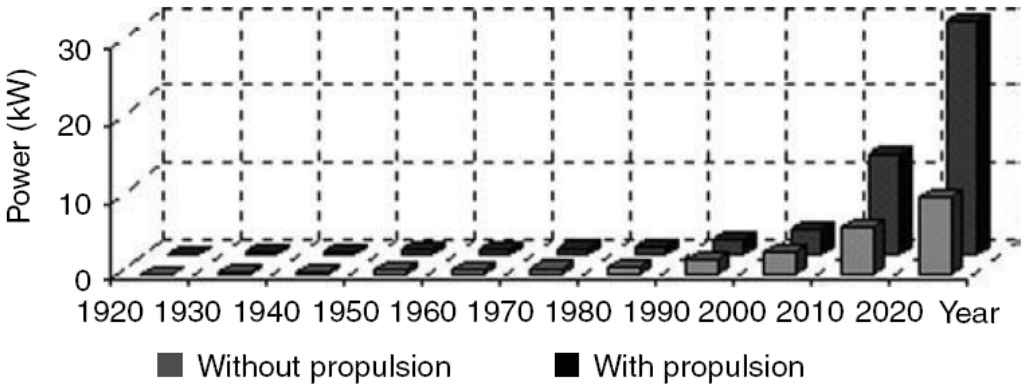

Fig. 2. Trend in vehicle electric load [18].

Power density, or specific power, of a generator is the amount of electric power generated divided by its weight. Sometimes this power is measured per volume. For many applications like vehicular and wind power generation, the weight and size of

generators become a key factor, and can change the cost and overall system efficiency. Therefore, power density maximization is one of the primary design objectives.

Regenerative braking is the principle means through which kinetic energy of the vehicle is returned to the electric energy storage, rather than being lost as heat in the brake pads. Usually the braking time is much shorter than the acceleration, so braking power is much higher than motoring power. So, the peaking power of an electric machine used for traction is defined by its regenerative braking characteristics rather than its motoring operation characteristics. This concludes the importance of power density maximization for generators in hybrid electric vehicles. According to the US DOE's Partnership for a New Generation of Vehicles (PNGV) program, design targets for electric machines used for propulsion of hybrid electric vehicles and their associated power electronics are listed in Table I. To illustrate the demand for improvement, one can compare the 0.24 kW/kg specific power of an existing Lundel alternator rated for 120 A continuous at 14.2 V with the 1.6 kW/kg specific power as the target for hybrid electric vehicles [19].

Table I. Electric Machines and Power Electronics Goals for HEV (Based on PNGV)

Electric Machines	Unit	Target
Peak Specific Power	kW/kg	1.6
Volumetric Power Density	kW/L	5
Specific Power	$/kW	4
Power Load Efficiency (@20% peak torque)	%	96
Power Electronics		
Peak Specific Power	kVA/kg	5
Volumetric Power Density	kW/L	12
Specific Cost	$/kVA	7
Part Load Efficiency (@ 20% Current)	%	97–98

There is a trend for more electricity in aircraft and spacecraft because of more electric actuators and increased complexity. This in turn demands for modern generator with high degree of reliability, power density, and efficiency.

B. The SRG Drive, Advantages and Challenges

The switched reluctance machine has salient poles, both on the stator and the rotor. It has concentrated windings on the stator and no winding or permanent magnet on the rotor. There are several configurations for the SRG depending on the number and size of the rotor and stator poles and the field direction [20]. The structure of a generator with eight poles on the stator and six poles on the rotor is shown in Fig. 3.

The stator and rotor are made from iron laminations stacked together. This structure is very simple and low cost to manufacture. Due to the lack of copper and permanent magnets on the rotor, it is very rugged and can be designed to operate at very high speeds and in harsh environments. Because the SRG is singly excited and there is no permanent magnet in this generator, during start up and initial conditions, it needs an external source such as a battery to deliver energy to the phase. After a transient time, this external source can be disconnected.

The magnetic field is rotating synchronously with the rotor by switching current from one phase to another. Knowing the rotor position to commutate current from one phase to another in synchrony with the rotor is a necessity for this machine. Position

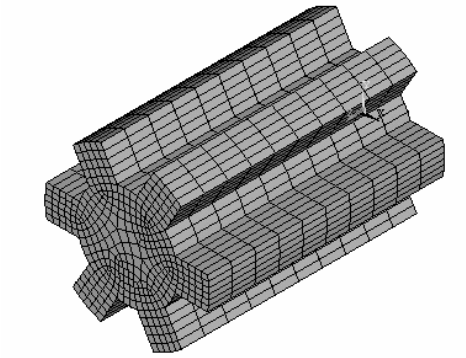

(a) 3D model of rotor with six poles.

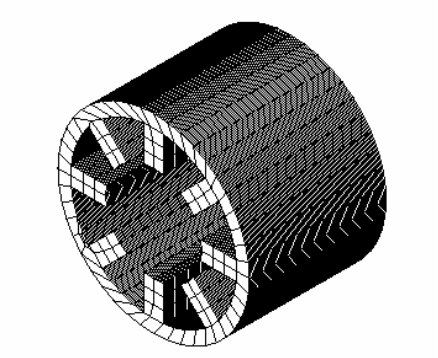

(b) 3D model of stator with eight poles.

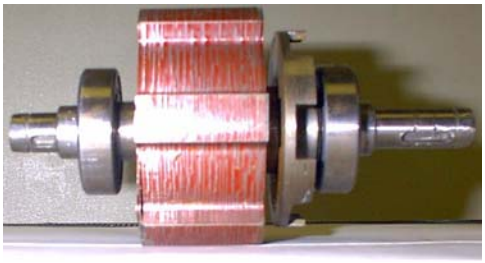

(c) Rotor of a ½–hp SRG with six poles.

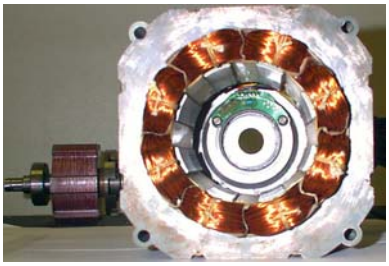

(d) Stator of a ½ –hp SRG with eight poles.

Fig. 3. Structure of a SRG with eight poles on the stator and six poles on the rotor.

information can be measured by a shaft position sensor or calculated with a sensorless algorithm.

Phase current is not sinusoidal, thus a converter is always used to drive this machine. The SRG converter is reliable and fault tolerant. Generator phases are in series with power switches, which avoids shoot-through problem. Phase currents work independently, so in the case of fault for one of the phases, other phases can continue working. The output power of this machine increases with the converter dc-bus voltage, so it is immune to a short circuit.

This machine has a poor power factor, which implies an oversized converter. Also due to large current spikes on the output of converter, the size of line filter for

enhancing power quality is very large. This can increase the size and cost of the SRG drive. On the other hand, the spiky shape of the current produces high torque ripple on the prime mover and acoustic noise, which may not be acceptable for some applications. Current profiling can mitigate torque ripple and acoustic noise vibrations.

One of the key advantages of the SRG is that it can generate power efficiently with variable speed and variable output voltage. The magnetic field is controlled with phase current, so the generator can run easily in the field-weakening region. The SRG's characteristics due to its doubly salient structure and saturation of iron in the flux path are highly nonlinear, so it requires a special controller compared to the other machines.

Back electromotive force (EMF) voltage produced in the SRG is a function of the phase current and the shaft speed. If the rotor shaft speed and phase currents are high enough, the back EMF voltage can be greater than the bus supply voltage, so the current increases even after turning off the phase. This can be very dangerous for the power electronic converter and its output filter. In addition, it produces high torque ripple that can be harmful for the prime mover. This problem can be avoided by proper selection of the phase switching angles that can keep the current in the safe region.

Peaking output power of this machine is generally limited by the volt-ampere rating of the power electronic converter, and it is superior to permanent magnet generators, which are limited by the risk of demagnetization of magnets. Also, because copper losses are on the stator, thermal management in the SRG is much easier than for induction machines. The power density of the switched reluctance machine is comparable with induction machines. However, the switched reluctance machine needs a

smaller air gap, better concentricity, and tighter manufacturing tolerances compared to the induction machine to achieve comparable performance and/or power density [21].

The power density can be improved by selecting materials that have a higher saturation flux density, such as cobalt. However, these materials can be extremely expensive and it may not be practical for many applications. Using a smaller air gap can improve the power density and efficiency of the machine in the expense of manufacturing cost and higher acoustic noise. Having selected the right design geometry and number of stator and rotor poles, the power density of the SRG can be enhanced [22].

Design optimization objectives of the SRG such as efficiency improvement, power density maximization, torque ripple, and acoustic noise level mitigation are not in the same direction. Improvement of one objective can trade off for others. The designer should select a set of objectives favorable for each application [21].

In summary, using the SRG has the following benefits:

- Low cost and rugged structure;
- Fault tolerant operation;
- Variable voltage operation;
- High efficiency in wide speed range;
- Reliable converter topology.

Some disadvantages and challenges of using the SRG are as follows:

- Highly nonlinear behavior;
- Torque ripple and acoustic noise;

- Large current ripple on the output terminal;
- Need to position sensor information for operation;
- Possible excessive current problem at certain speeds and currents.

C. Previous Research Work

The generating mode of the switched reluctance machine has been one of the research topics in recent years; some papers [23–25] and a few patents [26–29] have been published on this topic. These publications are describing modeling, analysis of characteristics, control methods and suitability of the SRG for different applications.

In [25], the generating mode of the switched reluctance machine is described and duality of motoring and generating modes are shown. Based on this conclusion, control methods developed for the motoring mode can be adapted for the generating mode also. This paper points out that the phase current in the generating mode mirrors the one in the motoring mode about the rotor's aligned position. It has been shown, when the dc-bus voltage of the switched reluctance generator is not fixed; the SRG needs a closed loop control for controlling output voltage. The average and detailed model of the SRG has been proposed [30]. The SRG has been modeled as a controlled-current source for the average model and it is adequate for predicting the stability of the system. For finding the output ripple voltage and device stresses, a detailed model is required [31].

The SRG has been used for several applications, such as a high-speed switched reluctance machine in a starter/generator for aircraft jet turbines [1]. The switched

reluctance machine starts as a motor up to the rated speed of the jet turbine, and then it begins to operate as a generator. The effect of the capacitive load and constant power load on the output power generation of the switched reluctance machine has been shown [32].

Due to several inherent advantages, especially the ability to have an extended constant-power range, the switched reluctance machine is a good candidate as traction machines for electric vehicles and hybrid electric vehicles. A design and control strategy of this machine for regenerative braking has been proposed [8]. The paper [9] suggests using the switched reluctance machine as started/alternator for vehicles and a method has been introduced for active damping of engine torque pulsations by controlling the braking torque of the SRG. A comparison between switched reluctance machine and induction machine for using as a starter/alternator of hybrid electric vehicles has been performed [11]. The controller has not been optimized, but the results show the similar performance for both machines. Different designs of a 300-kW SRG for hybrid electric vehicles have been investigated to obtain the trend of important variables such as size, weight, efficiency and torque [33].

The SRG's high efficiency operation over a wide speed range, rugged structure, low cost, and reliable drive make it a good candidate as a wind power generator. Several papers have been published on design and control of the SRG for this application [6, 7]. These results show the superiority of the SRG compared to other conventional wind power generators.

The SRG is inherently fault tolerant. Phase currents are independent so in the case of disconnecting one phase, the other phases can generate power independently. The output power is a function of the dc-bus voltage. So if there is no other source connected to the dc-bus of the SRG, the output power voltage will drop after short circuit. Fault analysis of the SRG has been studied [34]. Some converter topologies have been proposed that separate the machine's excitation from its load, so the SRG can clear a load fault or recover from one [28]. A multi-pole single phase SRG has been employed as a low cost generator for higher fault tolerance [35]. This research has investigated operation with a split-winding converter under open- and short-circuit faults.

One of the main control problems of the SRG is the excessive phase current at high speed. This can damage the converter or force high torque ripple on the shaft. This problem can be avoided by carefully selecting phase switching angles as a function of output voltage and shaft speed. A predictive control method is developed [9]. This controller selects the right turn-off command to maintain the peak phase current below the maximum rating of the drive. This will remove the need for an oversized converter.

In contrast to the considerable progress in designing of controllers for motoring operation, less attention has been paid to the design of the SRG controller. This is primarily due to the highly nonlinear characteristics of the SRG. The output power depends on several design parameters and control variables; the main purpose of the controller is to select of the control variables to deliver the output power to the load with the best performance. The best performance can be defined as the best efficiency, maximum output power throughput, or etc. A control method to cope with different

speed region of the SRG is published [1]. In the low-speed region, the phase turn-on angle is fixed and pulse width is varied to achieve the required power. For higher speeds, the output power is controlled with the turn-on angle, and the generator phase is turned off when it reaches a predefined level. Simulation results show the linear variation of dc-bus current with the turn-on angle over a speed range. This method does not include the effect of dc-bus voltage variations and it needs prior knowledge of the SRG model. Another control technique based on the inverse model has been introduced [36]. In this method, the turn-off angle is fixed and determined with a curve fitting method on the piecewise linear model of the SRG. The net output power is described as an analytical function of dc-bus voltage, shaft speed and turn-on angle. This method needs the prior knowledge of the machine and does not lead to maximum efficiency.

Control of the SRG to generate power with maximum efficiency has been proposed in [37]. In this method optimal turn-on and turn-off angles for just one operating mode has been discussed. The turn-on angle is set based on the output of the voltage controller and the turn-off angle is selected to achieve the optimal excitation. The optimal turn-off value is calculated from a polynomial function approximation. The polynomial function is obtained from the off-line optimal data.

Two-step switching of the SRG is another method for enhancing its output power [38]. In this method, a zero-voltage switching step has been added to the conventional method. During this step, the phase is short-circuited and the current increases due to the back EMF. This produces more power than the conventional switching method, for the

same amount of magnetization current. No control strategy for online selection of parameters has been reported.

D. Research Objectives

The first objective of this research is to analyze fundamental principles of energy conversion in the switched reluctance generator in a systematic approach. Current status, benefits, and control challenges are explored. As a result of this analysis, design parameters and control parameters that affect the average output power of the SRG drive are identified.

The second objective is to characterize design and control of the generator for the range of parameters and control variables. New performance criteria are defined and models are developed and numerically simulated, iterative simulations of the machine under all useful conditions are done. The main outcomes are:

- To characterize the output power of the SRG for the range of design parameters and control variables.
- To prove the existence of a maximum output power point.
- Finding the optimal design parameters and control variables of the machine to generate maximum output power.

The third objective is to develop a control method for optimal operation of the SRG. The fourth objective is to experimentally validate of the controller for different operating points. The fifth objective of this research is to develop a control method for

online tuning of controller. The final objective is to do a detailed study on the various attributes of the proposed control method, such as the resolution, accuracy and sensitivity to parameters.

E. Dissertation Organization

The dissertation starts with the introduction presented earlier in this chapter. The current status of power generation and requirements for electric generators was also discussed earlier. The merits of the switched reluctance generator were briefly introduced, and challenges for its design and control have been described. Then previous research works on design, control, and application of this machine have been reviewed. Objectives of this research work were also presented.

The fundamental principle of the SRG drive is presented in Chapter II. This covers the mechanical structure and the electromagnetic behavior of the SRG, the principles of power generation in the SRG, the topology of the SRG drive converter, the mathematical model of the SRG drive, and the operating modes of the SRG. This chapter introduces the basics of the SRG drive that will be used in later chapters.

Design and control characterization of the average output power of the SRG for the range of design parameters and control variables will be introduced in Chapter III. The design parameters and control variables affecting output power are identified in this chapter. An analytical approach for finding the effect of design parameters and control variables on the output power has been shown. An iterative search method for finding

output power for the range of design parameters and control variables has been proposed. Simulation and experimental search results for finding the maximum output power has been presented.

In Chapter IV, a model-based, real-time control method of the SRG drive for output power maximization has been developed. A self-tuning controller has been proposed to remove the dependency of the controller on the machine parameters. This method is experimentally tested and the results have been presented. Current ripple mitigation on the dc-bus output of the generator drive has been investigated in this chapter, a control method for reducing the dc-bus current of the generator has been proposed. Also, the simulation and experimental results of this method have been presented.

Chapter V concludes the dissertation and discusses future research work in this area.

F. Conclusion

The current status of electric power generation and requirements for electric generators has been reviewed briefly in this chapter. The reasons for the preference of output power maximization for electric generators have been described. State-of-the-art switched reluctance generators have been presented. Design and control characterization of the switched reluctance generator to maximize the average output power will be

presented in this dissertation. The organization of this dissertation is briefly introduced in this chapter.

CHAPTER II

FUNDAMENTAL PRINCIPLES OF THE SRG DRIVE

A conventional switched reluctance generator drive system consists of the switched reluctance generator, power converter, sensors such as voltage, current, and position sensors, and control circuitry such as the DSP controller and its peripherals.

The controller is a crucial part of the SRG drive and it is necessity to have closed-loop control for stable power generation in most of applications [25]. Phase windings of the SRG are connected to the power converter, which provides field excitation for the phases and rectifies the generated current to the output dc-bus. Field excitation can be either from the output dc-bus, or a separate bus. Controller according to the information from sensors sends switching signals for gate drivers to control current in each phase. Basic principles and operations of the SRG drive will be presented in detail in following paragraphs.

A. Mechanical Structure of the SRG

The switched reluctance generator has doubly saliency both on the rotor and the stator. It can be built as a linear or rotary machine with either radial or axial flux. It has concentrated windings on the stator and no winding or permanent magnet on the rotor [20]. The number of rotor and stator poles can be the same or different, so there are

several configurations for SRG, cross section view of a four phase radial flux rotary SRG with six poles on the rotor and eight poles on the stator is shown in Fig. 4.

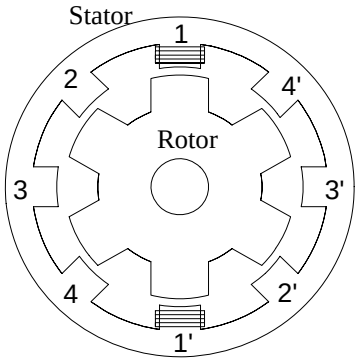

Fig. 4. Cross section view of a four phase 8/6 SRG.

B. Magnetic Characteristic of the SRG

Due to its double salient structure, the reluctance of the flux path for a phase winding varies with the rotor position. As one of the rotor poles moves toward the stator pole of the phase, the phase self-inductance increases until it reaches its maximum value, when it is completely aligned with the stator pole; this position is called the *aligned position*. As the rotor moves away from the stator pole, the self-inductance decreases until it reaches its minimum value when it is between two consecutive stator poles. This position is called the *unaligned position*. Also, because the switched reluctance machine is commonly designed such that the stator enters the magnetic saturation region with phase excitation, the reluctance of the flux path varies with the phase current. As a result, the phase flux linkage and phase self-inductance vary with both the rotor position

and the phase current. The profile of flux linkage and phase self-inductance of an 8/6 1-hp switched reluctance machine is shown in Figures 5 and 6. The mechanical and electrical data of this machine is given in Appendices A and B and graphs and waveforms in this chapter and the following chapters are based on the simulation and experimental measurements of this machine.

It has been shown a Fourier series of rotor position (θ) which has current dependent coefficients, can approximate the phase self-inductance (L) with high accuracy [39]. Each coefficient can be represented as a power series of the phase current (i). This analytical representation of the phase self-inductance of Phase-1 is given by

$$\begin{aligned} L(i,\theta) &= L_0(i) + L_1(i)\cos N_r\theta + L_2(i)\cos 2N_r\theta \\ &= \sum_{n=0}^{k} a_{1n} i^n + \sum_{n=0}^{k} a_{2n} i^n \cos(N_r\theta) + \sum_{n=0}^{k} a_{3n} i^n \cos(2N_r\theta) \end{aligned} \tag{2.1}$$

where N_r is the number of rotor poles; a_{1n}, a_{2n}, and a_{3n} are the coefficients of the polynomial functions $L_0(i)$, $L_1(i)$, and $L_2(i)$, respectively. In equation (2.1),

$$L_0 = \frac{1}{2}\left[\frac{1}{2}(L_a + L_u) + L_m\right] \tag{2.2}$$

$$L_1 = \frac{1}{2}(L_a - L_u) \tag{2.3}$$

$$L_2 = \frac{1}{2}\left[\frac{1}{2}(L_a + L_u) - L_m\right] \tag{2.4}$$

where

$$L_a = L(\theta = 0^\circ) = \sum_{n=0}^{k} a_n i^n \tag{2.5}$$

is the aligned position self-inductance as a function of the phase current;

$$L_m = L(\theta = \frac{\pi}{2N_r}) = \sum_{n=0}^{k} b_n i^n \tag{2.6}$$

is the self-inductance at the midway between the unaligned and the aligned positions as a function of current;

$$L_u = L(\theta = \frac{\pi}{N_r}) \tag{2.7}$$

is the self-inductance at the unaligned position and is assumed to be independent of the phase current. k is the degree of approximation (in the present case k= 5 yields a good accuracy). Coefficients a_n and b_n are determined by curve-fitting methods such that L_a and L_m obtained from Equations (2.5) and (2.6) would fit profiles obtained using finite element analysis or experimental measurement. After a_n and b_n are obtained from curve fitting, a_{1n}, a_{2n}, and a_{3n} can be easily calculated.

The analytical representation of self-inductance of other phases are the same as Equation (2.1) but shifted by 90° (electrical) from each other. In this research, this model has been used for analysis and simulations otherwise stated. It should be noticed that more terms could be added to the right side of Equation (2.1) to enhance the accuracy of the developed analytical model.

If the current level is low, iron core does not become magnetically saturated and variation of the self-inductance with current can be neglected, thus the phase self-inductance can be approximated with a piecewise linear function (Fig. 7). This model is easier for analysis and shows better relationship between geometry of the machine like the stator pole width (β_s) and the rotor pole width (β_r) with the self-inductance. In this

research, this model has been adopted for studying the geometry impact of the generator on the output power [20].

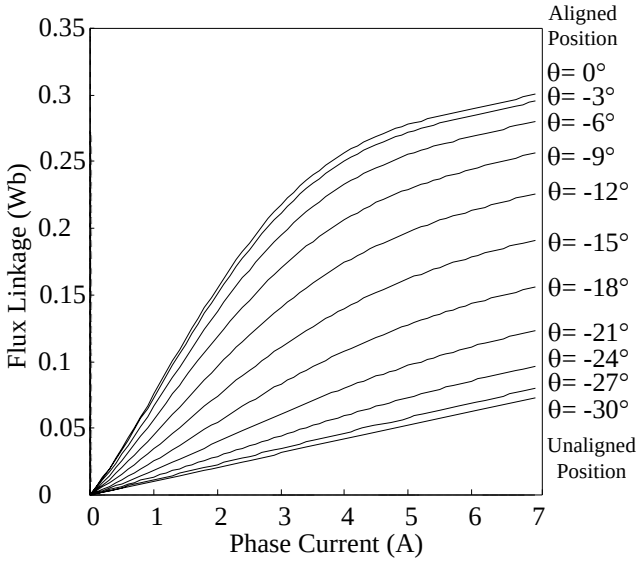

Fig. 5.Variation of the phase flux linkage with the rotor position and phase current.

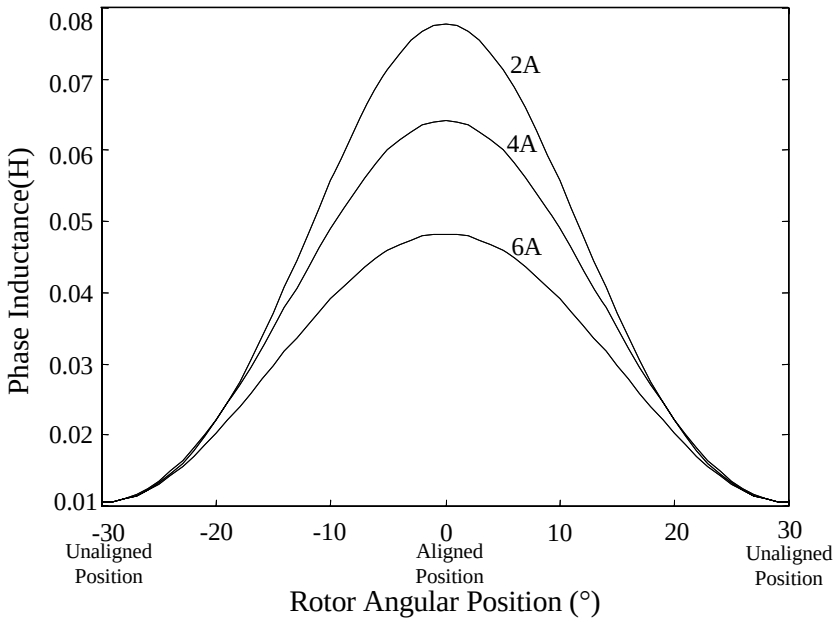

Fig. 6.Variation of the phase self-inductance with the rotor position and phase current.

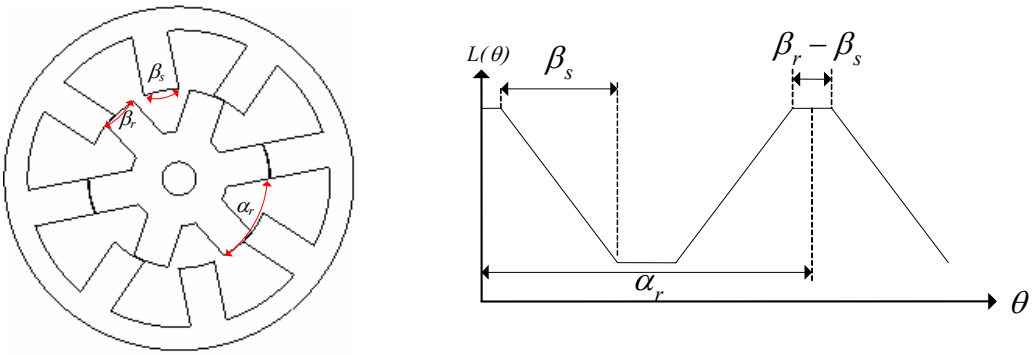

(a) Stator and rotor pole width and rotor pole pitch shown on the cross section of an 8/6 SRG.

(b) A simplified piecewise linear model of the phase self-inductance as a function of the rotor angular position.

Fig. 7. Cross section of a SRG and self-inductance variations of one phase.

C. Principles of Power Generation in SRG

If an electric source is connected to the phase coil while the rotor is aligned with it, energy will be stored in the magnetic path of the coil (Fig. 8.a). Magnetic reluctance is at the minimum value, and the stator pole tends to keep the rotor at this position. As the rotor moves away from the stator pole, the stator pole attracts the rotor pole to keep it at the aligned position. This produces opposing torque on the prime mover and increases the energy stored in the magnetic field, which can be transferred to the electric supply (Fig. 8.b). When the rotor is unaligned with the stator, there is no energy conversion from mechanical to magnetic and all the stored energy in the coil will be returned to the supply (Fig. 8.c). This concludes that any current pulse in the decreasing slope of self-inductance (Fig. 9) (i.e., when the rotor pole moves away from the stator pole) can generate power.

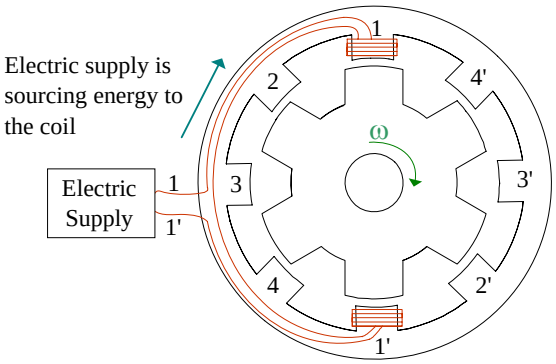

(a) Magnetizing the coil.

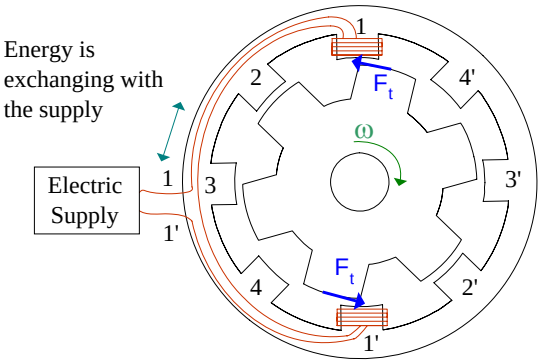

(b) Mechanical-to-electromagnetic energy conversion.

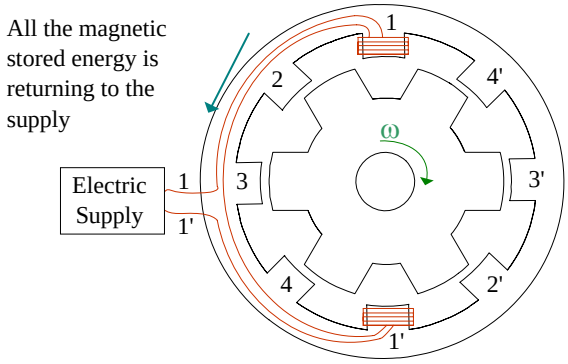

(c) Return of energy to the supply.

Fig. 8. Energy conversion process in SRG.

This process can be shown in flux linkage-current plane (λ-i) (Fig. 10). If at the aligned position a pulse of current is applied to the generator phase, electromagnetic

energy *(W_I)* will be stored in the phase coil. If it is assumed that the machine is in linear magnetic region, W_I can be calculated from:

$$W_I = \int_0^{I_o} i.d\lambda = \frac{1}{2} L_a I_o^{\,2} \tag{2.8}$$

where I_0, L_a, λ, i are current level, phase self-inductance at the aligned position, flux linkage and current of Phase-1 respectively. As the rotor moves from the aligned position toward the unaligned position, phase inductance is changing from L_a to L_u and energy W_{II} is returned to the supply.

$$W_{II} = (L_u - L_a) \cdot I_o \tag{2.9}$$

At the unaligned position, the remained stored energy in the coil (W_{III}) is sent back to the supply.

$$W_{III} = \int_{I_o}^{0} i.d\lambda = \frac{-1}{2} L_u I_o^{\,2} \tag{2.10}$$

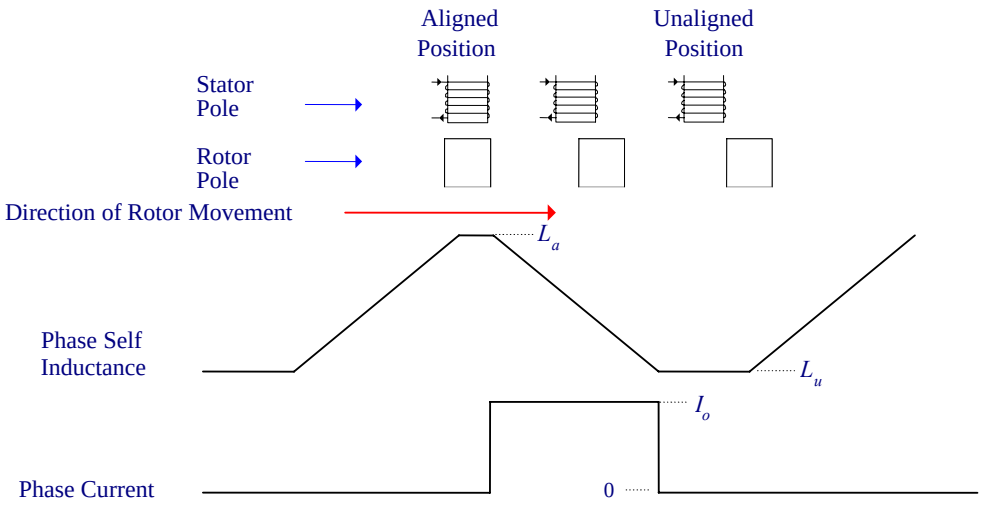

Fig. 9. Applying current pulse on the decreasing slope of the phase self-inductance.

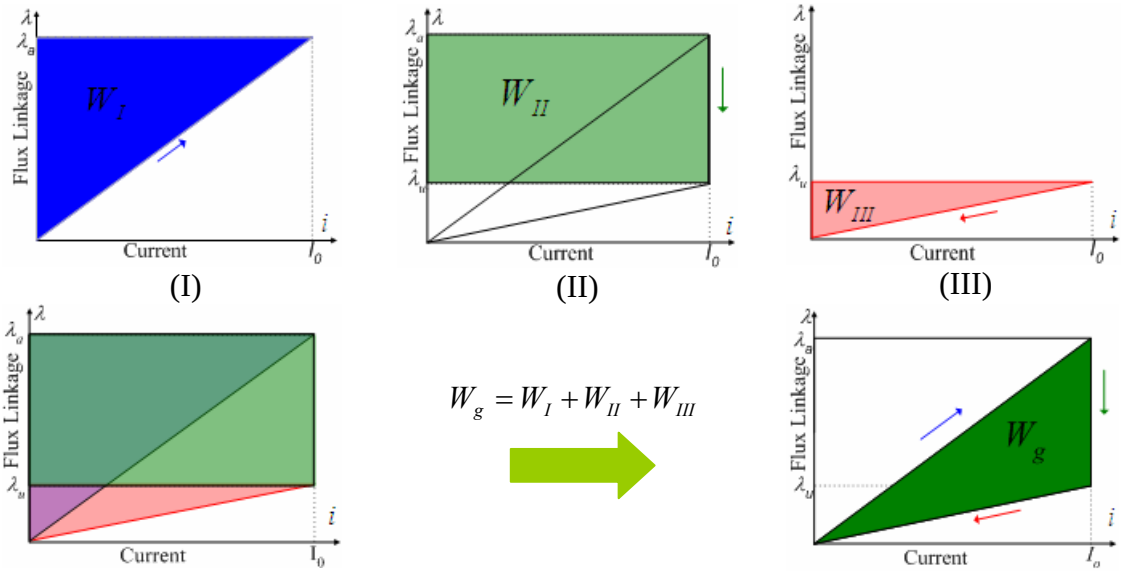

Fig. 10. Energy conversion process in flux linkage and current plane.

The total energy generated energy (W_g) is the summation of these three energies.

$$W_g = W_I + W_{II} + W_{III} = \frac{1}{2}(L_u - L_a) \cdot I_o^{\,2} \qquad (2.11)$$

In practice, usually (λ-i) curves are not linear due to saturation effect and current is not flat top. The phase coil is magnetized close to aligned position and is demagnetized near to the unaligned region in each cycle. This process can be shown as a loop in (λ-i) plane which is called energy conversion loop (Fig. 11) and the average output power of the generator is proportional to the area inside the loop (W_g) [23].

D. Mathematical Model of the SRG Drive

The average electric power of SRG phases (P_{out}) is the summation of output power of each phase in one electric cycle

$$P_{out} = \frac{1}{T}\sum_{j=1}^{N_s}\int_0^T v_j i_j dt \tag{2.12}$$

where N_s, T, V_j, i_j are the number of motor phases, the conduction period of one phase, voltage and current of Phase j. It must be remembered that each phase of the SRG, ideally, can be considered as a de-coupled magnetic circuit. whose dynamics are given by its phase voltage differential equation.

$$v_j = Ri_j + \frac{d\lambda_j}{dt} \tag{2.13}$$

Where R is the winding resistance per phase, λ_j represents the flux linkage of Phase j due to the current i_j, and t is time. The phase flux linkage λ_j is given by

$$\lambda_j = L_j(i_j, \theta) i_j \tag{2.14}$$

where L_j is the self inductance of Phase j. Substituting (2.14) into (2.13), one can have

$$v_j = Ri_j + (L_j + i_j \frac{\partial L_j}{\partial i_j})\frac{di_j}{dt} + i_j \frac{\partial L_j}{\partial \theta}\omega \tag{2.15}$$

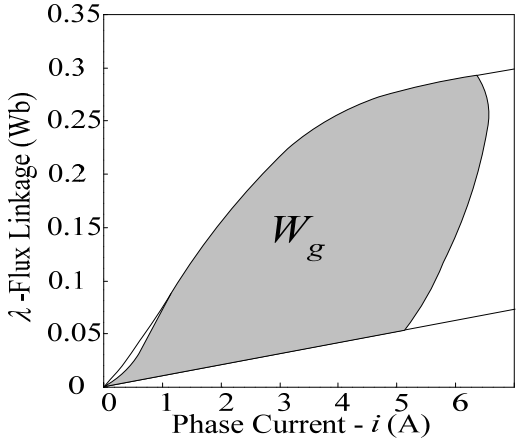

Fig. 11. Energy conversion loop.

The third term in Equation (2.15) is motional back EMF and it can be modeled as a resistance, which can have positive or negative value depending on the slope of inductance.

$$e = i_j \frac{\partial \lambda_j(i_j,\theta)}{\partial \theta} = i_j \frac{\partial L_j(i_j,\theta)}{\partial \theta} \omega = K_e(i_j,\theta) \cdot i_j \cdot \omega \tag{2.16}$$

The profile of the back EMF (K_e) constant with respect to the phase current and rotor position of an 8/6 1-hp SRG is shown in Fig. 12.

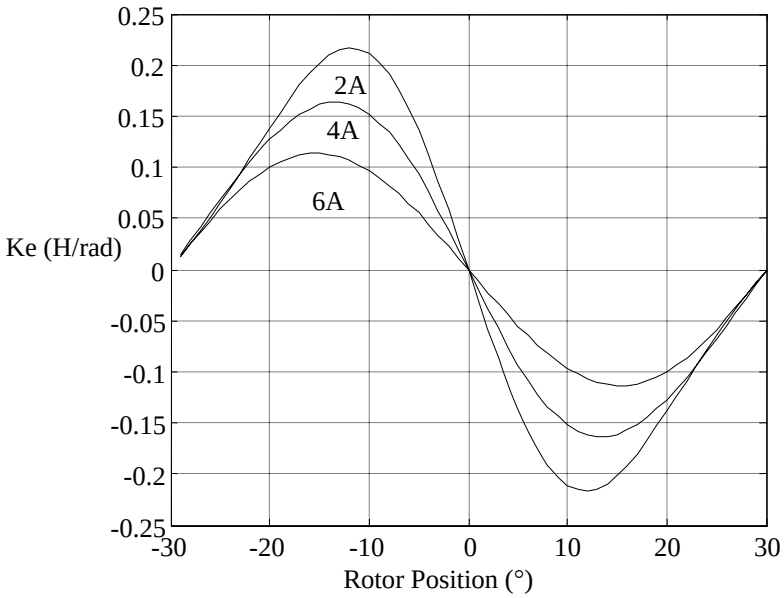

Fig. 12. Back EMF constant (K_e) versus the phase current and rotor position.

The phase incremental inductance is defined as the derivative of the phase flux linkage against the phase current as

$$\ell_j(i_j,\theta) = \frac{\partial \lambda_j}{\partial i_j} = L_j + i_j \frac{\partial L_j}{\partial i_j} \tag{2.17}$$

The incremental inductance is equal to the phase self-inductance, if the machine is operating at the linear magnetic region. However, if the machine is saturated at certain phase currents and rotor positions, the phase incremental inductance does not equal the phase bulk inductance any more. The variation of the phase incremental inductance with respect to the phase current and rotor position of an 8/6 1-hp SRG is shown in Fig. 13.

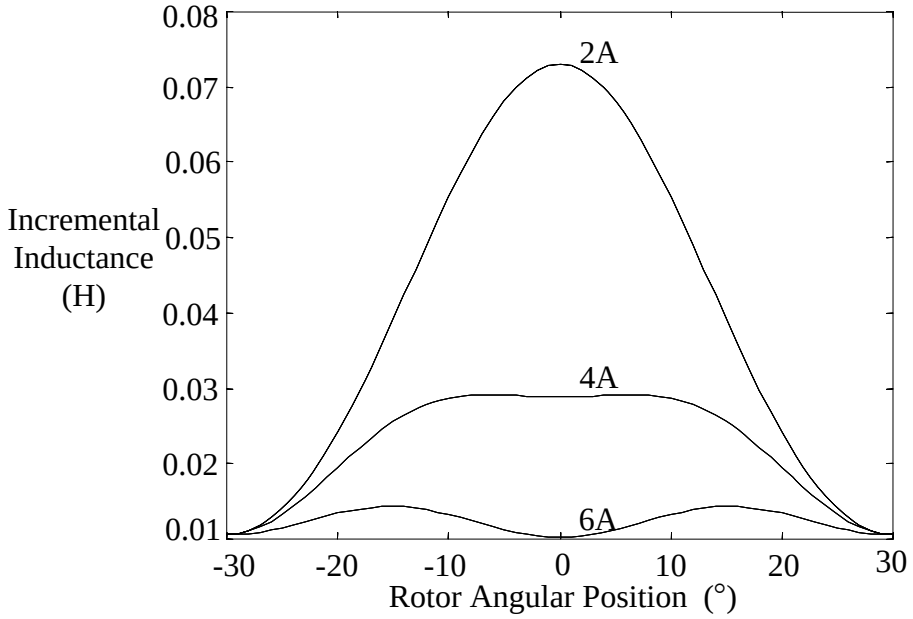

Fig. 13. Variation of the phase incremental inductance with the rotor position and phase current.

The equivalent circuit of one phase has been depicted in Fig. 14. If a constant current is applied to the decreasing inductance region of machine, a negative voltage will be induced on the coil, which shows the return of energy back to the electrical supply.

$$v_j = Ri_j + \ell_j \frac{di_j}{dt} + i_j \frac{\partial L_j}{\partial \theta}\omega = (R + \frac{\partial L_j}{\partial \theta}\omega) i_j < 0 \qquad (2.18)$$

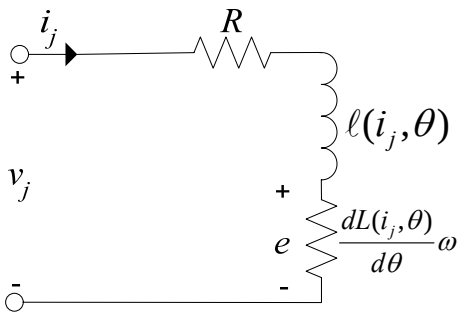

Fig. 14. Equivalent circuit of one phase of SRG.

E. SRG Drive Converter

SRG drive converter for every excitation cycle of each phase should be able to magnetize the phase coil, retrieve the converted energy, and demagnetize the phase coil. The power produced by each phase can be controlled by varying the amplitude and the timing of current pulses in synchrony with the rotor position. It should be excited near the aligned position and then turned off before the unaligned position. Because there is no ideal current source, it can be implemented with an asymmetric half-bridge voltage source, current controlled converter as shown in Fig. 15.

Capacitor C is for filtering output current of the generator. Because the SRG is singly excited and there is no permanent magnet in this generator, it needs an external source such as a battery to deliver energy for start-up. After transient time, the capacitor is charged up to the output voltage. Depending on the output voltage during phase-magnetization time, both the capacitor and the external source, or just the capacitor provides current to the load and the phase coil. The external source can be designed to be

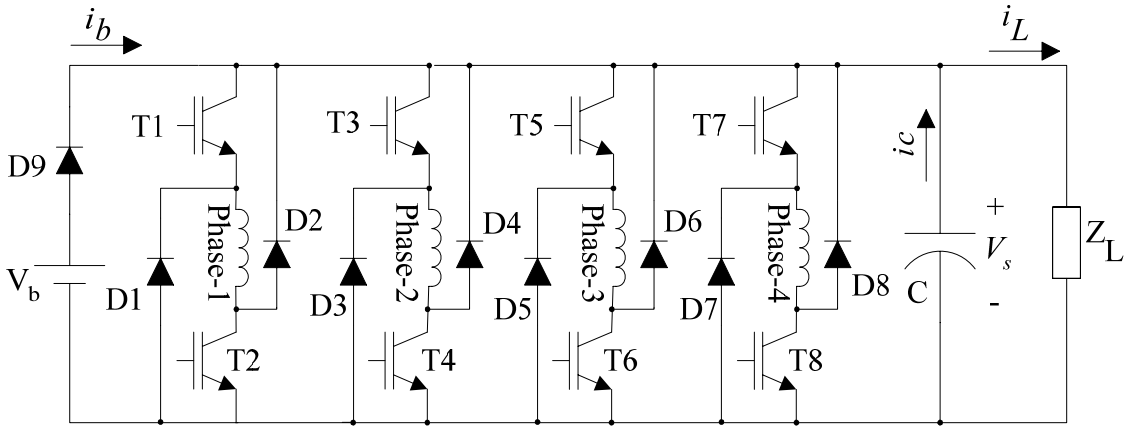

Fig. 15. The conventional SRG converter.

charged or can be disconnected from the system after the system reaches its operating point, like Fig. 15.

The operation of the conventional converter is shown in Fig. 16 by taking Phase-1 as an example. When the two switches T1 and T2 are turned on as in Fig. 16.a, the dc-bus voltage (V_s) will be applied to the phase-1 winding. Phase-1 current will increase as it flows through the path consisting of dc-bus positive terminal, T1, Phase-1 winding, T2, and dc-bus negative terminal. In this mode, flux linkage of the phase is increasing, so it is called magnetization mode.

$$\ell \frac{di_1}{dt} + Ri_1 = V_s - e \tag{2.19}$$

By turning off T1 and holding on T2 (i.e., Fig. 16.b), while the phase is energized, the current freewheels through the T2 and D1. At this mode, Phase-1 does not sink or source energy to the power supply, but the current increases due to the back EMF voltage in

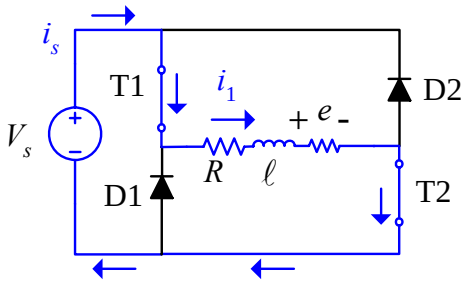

(a) Magnetization mode.

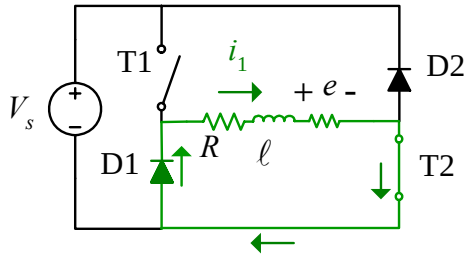

(b) Zero-voltage mode.

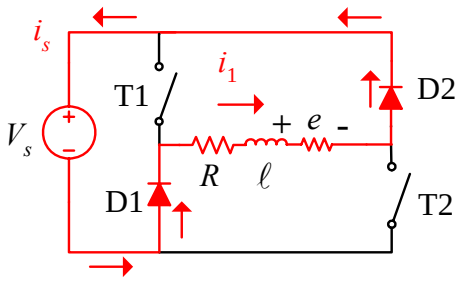

(c) Demagnetization mode.

Fig. 16. Modes of operation for conventional converter.

the coil. In this mode, flux linkage of the phase is constant and it is called zero-voltage mode.

$$\ell \frac{di_1}{dt} + Ri_1 = -e \tag{2.20}$$

When T1 and T2 are turned off (Fig. 16.c), the phase-1 current will flow through D2, dc-bus positive terminal, dc-bus negative terminal, D1, and Phase-1 winding. During this

time, the motor phase is subjected to negative dc-bus voltage through the freewheeling diodes and the energy trapped in the magnetic circuit is returned to the dc-bus. In this mode, flux linkage of phase is decreasing and it is called demagnetization mode.

$$\ell \frac{di_1}{dt} + Ri_1 = -V_s - e \tag{2.21}$$

If the back EMF voltage is smaller than the phase voltage, the phase current drops due to the negative applied phase voltage and by turning on and off T1 and T2, the Phase-1 current can be regulated.

F. Modes of Operation of the SRG Drive

Depending on the dc-bus voltage, rotor shaft speed and phase commutation angles of SRG, the phase-current waveform can be very different. Based on the current waveform different modes of operation for SRG can be defined.

According to Part C of this chapter, the SRG phase should be energized during the decreasing phase inductance slope as the rotor rotates. If the generator speed is low enough, the phase current can reach its peak value and the back EMF is smaller than the dc-bus voltage. So the phase current can be controlled by switching on or off to energize or de-energize the phase as shown in Figures 17.a. and 18. This mode is called low-speed or sometimes, chopping mode.

As the speed increases, back EMF will increase until a speed that back EMF equals the dc-bus voltage. At this speed, the current waveform has a flat top shape (Fig. 19). Above this speed, the phase current will increase even after de-energizing the phase;

this can damage the SRG drive and its prime mover. For avoiding excessive current problem, the controller should de-energize the phase earlier. The effect of phase turn-off angle on the peak current waveform has been shown in Fig. 20. This mode of operation is called high-speed or single-pulse mode.

If the phase is energized for more than half the electric cycle, the phase current cannot reach to zero before the start of next cycle. Keeping the same phase excitation pattern, phase current can reach to steady state waveform after some cycles, where it has a dc offset and oscillating between two maximum and minimum values like Fig. 21. At low-speed maximum phase current can be very high and may damage the drive. However, it is good way to increase the output power of generator at very high speed. Optimal phase excitation for output power maximization is discussed in the next chapter.

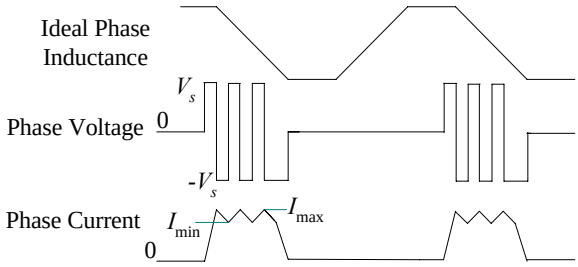

(a) Low-speed operation of SRG.

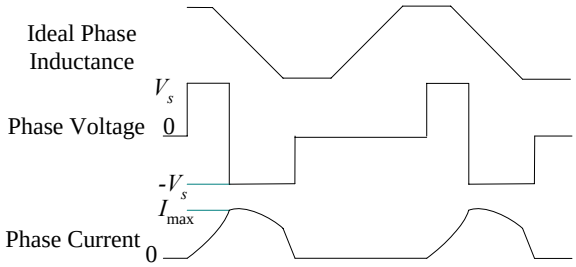

(b) High-speed operation of SRG.

Fig. 17. Low-speed and high-speed operation in the generating mode.

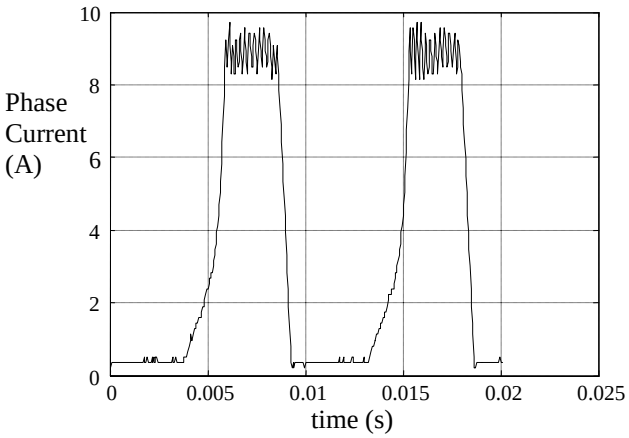

Fig. 18. Phase current of a 1-hp SRG running at ω= 1000 r/min and V_s= 120 V.

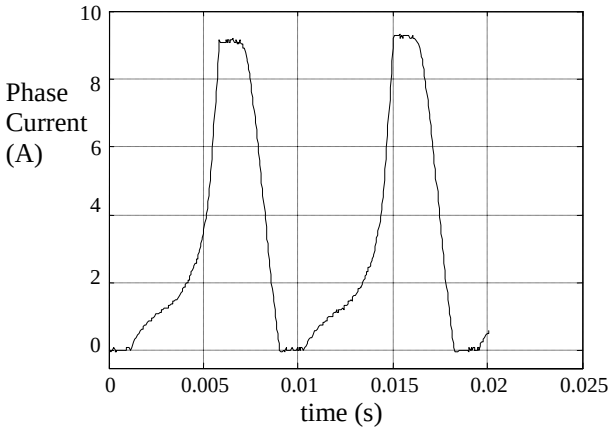

Fig. 19. Phase current at a speed that back EMF equals the dc-bus voltage.

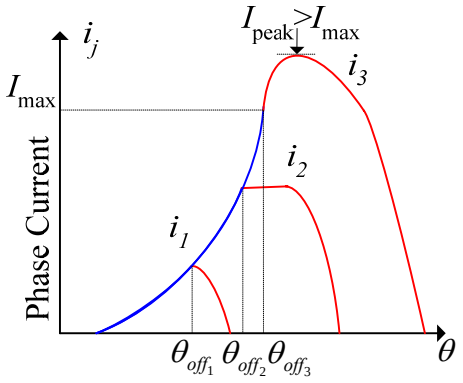

Fig. 20. Variation of the phase current with respect to the turn-off instant in SRG.

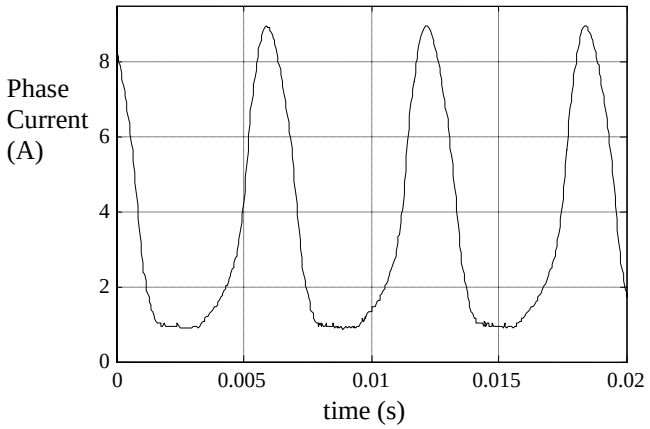

Fig. 21. Continuous conduction operating mode of the phase current.

G. Power Losses in the SRG Drive

The average output electric power of a SRG drive at steady-state operation (P_{out}) equals the difference between mechanical input power from the prime mover (P_{mech}) and total power losses (P_{loss}) in the drive.

$$P_{out} = P_{mech} - P_{loss} \tag{2.22}$$

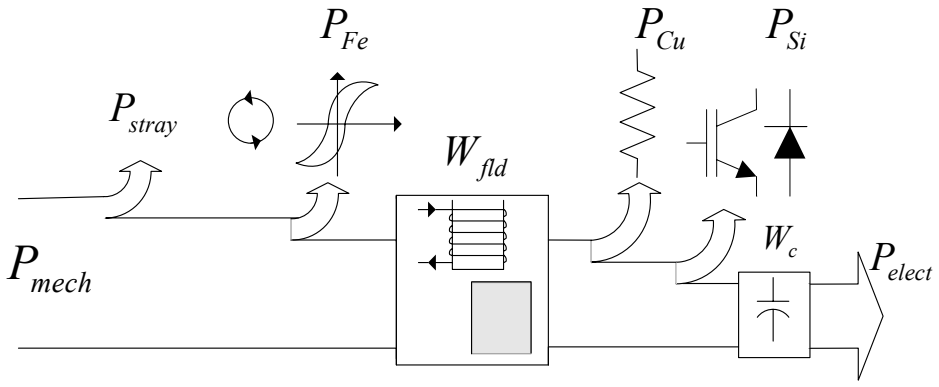

Fig. 22. Power flow in the switched reluctance generator.

Due to highly nonlinear operation of the SRG, exact estimation of losses is a big challenge. However, in searching for maximum output power, the designer only needs to make sure that the total power loss is less than the maximum rating of the machine. Power loss is the summation of several components (Fig. 22)

$$P_{loss} = P_{Si} + P_{Cu} + P_{Fe} + P_{stray} \tag{2.23}$$

where P_{si}, P_{cu}, P_{Fe}, and P_{stray} are inverter loss, copper loss, iron loss, and mechanical losses, respectively. Assuming all phases are carrying identical current waveform, the average copper loss can be easily calculated as

$$P_{Cu} = N \cdot I_{rms}{}^{2} R \tag{2.24}$$

where N, R, and I_{rms} are number of phases, resistance, and phase-current rms value, respectively. The windage loss is the main component of mechanical loss and it is a function of generator shaft speed and rotor shape. The mechanical loss of a 1-hp machine connected to a permanent magnet brushed dc machine with the specification in Appendix A is shown in Fig. 23. Losses in power converter are mostly composed of switching loss and conduction loss. In low speed operating mode, switching loss is higher and at high-speed operating mode, conduction loss in freewheeling diodes is dominant. Therefore, keeping the rms value of phase current below maximum rating of the machine will limit both copper and converter losses in single pulse-mode. Iron losses are composed of hysteresis and eddy current losses. Due to the highly nonlinear magnetic structure of the machine, it is hard to predict the iron losses. Some simple methods for estimating iron losses have been proposed in literature; however, usually the best way to estimate iron losses are using appropriate finite element methods [20].

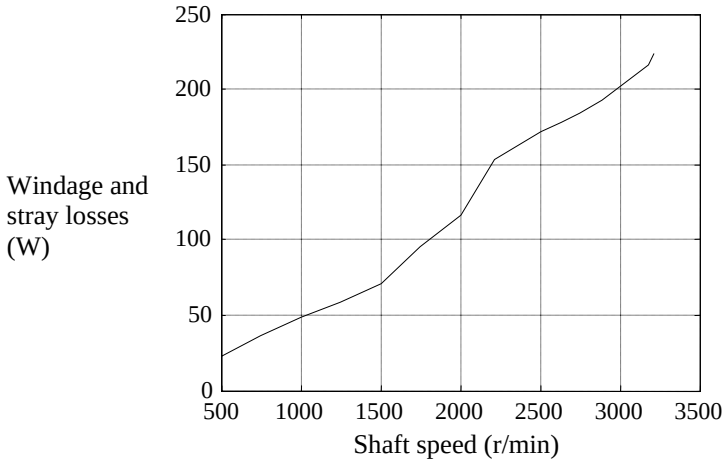

Fig. 23. Mechanical power losses in a SRG dynamometer.

H. Conclusion

In this chapter, the fundamental principles of the SRG drive were introduced. The magnetic behavior of the SR machine along with the mechanism of energy production was presented. The mathematical model of the SRG has been presented with electrical equivalent circuit. The conventional SRG drive and its different modes of operation were also discussed. Also a review on power losses has been presented.

CHAPTER III

DESIGN AND CONTROL CHARACTERIZATION OF THE SRG FOR THE MAXIMUM OUTPUT POWER

The ultimate goal in design and control of the stand-alone generator is power-density maximization, that is, maximum power throughput for a given size. In other words, it is desirable to have minimal size and lighter weight in the same rated machine. Power maximization can be accomplished in design and control by optimal selection of design parameters and control variables. Hence, exploring characteristics for the maximum output power on the range of design parameters and control variables are essential for utilizing the SRG across many applications.

In this chapter, control variables and design parameters affecting the output power are identified based on the terminal voltage equation of the SRG. As mentioned in previous chapters, the SRG has highly nonlinear characteristics. Thus, it is not possible to find an equation to calculate the output power in terms of all design parameters and control variables. However, by some approximations, this equation can be derived analytically. To find more accurate profile along with considering practical limitations, an iterative search method has been proposed. Results from the simulation of a 1-hp generator covering the whole range of design parameters and control variables have been presented and verified by experiment.

A. Design Parameters and Control Variables Affecting the Output Power

The average output power (P_{out}) of the SRG, ignoring power electronic losses, is calculated from Equation (2.12):

$$P_{out} = \frac{1}{T}\sum_{j=1}^{N_s}\int_0^T v_j i_j dt \tag{2.12}$$

Finding the average power requires the knowledge of phase current for a given terminal voltage by solving Equation (2.15).

$$v_j = Ri_j + (L_j + i_j \frac{\partial L_j}{\partial i_j})\frac{di_j}{dt} + i_j \frac{\partial L_j}{\partial \theta}\omega \tag{2.15}$$

Phase current depends on the following design parameters and control variables:

1) Phase Inductance $L(i_j, \theta)$: Because energy generation in this machine is based on the inductance variation, phase inductance plays a great factor in power generation. It is determined during the design step and its value may deviate from the designed value due to manufacturing imperfections, aging, or eccentricity of rotor [30].
2) Phase Resistance (R): It is always desired to minimize the copper loss. The phase resistance variation is small and ohmic drop on the phase resistance is usually negligible compared to the phase voltage at low current levels, thus it is not considered a design parameter. However, the effect of the phase resistance on the output power will be discussed in this chapter.

3) Rotor Shaft Speed (ω): It can change from zero up to more than 5–6 times of the rated speed of the generator and it is determined by the dynamic of prime mover and generator, which usually has much bigger time constant than the phase-conduction period. Thus, in one period of the phase current, it is assumed that the shaft speed is constant.

4) Phase Voltage (v_j): It can be identified with the dc-bus voltage level (V_s) and switching times. Assuming the generator shaft speed is constant in one period, the switching angles can be used instead of the switching times. Usually, the SRG is derived with a voltage source inverter, thus the dc-bus voltage is almost constant in one period of the phase current. Using conventional asymmetric half bridge as the topology of converter, the phase voltage has a general waveform as shown in Fig. 24. The phase voltage can get any value of zero, positive dc-bus voltage, or negative dc-bus voltage. It changes its value at switching angles. Switching angles and dc-bus voltage level are named as $\theta_1..\theta_5$ and V_s respectively in Fig 24.

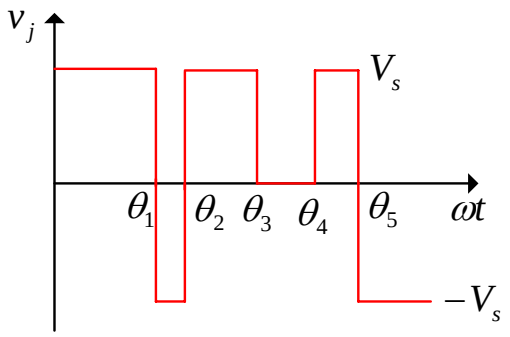

Fig. 24. A general phase voltage waveform.

Assuming all generator phases are identical, current of phases are the same and just time-shifted. Thus, the phase voltage and current will be referenced without index *j* as *v* and *i*, respectively in the following analysis.

B. Comparison of the Phase Voltage Switching Strategies for Output Power Maximization

Careful selection of the phase voltage switching is crucial to optimal excitation of the generator and the best voltage switching depends on the operating point of the generator and its operational limits. In the following section, a qualitative comparison of different voltage switching schemes has been presented. The conclusions can be used for selecting voltage switching algorithm for output power maximization.

B.1. Optimal switching strategy with no limit on the phase current

In this case, there is no constraint on the peak or rms value of the phase current. For finding the optimal phase voltage of the generator, the output power with three voltage waveforms as shown in Fig. 25 are compared. Any other voltage waveform can be constructed with a combination of these voltage waveforms. All voltage waveforms start at the same angle (θ_{on}) and have the same conduction period, which means that the phase current extinguishes to zero at the same position (θ_e). The comparison is based on an ideal motor that has no phase coil resistance and no magnetic saturation in its core.

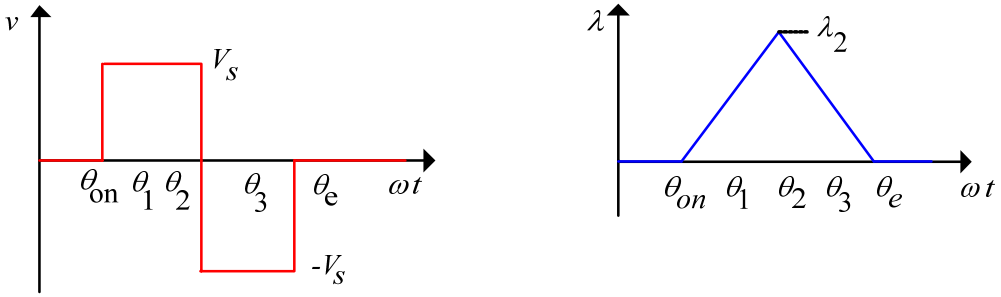

(a) The phase voltage and flux linkage waveforms with one-step switching pattern.

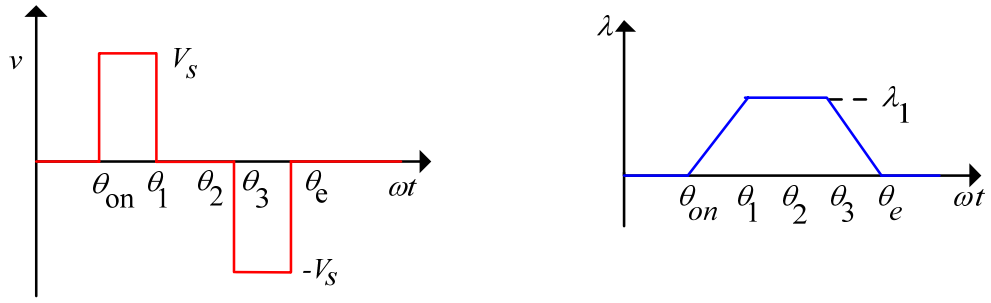

(b) The phase voltage and flux linkage waveforms with two-step switching pattern.

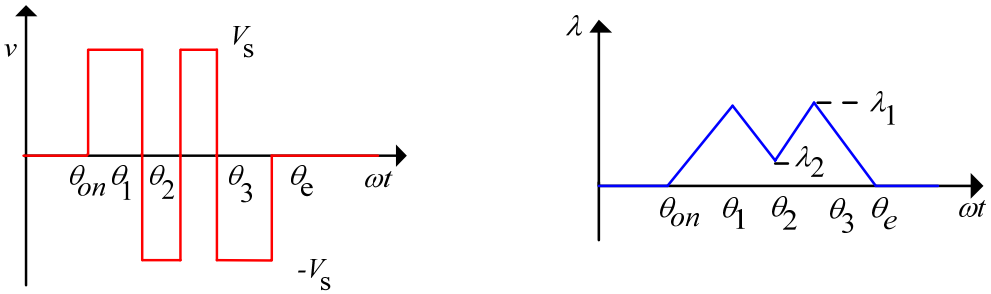

(c) The phase voltage and flux linkage waveforms with three-step switching pattern.

Fig. 25. Three basic phase voltage and flux linkage patterns.

Before comparing the output power for the three phase voltage waveforms in Fig. 25, let us prove the following lemma:

Lemma 1-Any increase in the phase flux linkage followed by its decrease to reach the initial value on the negative slope of inductance region, generates electric power.

Proof: Suppose that a positive voltage is applied to the phase coil from θ_1 to θ_2, this increases the flux linkage linearly from λ_1 to λ_2. From θ_2 to θ_3, the flux linkage decreases linearly to reach λ_1 again (Fig. 26). The flux linkage is calculated in Equation (3.1).

$$\lambda = \frac{1}{\omega}\int_0^{\theta} v \cdot d\theta = \begin{cases} \frac{V_s}{\omega}.(\theta - \theta_1) + \lambda_1 & \theta_2 > \theta \geq \theta_1 \\ \lambda_2 - \frac{V_s}{\omega}.(\theta - \theta_2) & \theta_3 > \theta \geq \theta_2 \\ \lambda_1 & else \end{cases} \tag{3.1}$$

The energy transferred to the phase during this period equals

$$\Delta W = \frac{1}{\omega}\int_{\theta_1}^{\theta_3} i \cdot v d\theta = \frac{V_s}{\omega} \cdot (\int_{\theta_1}^{\theta_2} \frac{\lambda}{L(\theta)} d\theta - \int_{\theta_2}^{\theta_3} \frac{\lambda}{L(\theta)} d\theta) = V_s \cdot (Q_m - Q_d) \tag{3.2}$$

where Q_m and Q_d are total charges during magnetization period (θ_1-θ_2) and demagnetization period (θ_2-θ_3), respectively.

It can be proved easily that Q_d is always greater than Q_m. For this reason, two small intervals of position ($d\theta$) have been selected with equal fluxes in magnetization and demagnetization periods as shown in Fig. 27. To distinguish the variables in the magnetization and demagnetization periods, variables in the magnetization period have been labeled with *m* argument (e.g., θ_m) and ones in the demagnetization period have been labeled with *d* argument (e.g., θ_d).

$$dQ_m = \frac{1}{\omega} \cdot i_m \cdot d\theta_m = \frac{\lambda \cdot d\theta_m}{\omega \cdot L(\theta_m)} \tag{3.3}$$

$$dQ_d = \frac{1}{\omega} \cdot i_d \cdot d\theta_d = \frac{\lambda \cdot d\theta_d}{\omega \cdot L(\theta_d)} \tag{3.4}$$

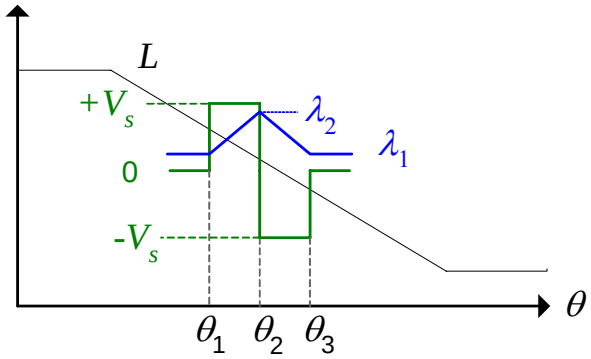

Fig. 26. A single pulse voltage applied in the decreasing inductance slope.

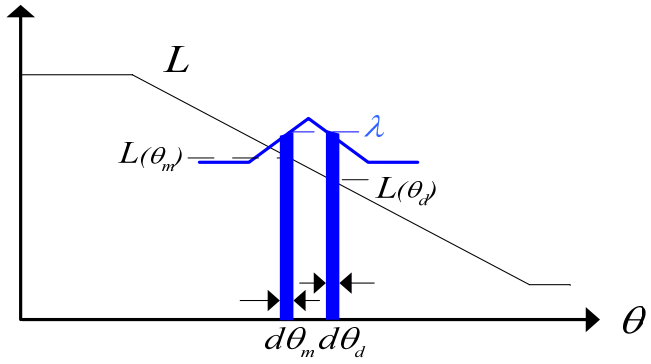

Fig. 27. The magnetization and demagnetization bands with the same flux linkage.

Because $L(\theta_m) > L(\theta_d)$, it can be concluded that

$$dQ_m < dQ_d \tag{3.5}$$

This is valid on the entire magnetization and demagnetization period. Since magnetization and demagnetization periods are equal, the total summation of Equation (3.5) is also valid, which means power is generating.

$$Q_m < Q_d \Rightarrow \Delta W < 0 \tag{3.6}$$

Similarly, one can prove that any decrease in the flux linkage followed by increase to reach its initial value within the decreasing slope of inductance, consumes energy. ■

Now we compare three different voltage patterns in Fig. 25, which the average output power for each one can be calculated as

$$P_{out} = \frac{N_s N_r}{2\pi} \int_{\theta_{on}}^{\theta_e} i \cdot v d\theta = \frac{N_s N_r}{2\pi} \left(\int_{\theta_{on}}^{\theta_1} i \cdot v d\theta + \int_{\theta_1}^{\theta_3} i \cdot v d\theta + \int_{\theta_3}^{\theta_e} i \cdot v d\theta \right) = P_I + P_{II} + P_{III} \qquad (3.7)$$

where N_r, P_I, P_{II}, P_{III} are the number of rotor poles, average power generated from θ_{on} to θ_1, θ_1 to θ_3 and θ_3 to θ_e, respectively. P_I and P_{III} are the same for three voltage switching waveforms. Hence, the switching waveform that has a bigger magnitude of P_{II} generates more output power.

In the one-step switching mode, Fig. 25.a from θ_1 to θ_3, the flux linkage increases and it returns to its initial value, which means power is generating according to *Lemma-1*. In the two-step switching mode, from θ_1 to θ_3 no power is generated and in the three-step switching mode, from θ_1 to θ_3, the flux linkage decreases and it returns to its initial value, which means that power is consuming according to *Lemma 1*. Thus, one-step switching pattern generates the highest power and the three-step switching pattern generates the least power.

One immediate question for output power maximization is optimal switching angles. It can be easily proved that in the decreasing inductance region, the output power increases by increasing the conduction angle. Fig. 28 shows the flux linkage of a one-step flux linkage waveform with two conduction periods. The output power with the conduction period from θ_{on_1} to θ_e can be calculated as

$$P_{out_1} = \frac{N_s N_r}{2\pi} \int_{\theta_{on_1}}^{\theta_e} i \cdot v d\theta = \frac{N_s N_r V_s}{2\pi} \left(\int_{\theta_{on_1}}^{\theta_{off_1}} \frac{\lambda_j}{L(\theta)} d\theta - \int_{\theta_{off_1}}^{\theta_e} \frac{\lambda_j}{L(\theta)} d\theta \right) = P_{on_1} + P_{off_1} \qquad (3.8)$$

where P_{on_1} and P_{off_1} are the average output power during magnetization and demagnetization periods. The output power with the conduction period from θ_{on_2} to θ_e can be calculated as

$$P_{out_2} = \frac{N_s \cdot N_r}{2\pi} \int_{\theta_{on_2}}^{\theta_e} i \cdot v d\theta = \frac{N_s \cdot N_r}{2\pi} \left(\int_{\theta_{on_2}}^{\theta_0} \frac{V_s \cdot \lambda}{L(\theta)} d\theta - \int_{\theta_{off_1}}^{\theta_e} \frac{V_s \cdot \lambda}{L(\theta)} d\theta + \int_{\theta_0}^{\theta_{off_1}} \frac{v \cdot \lambda}{L(\theta)} d\theta \right) \quad (3.9)$$
$$= P_{on_2} + P_0 + P_{off_2}$$

where P_{on_2}, P_0 and P_{off_2} are average output powers from θ_{on_2} to θ_0, θ_0 to θ_{off_1} and θ_{off_1} to θ_e, respectively. P_{off_2} and P_{off_1} are equal and P_0 is always less than zero. The conduction period from θ_{on_2} to θ_0 equals θ_{on_1} to θ_{off_1} and the phase inductance in the former period is bigger in the second period.

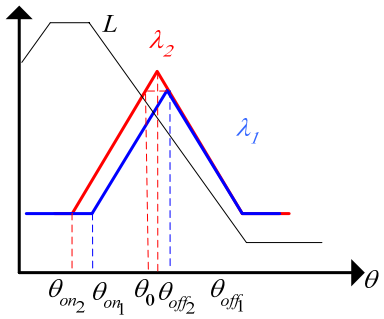

Fig. 28. Increase of the output power with the conduction band.

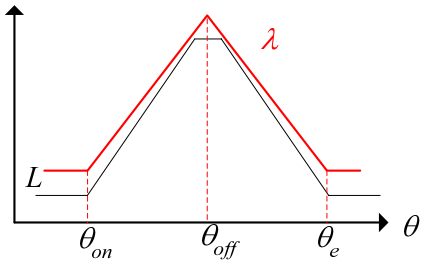

Fig. 29. Symmetrical switching which generates zero output power.

$$\theta_1 \in [\theta_{on_1}, \theta_{off_1}], \theta_2 \in [\theta_{on_2}, \theta_0], L(\theta_2) > L(\theta_1) \Rightarrow \frac{\lambda}{L(\theta_1)} > \frac{\lambda}{L(\theta_2)} \Rightarrow P_{on_1} > P_{on_2} \quad (3.10)$$

Hence, the total output power with a longer conduction period is more negative, which means more power is generated.

Advancing the switching angle even before the aligned position may increase the output power. This power increase continues to an optimal point and any further advancing the firing angle decreases the output power until the flux waveform becomes symmetrical around the aligned region, which means the generated power is zero (Fig. 29). It will be shown later in this chapter that finding the optimal values of θ_{on} and θ_{off} analytically is not practical; however, by using some numerical methods, one can find the optimal values easily.

B.2. Optimal switching strategy with the limited peak phase current

High current spikes can generate high radial and axial stress on the shaft and the generator body. It can cause high core losses and damage the power electronic converter. Hence, the maximum peak current of a generator should be limited by selecting firing angles that avoid current exceeding the maximum level. This can be defined in terms of the maximum flux linkage

$$i < I_{\max} \rightarrow \lambda(i, \theta) < \lambda(I_{\max}, \theta) \quad (3.11)$$

Anytime the phase flux linkage reaches to this value, the current should be regulated by applying negative voltage to the phase coil, as shown in Fig .30. For the maximum output power, one can start turning on the phase earlier until the flux linkage

reaches $\lambda_{\max}$. Assuming the position zero is at the aligned position and neglecting the voltage drop on the phase coil resistance, the turn-on angle for the maximum output power $\theta_{on\max}$ can be approximated as follows:

$$\theta_{on\max} = \frac{-\omega\lambda_{\max}}{V_s} + \theta_m \tag{3.12}$$

where θ_m is the position where the flux linkage has the maximum value (Fig. 31).

To control the phase current successfully below its maximum level, the back EMF voltage of the phase when the phase current reaches its maximum value should be smaller than the dc-bus voltage. This condition can be checked with Equation (3.13).

$$\frac{V_s}{\omega} \geq \left| \frac{\partial\lambda(I_{\max},\theta)}{\partial\theta} \right| \tag{3.13}$$

In other words, the slope of the flux linkage curve with respect to position at maximum current should be smaller than the dc-bus voltage over speed. In low-voltage or high-speed this condition may not be satisfied. For this reason, the phase should be a turned off earlier to avoid excessive current (Fig. 32).

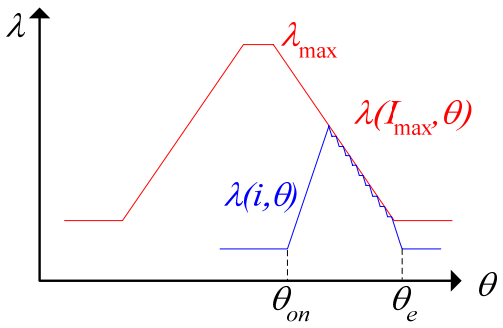

Fig. 30. Phase current excitation with limited maximum current.

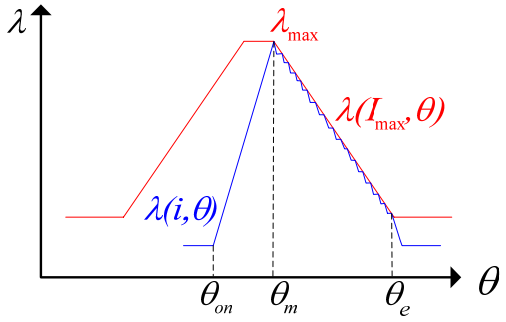

Fig. 31. Maximum output power when Equation (3.13) is satisfied.

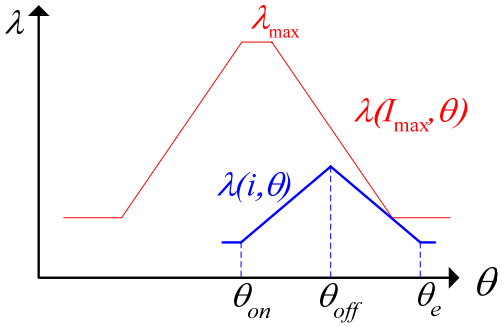

Fig. 32. Phase turn-off selection when Equation (3.13) is not satisfied.

B.3. Optimal switching strategy with limited rms value of the phase current

For any designed machine, the maximum machine loss is limited. Therefore, the rms value of the phase current should be less than the maximum rating of the machine. In low-speed and/or high dc-bus voltage, rms value of current can violate the maximum rating of the machine. In this case the optimal switching strategy should be identified again.

Suppose that the phase is excited with constant current I_p on the decreasing slope of inductance as shown in Fig. 33. The conduction period has been selected as the whole decreasing inductance region, due to the fact that for a square wave pulse with a fixed

average value, the longer the conduction period, the less the rms value is. Thus, the conduction period of the current almost equals stator pole width.

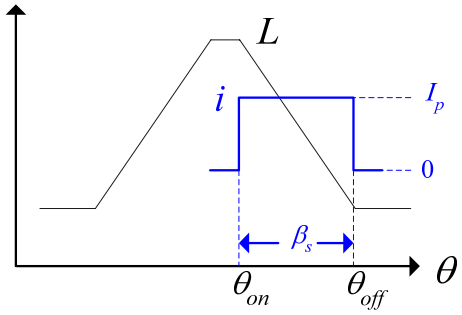

Fig. 33. Applying current pulse to the SRG phase for the maximum output power.

The maximum value of I_p can be found as

$$I_{p_{\max}} = \sqrt{\frac{\alpha_r}{\beta_s}} \cdot I_{rms_{\max}} \tag{3.14}$$

where $I_{rms_{\max}}$ is the rated rms value of the phase current. This current produces a back EMF voltage (e), which equals

$$e = \frac{dL}{d\theta} \cdot I_p \cdot \omega \tag{3.15}$$

It is easy to prove that this current has the minimum rms value for a fixed period of excitation and fixed average value. So, this pulse generates the maximum output power. The maximum output power of the generator in this situation equals

$$P_{out\max} = \frac{(L_a - L_u)}{2\pi} \cdot I_{p_{\max}}^2 \cdot N_r \cdot N_s \cdot \omega \tag{3.16}$$

This equation can be used as a rough estimate for the output power of generator which was obtained without considering magnetic saturation, iron and mechanical losses in the machine, and the voltage drop on the phase coil resistance. In practice, there is no ideal current source and SRM coils are excited with current controlled voltage converter. Moreover, the current cannot jump from zero to its maximum or vice versa in zero time because of the phase inductance. Therefore, the maximum peak current and the switching times should be calculated by considering these facts.

As the speed increases, back EMF voltage boosts up and at the speed which is called *base speed*, it equals the dc-bus voltage of the converter. Applying flat-top current, to get the maximum output power is not possible above the base speed, for which the current will increase even after applying negative voltage to the phase. Thus, the only way to regulate the current is to change the excitation angles.

In conclusion, for output power maximization of the SRG with limited rms current, a good strategy for exciting the phase is producing a flat-top current for below base speed, and tuning turn-on and turn-off switching angles for above the base speed. For the rest of our analysis, we emphasize the design and control on above the base speed region.

C. Analytical Approach for Finding the Output Power

Finding the output power requires solving Equation (2.15), which is nonlinear time varying with no general analytical solution. However, it can be solved with some

simplifying assumptions. For this purpose, it is assumed that the generator is operating at the high speed and the flux linkage is below the saturation limit, which is a common operating region for many applications of the switched reluctance generator. In this region, an effective way of the phase excitation is simply turning on and then turning off the phase as shown in Fig. 34.

Assuming the copper loss is negligible ($R = 0$), the flux linkage will be equal.

$$\lambda = \frac{1}{\omega}\int_0^{\theta} V d\theta = \begin{cases} \frac{V_s}{\omega}.(\theta - \theta_{on}) & \theta_{off} > \theta \geq \theta_{on} \\ \frac{V_s}{\omega}.(\theta_{off} - \theta_{on} - \theta) & \theta_e > \theta \geq \theta_{off} \\ 0 & else \end{cases} \tag{3.17}$$

Extinction angle (θ_e), is the position, where the current drops to zero after turning off and it equals

$$\theta_e = 2\theta_{off} - \theta_{on} \tag{3.18}$$

Also in the case of no magnetic saturation in the core ($L(i,\theta) = L(\theta)$) current can be obtained as

$$i = \frac{\lambda}{L(\theta)} = \begin{cases} \frac{V_s(\theta - \theta_{on})}{\omega \cdot L(\theta)} & \theta_{off} > \theta \geq \theta_{on} \\ \frac{V_s(\theta_{off} - \theta_{on} - \theta)}{\omega \cdot L(\theta)} & \theta_e > \theta \geq \theta_{off} \\ 0 & else \end{cases} \tag{3.19}$$

Substituting (3.19) in (2.12), the average power will be calculated as

$$P_{out} = \frac{N_s N_r V_s^{\,2}}{\omega}\left(\int_{\theta_{on}}^{\theta_{off}} \frac{(\theta - \theta_{on})d\theta}{L(\theta)} - \int_{\theta_{off}}^{\theta_e} \frac{(\theta_{off} - \theta_{on} - \theta)d\theta}{L(\theta)}\right) \tag{3.20}$$

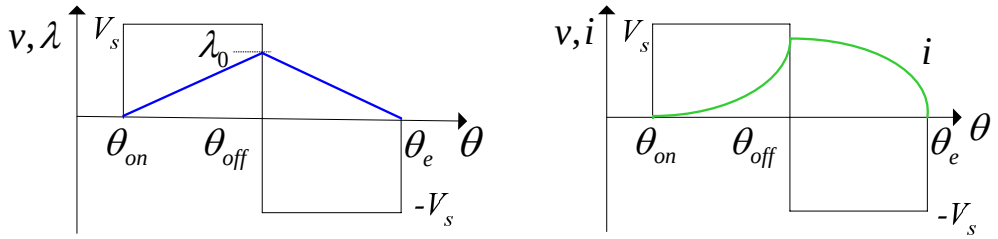

(a) The phase voltage and flux linkage (b) The phase current and voltage

Fig. 34. Phase voltage and current with one-step switching.

Equation (3.20) proves that for fixed commutation angles, the output power is proportional to V_s^2/ω and it is a nonlinear function of $\theta_{on}, \theta_{off}$ and L.

$$P_{out} = \frac{V_s^2}{\omega} \cdot f(L(\theta), \theta_{on}, \theta_{off}) \tag{3.21}$$

This equation implies, even in the simplified form, it is not clear to find the effect of switching angles and inductance shape on the output power. So an iterative search approach is used with engineering knowledge to find this relationship. This search has been implemented both on simulation and experimental.

D. Iterative Search for Finding the Maximum Output Power

The best way to find the profile of the output power is calculating it for all possible range of design parameters and control variables. Depending on application, the search space can be different. In order to narrow it down, we have used engineering knowledge to conduct the search toward the optimal operating point. This approach is composed of the following steps.

1. Identifying the parameters and variables that can affect the output power. Depending on the application the set of variables and parameters can change.
2. Determining limits on the operation of the SRG such as, maximum peak value of the phase current and maximum allowed losses.
3. Defining the possible range of parameters and variables.
4. Calculating the output power for one set-point of design parameters and control variables via experimental measurement or numerical simulation.
5. Excluding this operating point from the results, if it exceeds limits on the operation of machine, and based on that result, refining the search space.
6. Repeating step 3 to step 5, for the next point in the search space.

Because it is not possible to define a per unit generator for analysis, a 1-hp generator has been selected, the parameters of this generator has been shown in Table II and Table III. The detailed mechanical and electrical parameters of this machine are listed in Appendices A and B. The phase self-inductance and flux linkage as a function of the rotor position and the phase current are shown in Figures 5 and 6. The practical range of design parameters and control variables are defined and the model is simulated for different possible scenarios (Fig. 35). The range of design parameters and control variables that generate continuous current waveform (e.g., Fig. 21) are excluded from the simulation results. The simulation results of this particular machine are verified with experimental test. The results illustrate the general characteristics of the SRG. Moreover the same procedure can be used for the design and control of any other SRG.

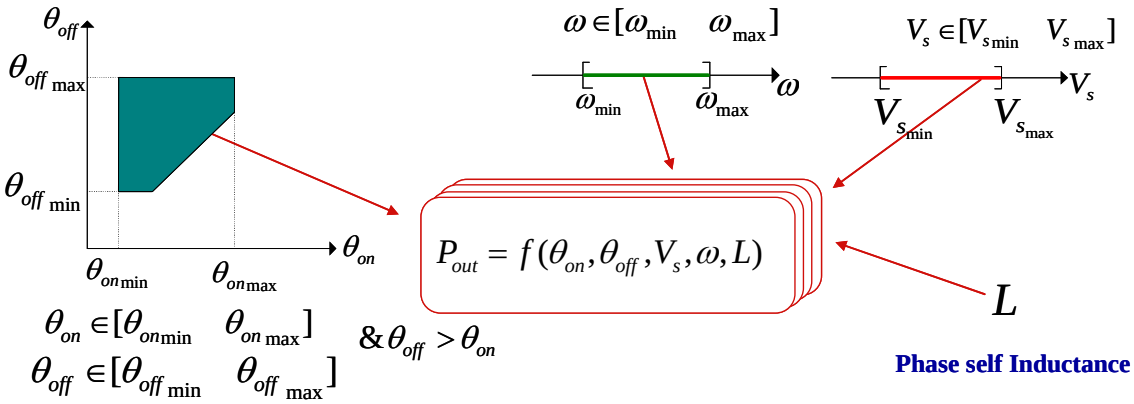

Fig. 35. The output power as a multidimensional space of design parameters and control variables.

Table II. Name Plate Specification of the SR Machine Used for Analysis

Power (P_{out})	1-hp	Number of Phases	4
Voltage (V_s)	120 V	Pole Configuration	8/6
Supply Current (I_L)	6 A	Unaligned Inductance (L_u)	8.25 mH
Base Speed (ω_b)	1000 r/min	Aligned Inductance (L_a)	53.753 mH

Table III. Maximum Rating of the SR Machine Used for Analysis

rms Value of the Phase Current	6A
Peak Value of the Phase Current	20A
Maximum Speed (ω_{max})	8000 r/min

D.1. Iterative simulation for finding the maximum output power

A detailed simulation model of the SRG with good accuracy is incorporated with the search algorithm [39]. The dynamic model of the SRG and the search algorithm is implemented in Simulink/Matlab environment. A user interface as shown in Fig. 36 is developed to get the range and step change of design parameters and control variables. Moreover, the user interface provides an interactive tool for visualizing the output power

variation versus different combinations of design parameters and control variables. The search algorithm runs the simulation model and analysis the results iteratively for the whole range of design parameters and control variables. The results can be plotted or stored for further analysis.

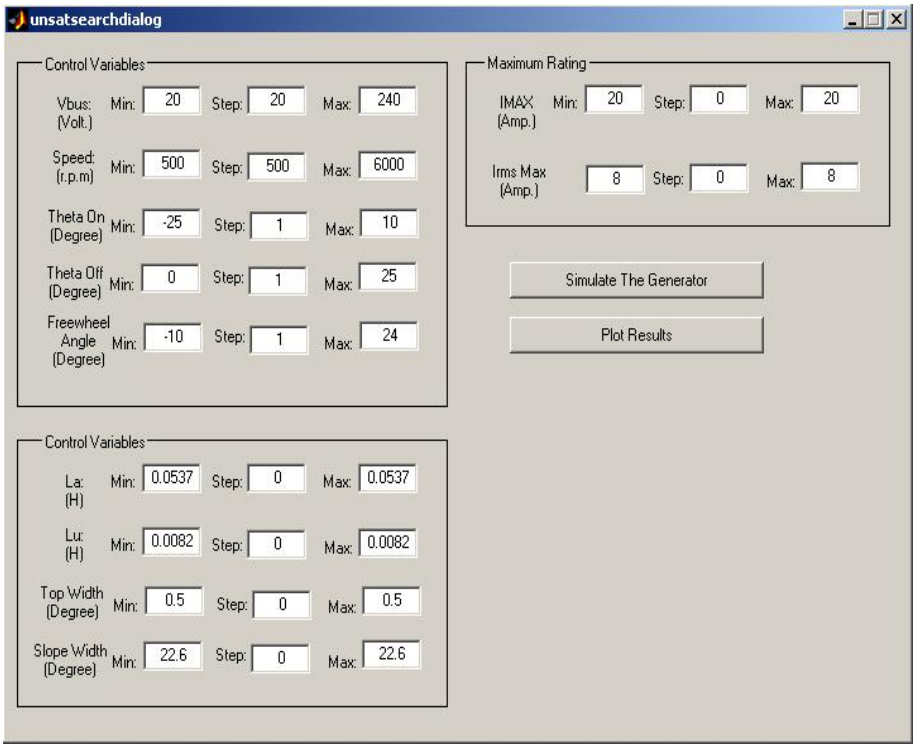

Fig. 36. A GUI designed for the search method.

Depending on the application, the range of design parameters and control variables will change. For better understanding the effect of design parameters and control variables on the output power, the search has been performed through different cases; each case represents an application of the SRG. In the first case, all the parameters and control variables except switching angles are considered constant. Other parameters

or control variables have been added one by one for other cases, thus the effect of design parameters and control variables on the output power have been further investigated.

D.1.1. Case I: $P_{out}= f(\theta_{on}, \theta_{off})$, $\omega, V_s=$ *const.*, $L= L(i, \theta)$

For the first case, we consider that the phase self inductance is a fixed function of current and position as shown in Fig. 6 and the dc-bus voltage and shaft speed are constant. Accordingly, the output power will be just a function of switching angles. This is a common situation when the SRG is connected to the utility line and a gas turbine running at constant speed. Variation of the output power for different values of turn-on angle and turn-off angle is plotted in Fig. 37. The data is gathered at the rated speed and rated terminal voltage. A two-dimensional version of this graph is shown in Fig. 38. The following can be observed from results:

- At a constant turn-on angle, increasing the turn-off angle increases the output power. (i.e., the longer conduction, the more output power at a fixed turn-on angle
- At a constant turn-off angle, by increasing turn-on angle, power decreases. (i.e., conduction period is decreased)
- There exists a pair of turn-on and turn-off angles, for which the power is maximum. For turn-on angle this point is before the rotor gets aligned with the stator ($\theta_{on} = -15^{\circ}$). This is in motoring region. In this region back EMF is opposing the phase supply voltage, hence the phase current cannot increase fast. However by the time the rotor reaches at the aligned

position, the phase coil will have enough current to build up a big back EMF for power generation. The optimal turn-off position is in the midway of aligned and unaligned positions of the rotor and stator ($\theta_{off} = 10^{\circ}$). This demagnetizes the phase before it gets into motoring region again.

- The output power is not very sensitive to turn-on and turn-off changes at its maximum point. Given this fact, one can define secondary control objectives and select a point that meets secondary objectives and also close to the maximum output power. Secondary objectives can be efficiency, productivity [38], or dc-bus current ripple minimization and so on.

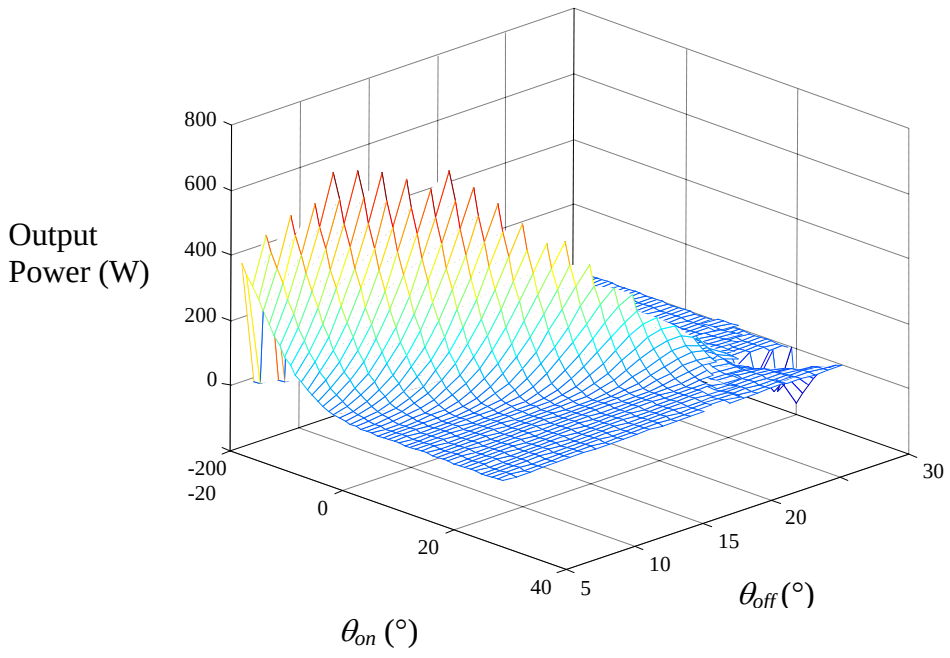

Fig. 37. The output power versus turn-on and turn-off angles at the rated output voltage and speed.

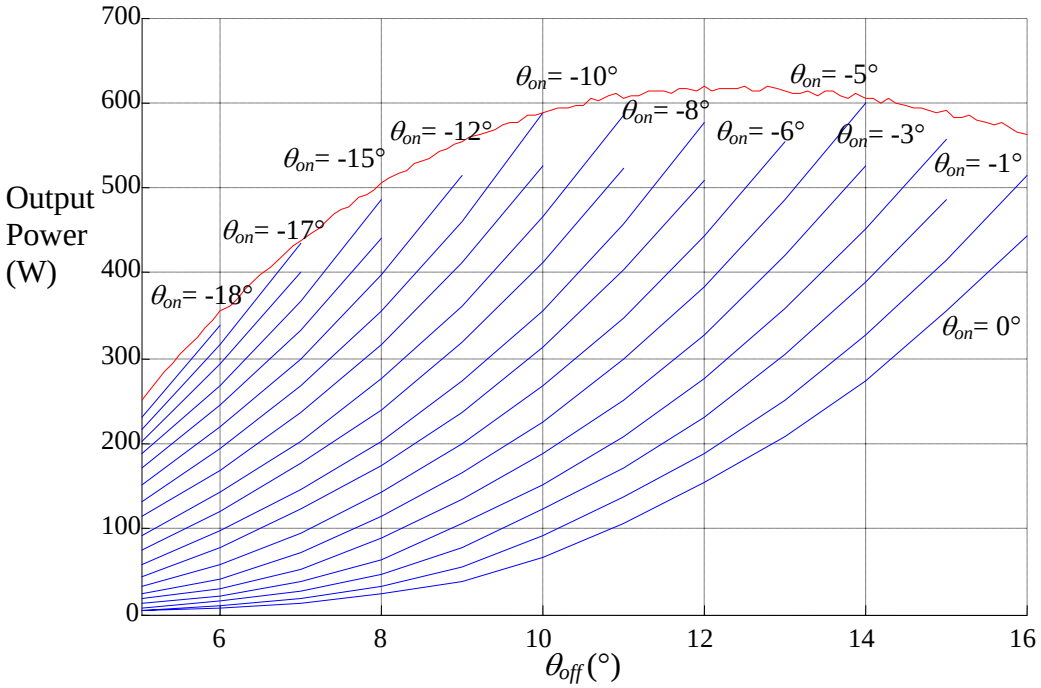

Fig. 38. 2D graph of the output power for the range of turn-on and turn-off angles at the rated output voltage and speed.

D.1.2. Case II: $P_{out}= f(\omega,\theta_{on}, \theta_{off}),V_s= const.,\ L= L(i,\theta)$

In this case, it is assumed that the phase self inductance is a fixed function and the dc-bus voltage is constant so the output power is a function of switching angles and shaft speed. An example of this case is a wind generator that is connected to a fixed-voltage dc-bus. Like previous case, the output power for all possible turn-on and turn-off angles at each shaft speed are calculated and it is shown in Fig. 39. At low speed which is below machine's base speed, the phase current is limited due to copper losses and the output power is increasing with speed. At speeds much higher than the base speed, it is inversely proportional to speed. So there exists a speed for which the output power is maximized.

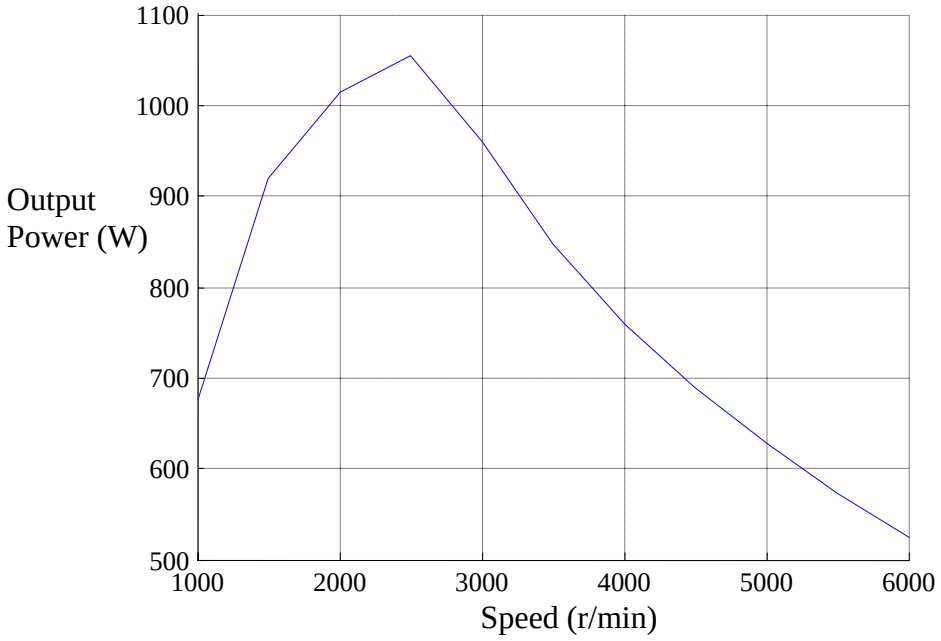

Fig. 39. The output power versus speed for optimal values of turn-on and turn-off angles at the rated dc-bus voltage.

D.1.3. Case III: $P_{out}= f(\omega, V_s,\theta_{on}, \theta_{off})$, $L= L(i,\theta)$

Now the effect of bus voltage variation is added, and the only fixed parameter is the phase inductance. The output power is a function of switching angles, dc-bus voltage and shaft speed. An example of this case is starter/alternator in cars where the generator terminal is connected to a battery and its voltage may change during charging or discharging periods. The output power for all possible turn-on, turn-off angles at each shaft speed and dc-bus voltage has been calculated and it is depicted in Fig. 40. It can be observed from the figure, the output power always increases with dc-bus voltage. At high speeds, it is proportional to V_s^2 and at low speeds and low dc-bus voltages it is also proportional to V_s^2 and with the increase of dc-bus voltage it is proportional to V_s, until it becomes almost constant.

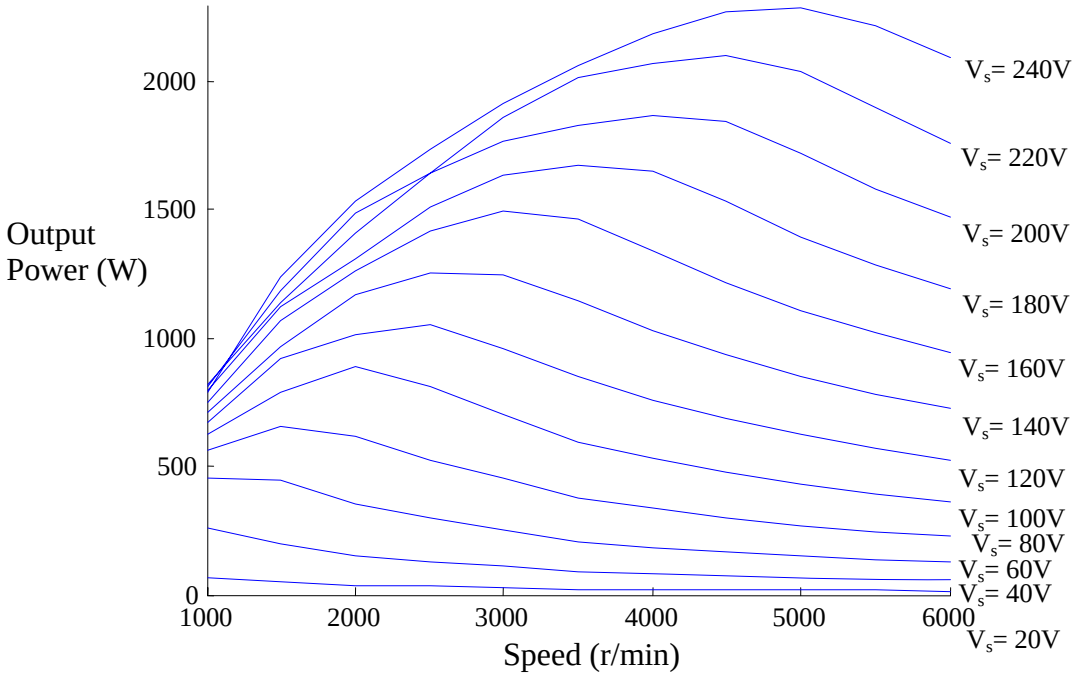

Fig. 40. The output power over the range of dc-bus voltage and speed at optimal turn-on and turn-off angles.

D.1.4. Case IV: $P_{out}= f(L,\theta_{on}, \theta_{off})$, ω, $V_s=$ *const.*

For this case, the effect of the phase inductance on the output power at the rated speed and dc-bus voltage is shown. For studying the effect of inductance modeling and saturation, the maximum output power with measured inductance (Fig. 6) has been compared to the simulation results of piecewise linear inductance model (Fig. 7). The maximum output power of the generator versus turn-on and turn-off angle for these two models are depicted in Fig. 41 and Fig. 42, respectively.

It can be observed from this figure that iron magnetic saturation causes decrease of the output power level. However, optimal turn-on and turn-off angles of both models are close. Similarly, the same conclusion holds for turn-off angle. This concludes that,

although linear inductance model is not accurate, but it can be used easily for finding the effect of rotor and stator pole sizes on the output power. The width of inductance slope in the linear inductance model equals the stator pole width and its top width equals the difference between the stator and rotor pole width.

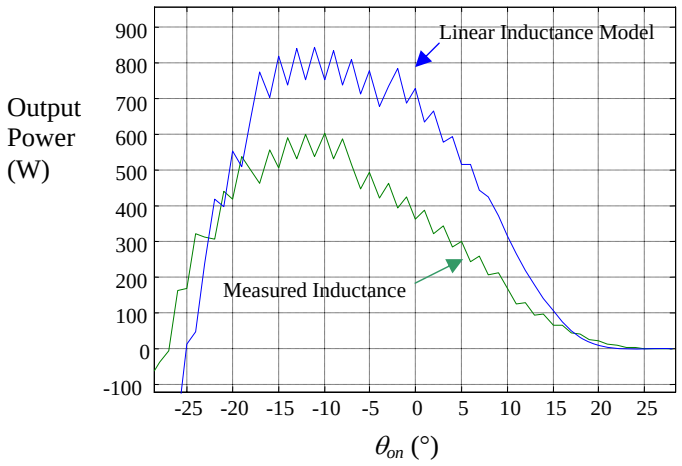

Fig. 41. The maximum output power versus turn-on angle for piecewise linear inductance and measured inductance models.

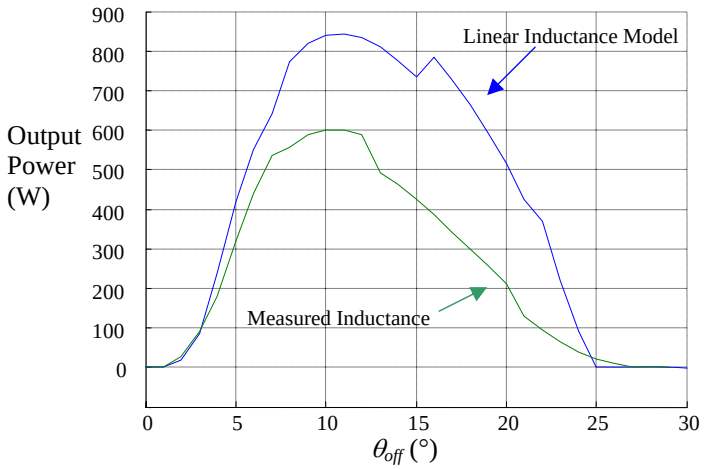

Fig. 42. The maximum output power versus turn-off angle for piecewise linear inductance and measured inductance models.

The maximum output power versus stator pole width (β_s) and rotor pole width (β_r) are shown in Figures 43 and 44, respectively. It can be concluded from these figures that by increasing the difference between the rotor pole width and the stator pole width the output power is decreasing, also there exists a stator pole size which gives the maximum output power. These values are close to the pole width of the existing 1-hp machine (β_s= 22.6°, β_r= 23.1°).

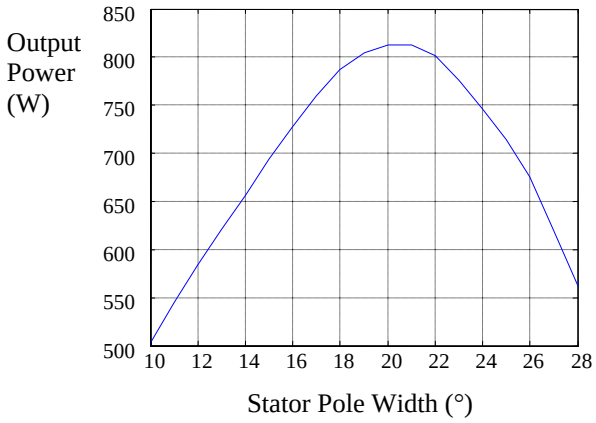

Fig. 43. The maximum output power versus stator pole width at the rated speed and dc-bus voltage $\beta_r = .5^\circ + \beta_s$, $10^\circ \le \beta_s \le 28^\circ$.

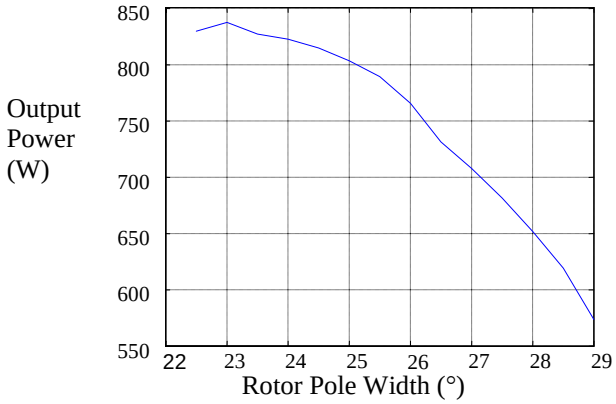

Fig. 44. The maximum output power versus rotor pole width at the rated speed and dc-bus voltage $\beta_s = 22.6^\circ$, $22.6^\circ \le \beta_r \le 29^\circ$.

D.1.5. The effect of phase resistance on the output power

Copper loss is a major component of losses in the SRG drive and it is a determining factor for the size of drive. Thus, it is always desired to be minimized. Furthermore, the phase resistance directly affects the phase current waveform and the output power of the SRG. Therefore, the effect of phase resistance on the output power of machine is carried out through some simulations on the 1-hp SRG model. The phase resistance on the existing SRG is 1.4 Ω. The simulation values are zero, 1.4 Ω, and 2.8 Ω. The phase current with these resistances at 120 V dc-bus with 2500 and 5000 r/min shaft speed has been depicted in Fig. 45. It can be observed that at high speed where the phase current is small, the voltage drop on the phase resistance is not comparable to the dc-bus voltage. Thus, its variation has less effect on the output power. The maximum output powers of these resistances at three shaft speed levels are compared in Fig. 46.

D.2. Iterative simulation with no limit on the phase current

In this part, we assume that there is no limit on the peak and rms values of the phase current. Based on this assumption, we investigate the maximum power on the range of design parameters and control variables. Although it may not be practical to run the generator at simulated values due to the excessive losses and mechanical stress in the machine, this analysis shows the inherent boundaries of the peaking power of the SRG. In many applications like regenerative breaking the peaking power can be a key factor in the selection of electric machine. Like the previous part, the analysis is carried out using different scenarios.

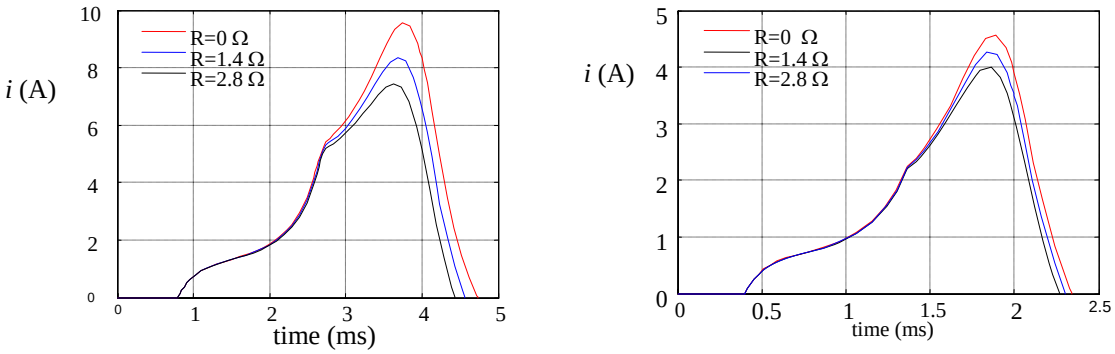

(a) Phase currents at 120 V and 2500 r/min.

(b) Phase currents at 120 V and 5000 r/min.

Fig. 45. Comparison of the phase current for three phase resistances.

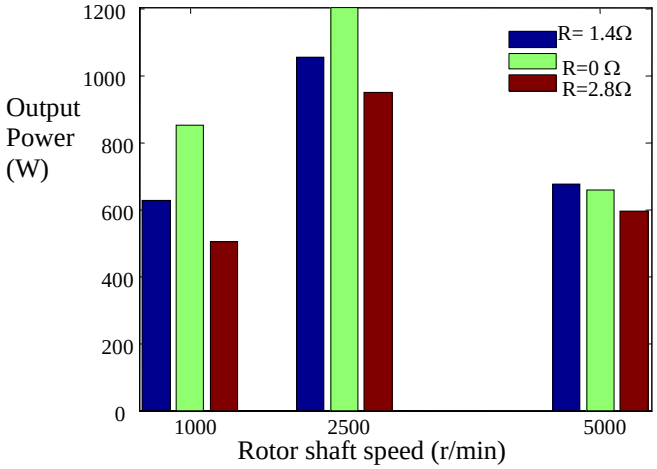

Fig. 46. Histogram of the output power.

D.2.1. Case I: $P_{out}= f(\theta_{on}, \theta_{off})$, ω, $V_s=$ *const.*, $L= L(i, \theta)$

In this case the only control variables are turn-on and turn-off angles and the rest of parameters are fixed at the rated values. Fig. 47 shows the variation of the output power for the range of turn-on and turn-off angles at 1000 r/min and 120 V. The maximum power is generated at θ_{on}= -15° and θ_{off}= 20° which gives 35° phase

magnetization interval. The variation of the rms value of the phase current on the range of turn-on and turn-off has been shown in Fig. 48.

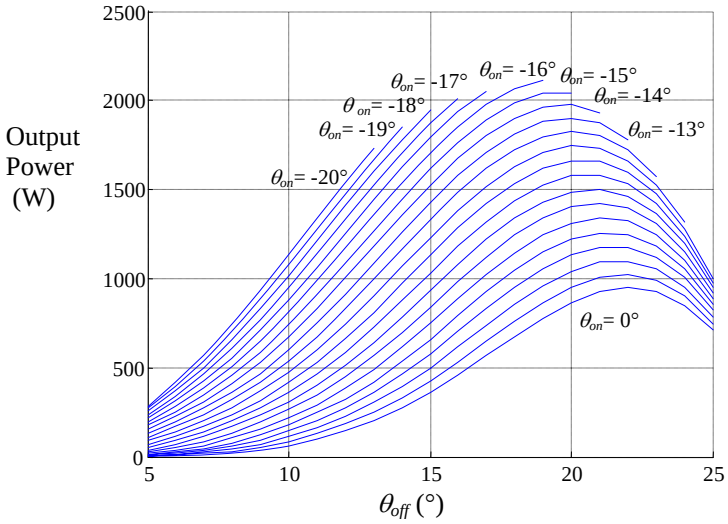

Fig. 47. The output power versus turn-on and turn-off angles at the rated output voltage and speed with no limit on the phase current.

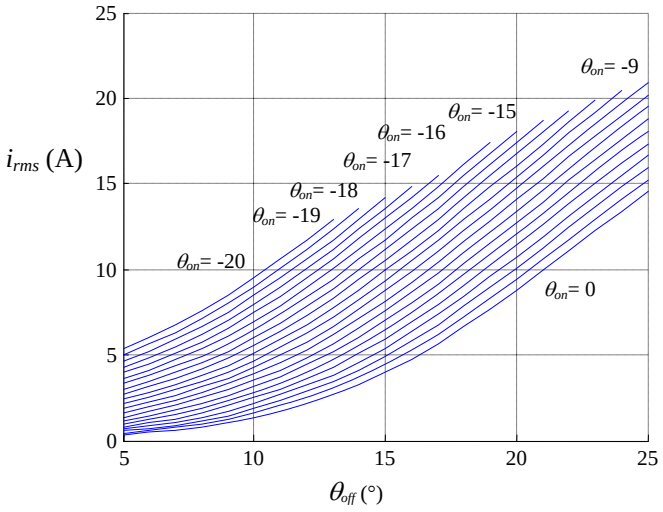

Fig. 48. The phase current rms-value versus turn-on and turn-off angles at the rated output voltage and speed with no limit on the phase current.

D.2.2. Case II: $P_{out}= f(\theta_{on}, \theta_{off}, \omega)$, $V_s=$ *const.*, $L= L(i, \theta)$

Compared to the previous case, shaft speed is added as another control variable. The output power and the rms value of the phase current for all possible turn-on and turn-off angles at each shaft speed are calculated and depicted in Figures 49 and 50. It is very remarkable that the maximum peak-power of the SRG and rms value of the phase current are monotonically decreasing with the shaft rotor speed.

D.2.3. Case III: $P_{out}= f(\theta_{on}, \theta_{off}, \omega, V_s)$, $L= L(i, \theta)$

Now the variation of the dc-bus voltage is included and the only fixed parameter is the phase inductance. The output power for all possible turn-on and turn-off angles at each shaft speed and dc-bus voltage is calculated and depicted in Fig. 51. It can be observed from Fig. 51 that the output power always increases with the dc-bus voltage. However, the slope of this increase is a function of the shaft speed.

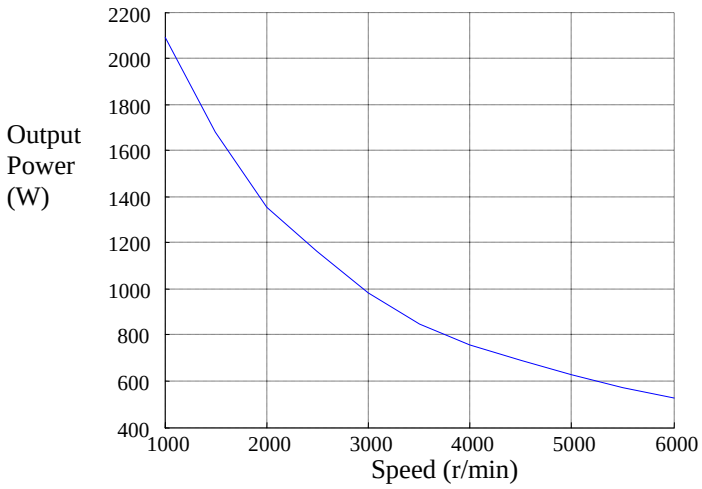

Fig. 49. The output power versus speed at 120 V dc-bus with no limit on the phase current.

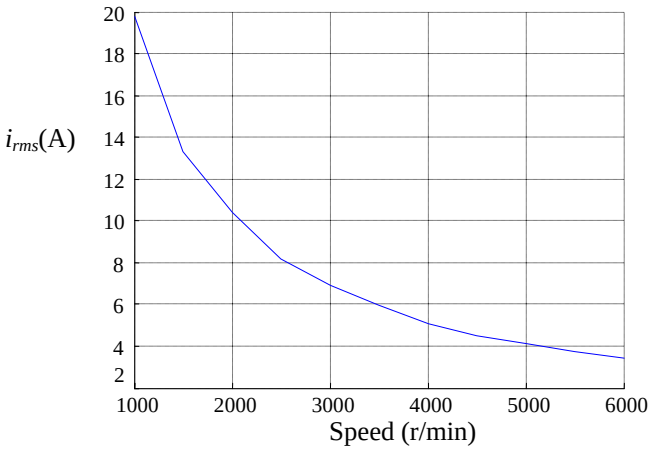

Fig. 50. The phase current rms-value versus speed at 120 V dc-bus with no limit on the phase current.

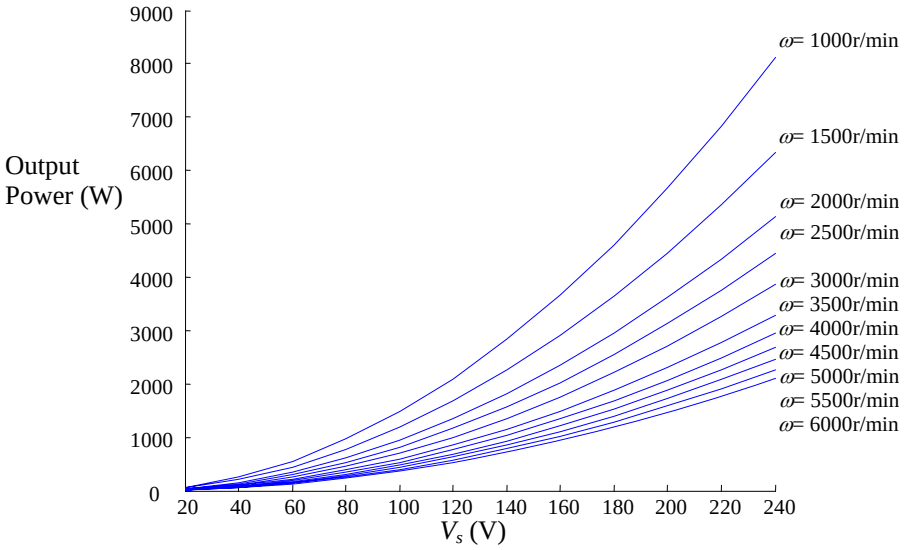

Fig. 51.The output power versus the dc-bus voltage at different shaft speeds.

E. Experimental Validation of the Simulation Results

For verifying simulation results, the output power has been measured on a test-bed in lab on the range of variations of dc-bus voltage, shaft speed, turn-on angle and

turn-off angle. The block diagram of the test-bed is shown in Fig. 52. Like simulation model, the SRG is an 8/6 1-hp machine with specification in Table II. A 2-hp permanent magnet brushed dc motor with the specifications listed in Table IV is used as prime mover. Its armature voltage is controlled with a PWM dc chopper.

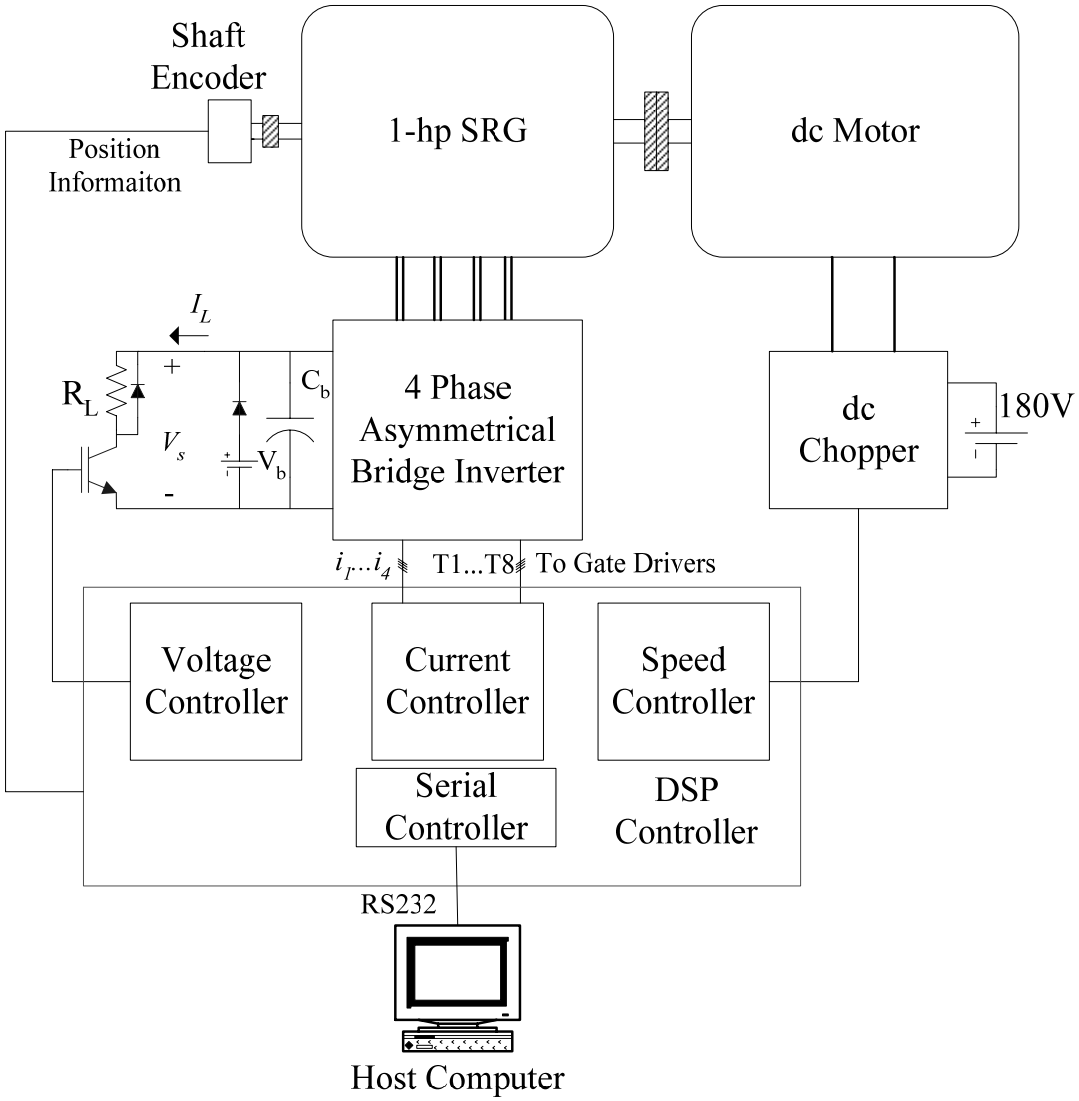

Fig. 52. Block diagram of the experimental test-bed.

Table IV. Name Plate Data of the Prime Mover

Type	Permanent Magnet Brushed dc
Voltage	180 V
Current	10 A
Rated Speed	2500 r/min

The load is a high power resistive load connected to the dc-bus voltage with a PWM dc chopper. A +24 V dc power supply is connected to the dc-bus by a diode. This power supply provides the initial magnetization current of the phases at start up. With the increase of dc-bus voltage above +24 volt, it will be disconnected automatically from the dc-bus and the capacitor on the dc-bus delivers current for the phase magnetization. The capacitor is 8800 μF which is big enough to filter current spikes on the bus. The converter is a four phase, two switches per phase, and asymmetric bridge converter as shown in Fig. 15. Shaft position information for commutation is obtained from a 3600 pulse per revolution incremental shaft encoder.

All of control and data acquisition algorithms have been implemented on a TI TMS320LF2812 DSP controller, which has 12 bit A/D and 150 MHz clock frequency. DSP is connected to a host computer via RS232 and receives desired dc-bus voltage, shaft speed, and commutation angles. Then, it calculates the shaft speed from shaft encoder pulses and a PI controller tunes the PWM command of the dc motor chopper to fix the speed at the desired value. The maximum speed has been limited to 3500 r/min for safe operation of the dc motor. Another PI controller sets the PWM command of load chopper to keep the dc-bus voltage at the desired value. The maximum dc-bus voltage is limited to 120 V for safety purposes. The output power of the SRG drive is calculated by

multiplying the average value of the current and voltage on the output terminal. The power electronic losses are reduced from the total output power of generator phases with this measurement method. Thus, it is expected to have some difference between the simulation and experimental results.

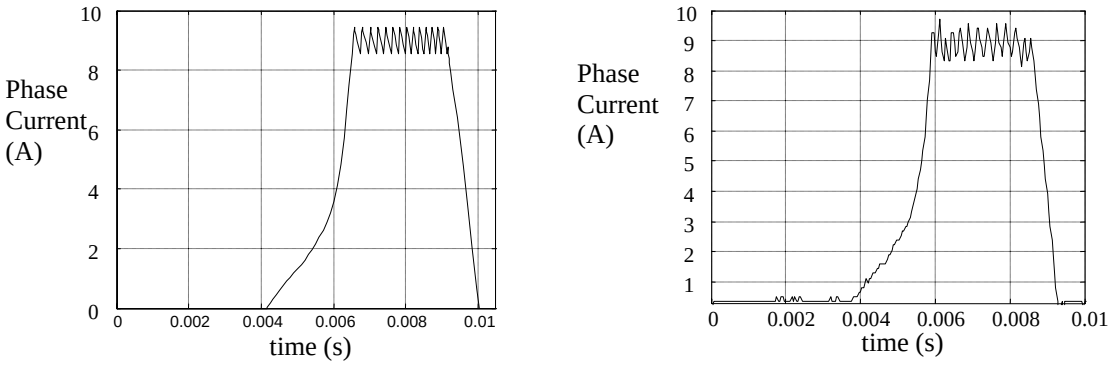

(a) Simulation result. (b) Experimental result.

Fig. 53. Phase current at 1000 r/min, 120 V dc-bus, 9 A flat-top current, turn-on angle -5°, and turn-off angle 25°.

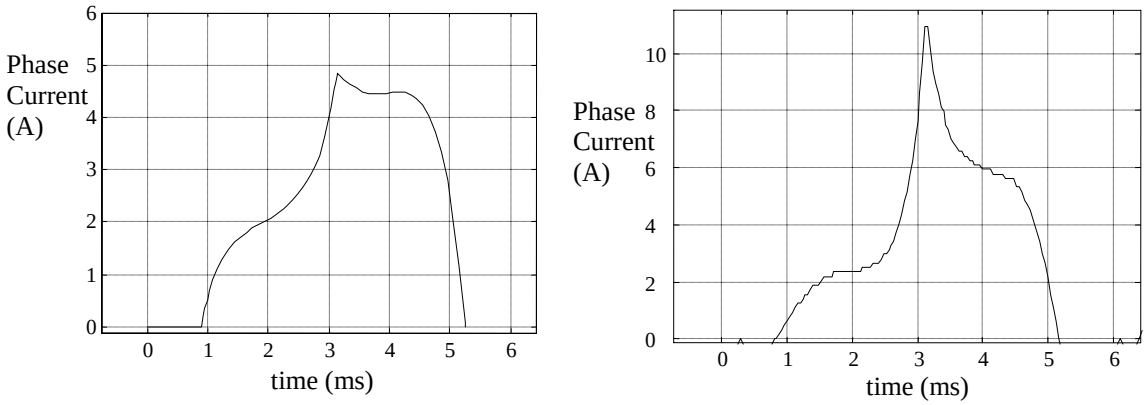

(a) Simulation result (b) Experimental result

Fig. 54. Phase current at 1850 r/min, 120 V dc-bus, turn-on angle -20°, and turn-off angle 5°.

Power measurements are performed iteratively over the ranges of turn-on angle, turn-off angle, shaft speed, and output voltage and transmitted to the host computer. A Matlab-based program logs and stores data for further processing. Experimental results show the same trend as the simulation results for the output power variation with respect to control variables. Phase current from the simulation and experimental results at 1000 r/min and 1850 r/min have been illustrated in Figures 53 and 54, respectively. The simulation and experimental results are matched at 1000 r/min. The experimental result at 1850 r/min shows a high spike of current compared to the simulation result. This fast current rise in the experimental result demonstrates the deep magnetic saturation of the core. This discrepancy arises from the fact that the inductance model (i.e., Equations (2.5) and (2.6)) was truncated at five terms. In order to match the simulation and experimental results additional terms should be added to the inductance model to match the simulation and experimental results at this region.

The variation of the output power versus turn-off angle for different values of turn-on angles from -19° to 18° is presented in Fig. 55. These data are measured at 2500 r/min rotor shaft speed and 120 V dc-bus. The graph shows the same trend as the simulation. The maximum turn-on and turn-off angles are located at -18° and 13°, respectively. The simulation and experimental results of the output power versus speed are compared at 120 V dc bus in Fig. 56. At each speed turn-on and turn-off angles are tuned to generate the maximum output power. A part of the difference between two curves is due to the power electronic losses that have not been included in simulation

results. These measurements have been repeated at other dc-bus voltages and illustrated in Fig. 57.

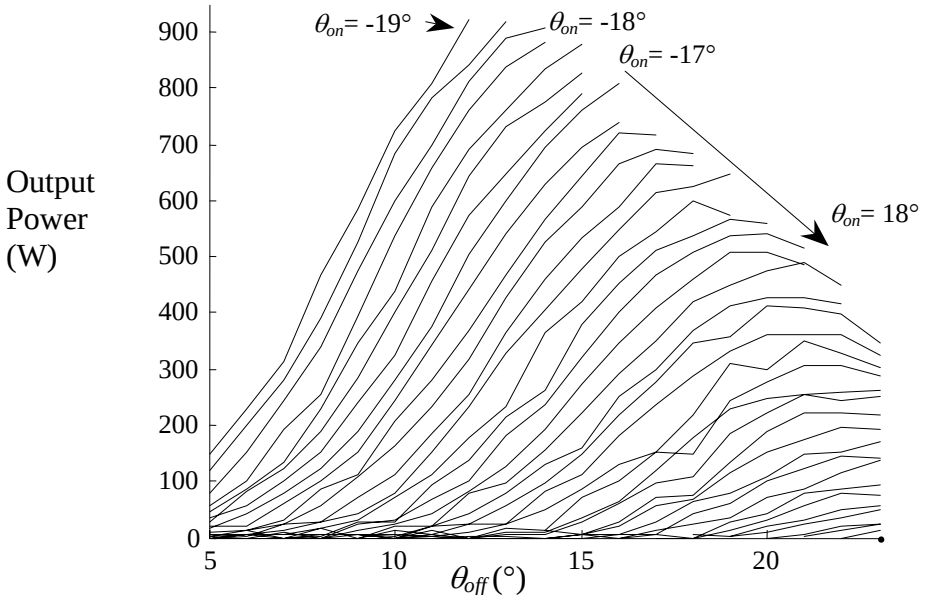

Fig. 55. The output power versus the turn-off and the turn-on angles at 120 V dc-bus and 2500 r/min.

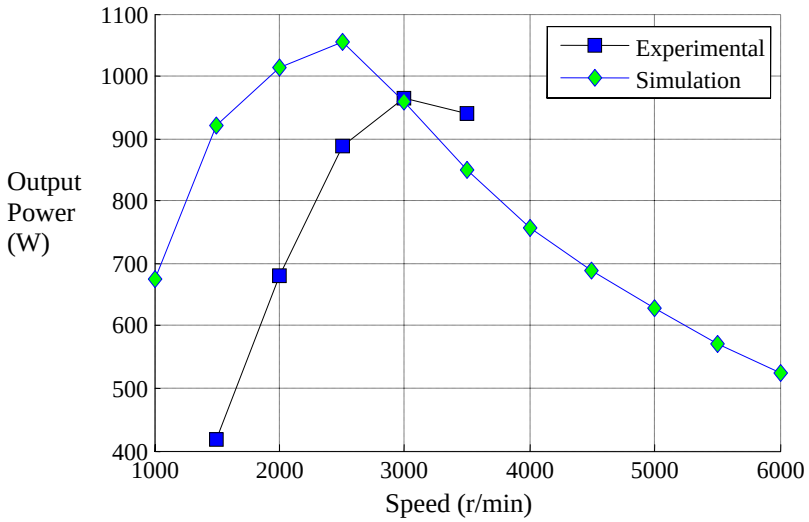

Fig. 56. The output power versus speed at 120 V dc-bus.

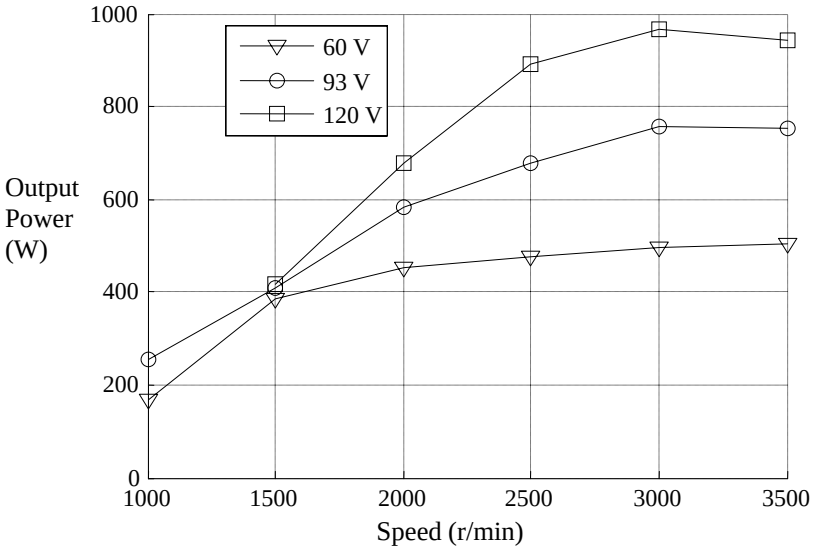

Fig. 57. The output power versus speed for 60 V, 93 V and 120 V on the dc-bus voltage.

F. Conclusion

The dc-bus voltage level, turn-on angle, turn-off angle, shaft speed and phase self-inductance have been identified as design parameters and control variables that affect the output power. Due to highly nonlinear characteristics of the SRG, there is no analytical solution for the output power in terms of design parameters and control variables. Thus, iterative simulation of the generator model on the range of design parameters and control variables is used as a technique for finding the output power profile. Because it involves a multidimensional search space with large number of iterations, theoretical knowledge about the generator and its practical limitations are used to narrow the search space and reduce simulation time. The output power profile of a 1-hp generator has been presented from simulation results. These results have been verified by experimental measurements on a test-bed in the lab.

The output power increases by increasing the dc-bus voltage, and its rate of change depends on the operating point of the SRG. At each dc-bus voltage level, there exists a shaft speed that generates the maximum output power. At any dc-bus voltage and shaft speed, there also exists a pair of turn-on and turn-off angles which maximizes the output power. The optimal turn-on angle is on the increasing slope of the phase self-inductance, and the optimal turn-off angle is on the decreasing slope of the phase self-inductance. The optimal values of rotor and stator pole width are obtained from the simulation.

The analysis and results of this chapter demonstrates the general characteristics of the SRG. The existence of a maximum output power in terms of design parameters and control variables has been proved. The results can be reference for design of any SRG and its controller.

CHAPTER IV

REAL-TIME CONTROL OF THE SRG DRIVE FOR OUTPUT POWER MAXIMIZATION

Once optimal design parameters have been selected, the controller should be able to select the optimal value for control variables. Control variables, depending on the application, can be any combination of switching angles, the dc-bus voltage, and/or the shaft speed. In low speed operation, flat-top phase current level can be added to the set of control variables. Among control variables, switching angles are always free to choose. However, the dc-bus voltage and shaft speed are determined based on the interaction of the load and the SRG, and the interaction of the prime mover and the SRG. So any controller should be designed at a system level with considering for all dynamics of the SRG drive, the prime mover, and the load. In this chapter, based on the simulation and experimental results that were presented in Chapter III, real-time control problem for output power maximization will be discussed and a self-tuning algorithm for on-line selection of control variables will be proposed. Also, a novel method for current ripple minimization on the output of the SRG drive will be presented.

A. Real-time Control of the SRG Drive for Maximum Output Power

Because the dynamics of the prime mover and the load are different from one application to another, there is no general solution to the control problem that can be

applied to the full range of applications. However, for most of the applications, the time constant of the load and prime mover are much longer than one period of electric excitation of the generator. For this reason, the output voltage and shaft speed of the generator can be assumed constant during one switching cycle. Thus, phase switching variables such as turn-on and turn-off angles can be separated from the dc-bus voltage and shaft speed controller. The dc-bus voltage controller and shaft speed controller should be designed at the system level, taking into account the dynamics of the prime mover and the load. The block diagram of the phase current controller is shown in Fig. 58.

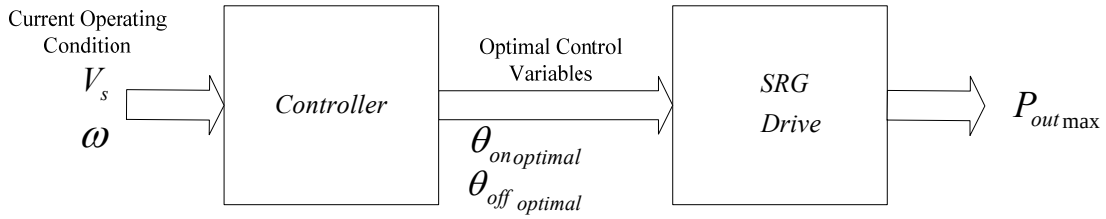

Fig. 58. Block diagram of the phase current controller.

As long as the values of dc-bus voltage and shaft speed are known, the controller doesn't need any information about the previous phase excitation. Therefore, the controller can be considered as a static controller with voltage and speed as inputs. Assuming the turn-on and the turn-off angles are the output parameters, the controller can be considered as a mapping from the voltage and the speed to the turn-on and the turn-off angles. Based on the simulation and experimental results, this mapping can be implemented as a look-up table, an artificial neural network, or any other types of

function approximation methods. For example, from the simulation results of the 1-hp machine in the previous chapter, optimal values of turn-on and turn-off variation versus shaft speed at 120 V dc bus voltage has been shown in Fig. 59.

It is very interesting to notice that the optimal turn-on angle does not change with the shaft speed, where as the turn-off angle increases linearly with the speed and stays almost constant above a certain speed. So it can be approximated with a piecewise linear curve. It should be noted that when the shaft speed is decreasing, the controller should switch to the chopping-mode. In the chopping-mode, control variables are the turn-on angle, the turn-off angle, and the flat-top level of the phase current. One can use the same procedure and select optimal control variables for output power maximization at this region of operation.

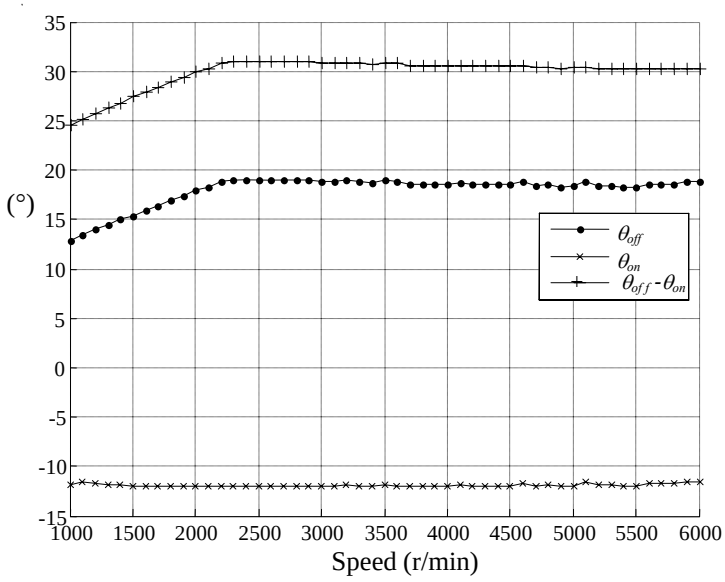

Fig. 59. Variation of optimal turn-on and turn-off angles with shaft speed at 120 V dc-bus voltage.

If the dc-bus voltage is changing, its variation should be taken into account. The variation of the turn-on and the turn-off angles versus the speed and the dc bus voltage are shown in Figures 60 and 61. Variation of the difference between turn-on and turn-off angles versus the speed and dc bus voltage is shown in Fig. 62. It is very remarkable to observe that the difference between the turn-off and the turn-on angles (θ_{off} - θ_{on}) results a smoother curve than the turn-on angle (θ_{on}) and the turn-off angle (θ_{off}) curves do. Accordingly, it is better to design the controller with (θ_{off} - θ_{on}) and either θ_{on} or θ_{off} as outputs.

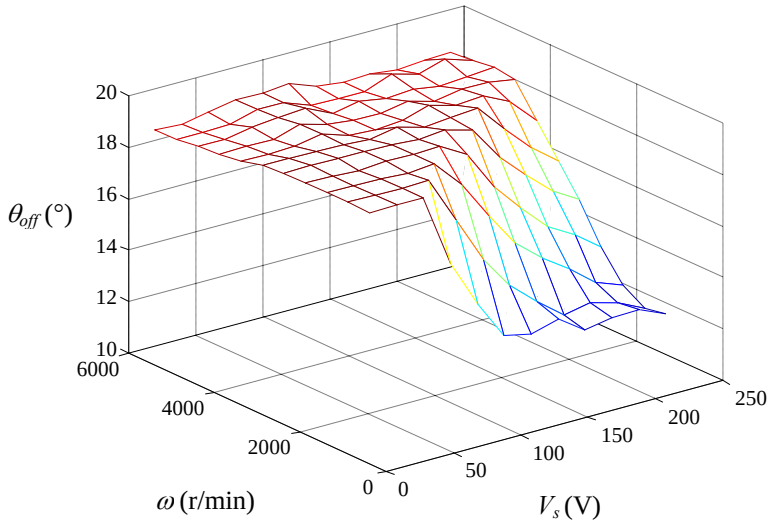

Fig. 60. Variation of the optimal turn-off angle versus the dc-bus voltage and speed.

B. Self-tuning Controller for Producing Maximum Output Power

In control theory, self-tuning is defined as the method of updating the control strategy in a control system. In the real world, the characteristics of a system and

environmental conditions are changing through time. The appealing feature of self-tuning controllers is that they automatically adjust themselves to these variations.

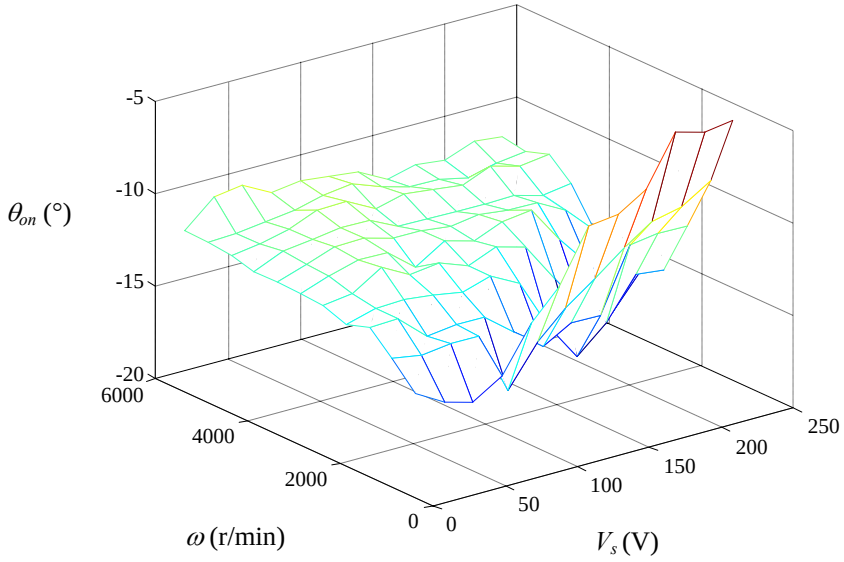

Fig. 61. Variation of the optimal turn-on angle versus the dc-bus voltage and speed.

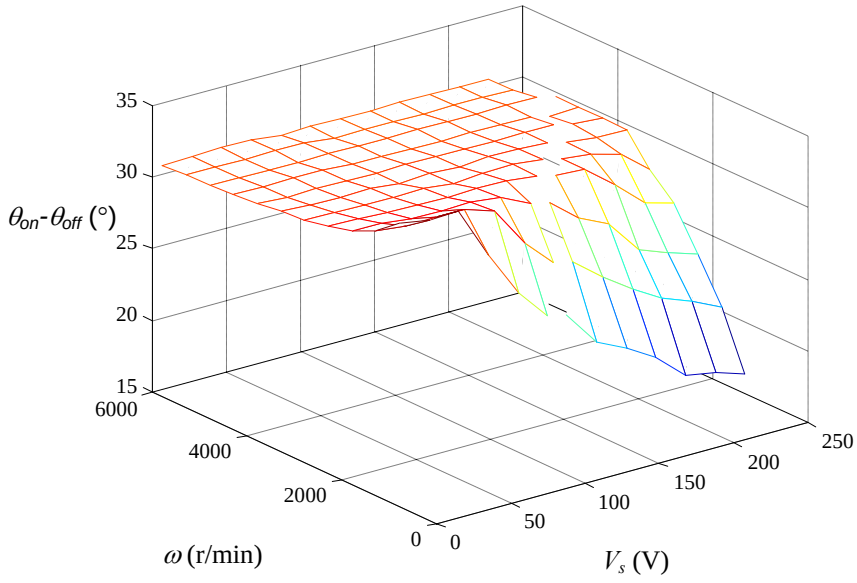

Fig. 62. Variation of the difference between the turn-off angle and the turn-on angle versus dc-bus voltage and shaft speed.

Finding the optimal turn-on and turn-off angles in the previous section relies on the exact knowledge of output power versus control variables at each operating mode, which depends on several machine parameters. The parameters deviate mainly because of mechanical and electrical variations in manufacturing, such as rotor eccentricity, bearing wear, winding partial failures, winding packing factor variations, temperature, etc. Moreover, due to the highly nonlinear characteristics of the machine, it is impossible to give an exact model for the variation of all of parameters that affect the output power. Therefore, self-tuning is inevitable in SRG drives especially in mass production, due to these unavoidable parameter deviations [40]. Block diagram of a self-tuning controller has been shown in Fig. 63. The current control loop has a fast dynamic compared to the load and the prime mover. Hence, a local search algorithm can be a very good candidate for this purpose.

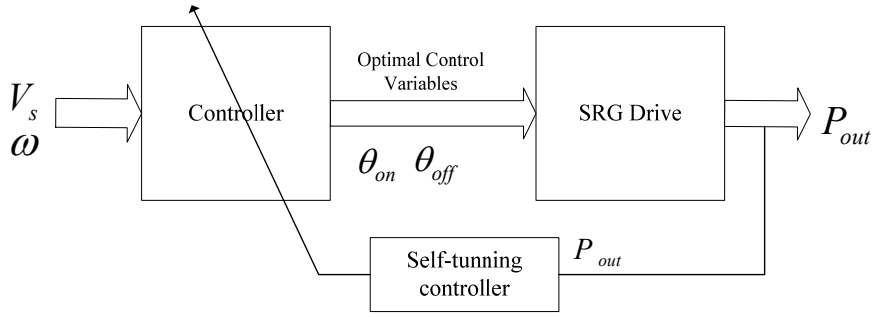

Fig. 63. Block diagram of the self-tuning controller.

It was proved in the previous chapter that there is a unique set of turn-on and turn-off angles that generates maximum power. Thus, one can use a search method to reach the maximum output power. For this search, turn-on angle (θ_{on}) is perturbed with a

small value; this value can be in the direction of either increasing or decreasing of θ_{on}, and then θ_{off} is perturbed until the maximum output power is found for this new value of θ_{on}. The new value of the output power is compared to the previous value of the output power and θ_{on} is perturbed again until the maximum output power is attained. The flowchart of this search algorithm is shown in Fig. 64.

The main controller of the SRG can call this algorithm whenever, the generator is operating under the steady state condition (i.e., constant shaft speed and dc bus voltage). One interesting feature of this controller is that it does not need any prior knowledge about machine parameters. Having initialized the controller with any arbitrary turn-on and turn-off angle, it will converge to the maximum output power.

Finding the optimal values of control variables for any arbitrary SRG requires extensive simulations and special hardware. However, by using this controller it is not necessary to go through all simulation and experiments. This novel technique saves a great amount of time and cost.

Turn-on angle, turn-off angle, and load current variations after running the self-tuning algorithm on the test-bed at 1500 r/min and 120 V dc-bus are shown Fig. 65. The initial values of the θ_{on}, θ_{off} are -15° and 13°, respectively. The average load current at this position is 1.86 A. The optimal value of θ_{on} and θ_{off} after running the search algorithm are -18° and 17°, respectively. The average load current at this position is 6.16 A, which is more than three times the initial value.

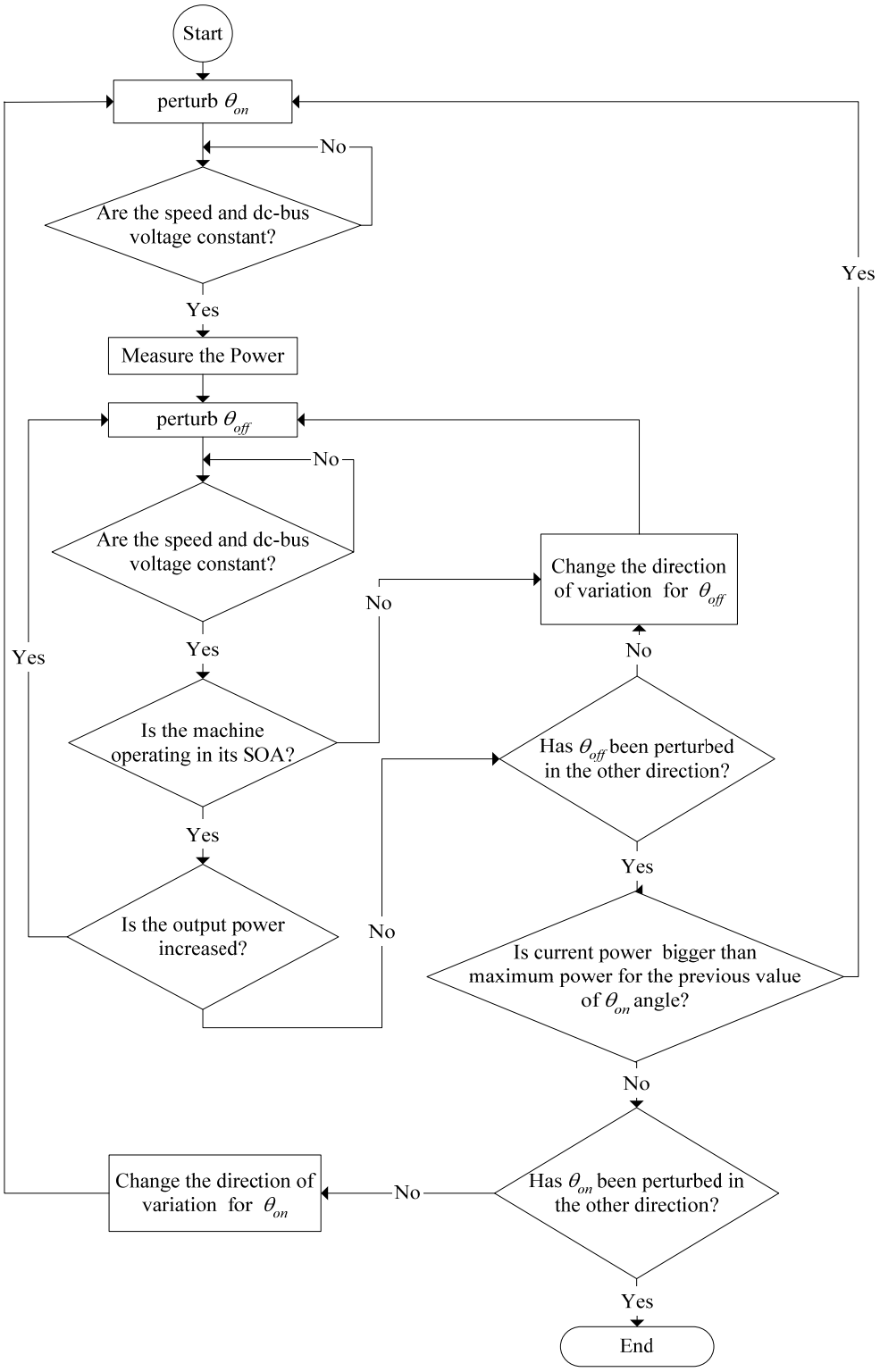

Fig. 64. Flowchart of the search algorithm.

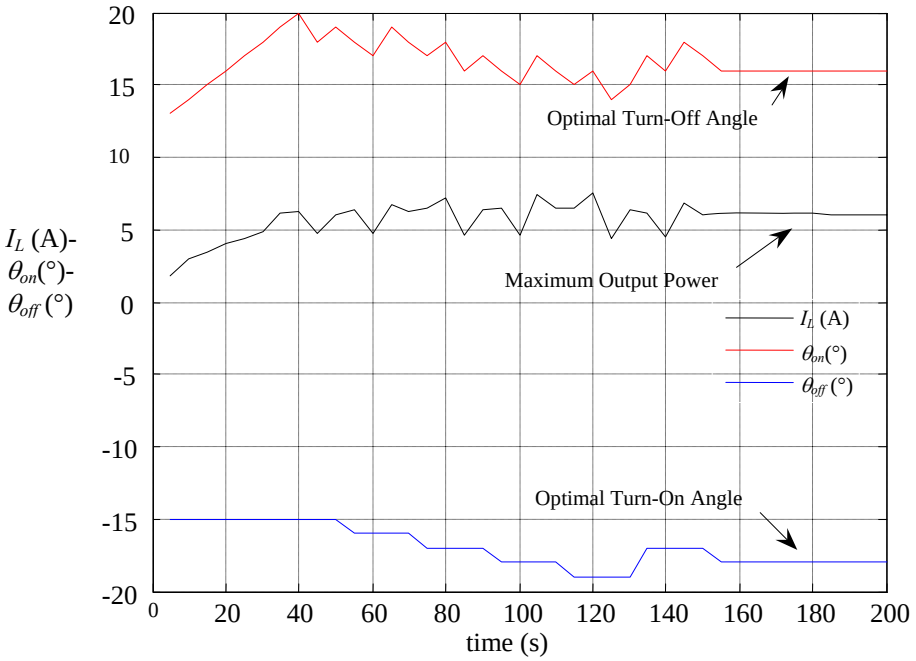

Fig. 65. Turn-on, turn-off, and load current variations after running the self-tuning algorithm.

In this method, it is assumed that all the phases are identical. For better results, one can define individual turn-on and turn-off angles for each phase and repeat the same procedure for each phase consequently to reach the maximum output power.

The step size for changing turn-on and turn-off angles should be selected carefully. If it is too big, the algorithm cannot converge to the maximum output power, and if it is too small, the measurement noise can be bigger than the power difference between two consecutive parameter perturbation and algorithm fails to finds the maximum output power. For the results on Fig. 65, a step size of 0.5° was selected. The algorithm was not able to find the maximum output power, if the step size was selected as 0.1°.

C. Output Current Ripple Mitigation of the SRG Drive

Maximizing the power density of generator drives should be considered on the system level rather than the optimization of components independently. The output filter can be very big and bulky in the SRG drive, due to the high output current ripple. In this section, by optimizing the control algorithm that was proposed in [38], the size of the output filter of the generator is minimized.

C.1 Sizing the capacitor filter on the dc-bus of the SRG converter

The simplified equivalent model of the SRG drive has been shown in Fig. 66, where i_o, i_C, and i_L represent output current of the SRG, capacitor current, and load current, respectively. The output current of the generator is the summation of the dc-bus current of each phase (i_{sj}).

$$i_o = \sum_{j=1}^{N_s} i_{sj} \tag{4.1}$$

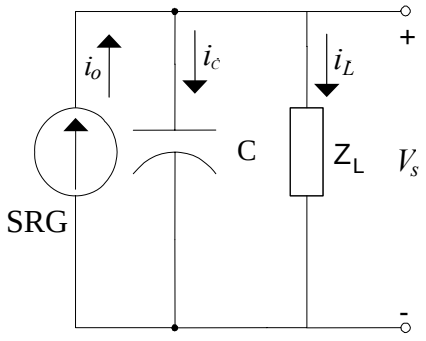

Fig. 66. A simple electric model of the SRG drive.

The dc-bus current of each phase is equal the phase current when the phase is magnetizing and it is equal the negative of the phase current when the phase is de-magnetizing. Thus, the output current of the generator depends on design parameters and control variables such as shaft speed, dc bus voltage, excitation pattern of the phases, number of phases, and the overlapping between phase currents. Output current of the generator and the phase current at 1000 r/min and 1800 r/min are measured and shown in Figures 67 and 68. Output current has a dc component which equals the load current (i_L) and an ac component which needs to be filtered inside the capacitor (i_C).

$$i_o = i_L + i_C \tag{4.2}$$

Neglecting the ESR of the capacitor, the size of the capacitor can be determined from maximum voltage ripple specification on the dc bus ($\Delta V_{\max}$) and the peak value of the integration of capacitor current ($\Delta Q_{m\max}$).

$$C = \Delta Q_{m\max} / \Delta V_{\max} \tag{4.3}$$

For the 1-hp SRG Drive with data in Figures 67 and 68, the minimum C will be 45 mF and 35 mF for the chopping and single pulse modes, respectively. These capacitor sizes are very big for a 1-hp drive with the existing capacitor technology. One way to reduce the capacitor size is reducing the current taken from the capacitor for the magnetization of the phases. A suitable index for comparison of methods that produce the same power is *Productivity*. It is defined as the ratio of the charge produced during de-magnetization of the phase (i.e., Fig. 16.c) to the charge used during magnetization of the phase (i.e., Fig. 16.a).

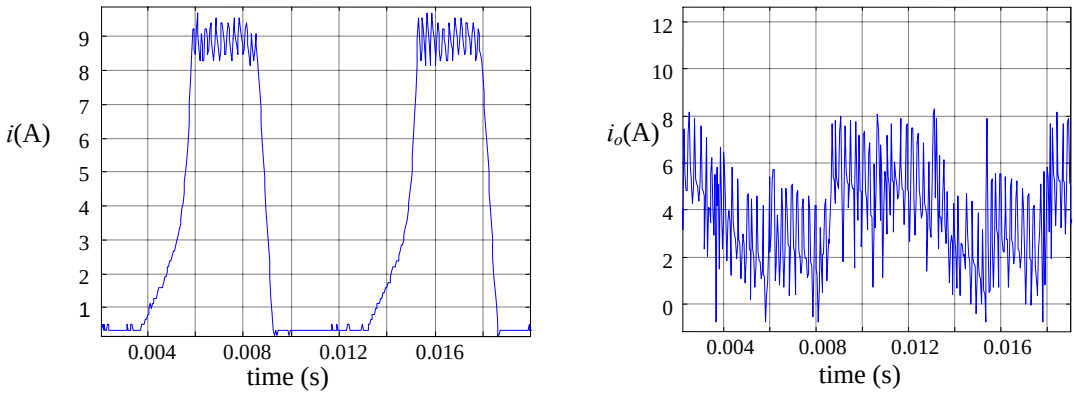

(a) Phase current. (b) Output current of the SRG drive.

Fig. 67. The phase and output current of the 1-hp SRG at 1000 r/min and 120 V (hard-chopping current control).

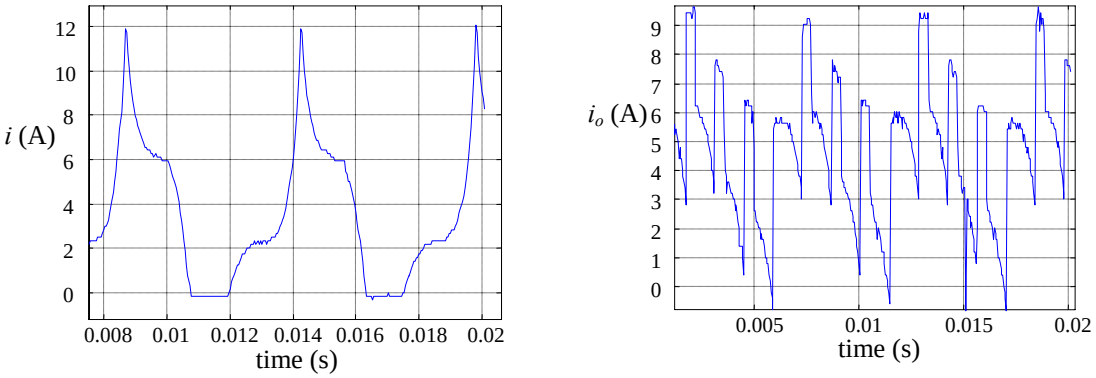

(a) Phase current. (b) Output current of the SRG drive.

Fig. 68. The phase and output current of the 1-hp SRG at 1800 r/min and 120 V.

$$\Gamma = \frac{Q_d}{Q_m},\ Q_m = \int_{T_m} idt,\ Q_d = \int_{T_d} idt \tag{4.4}$$

where Γ, Q_m, Q_d, T_m, and T_d are productivity ratio, magnetization charge, demagnetization charge, period of magnetization, and period of demagnetization,

respectively. Productivity of the generator at different operating points for maximum output power is shown in Figures 69 and 70.

C.2 Zero-voltage switching technique to enhance generation capability of the SRG

A current carrying phase on the decrementing inductance region will produce negative back EMF voltage, which is in the direction to increase the phase current. Thus, if one shorts the phase coil in this region, phase current increases without getting any charge from the source and the output power of the generator will be increased.

$$\ell \frac{di}{dt} + Ri = -e = -\frac{\partial L}{\partial \theta} \cdot i \cdot \omega \qquad (4.5)$$

Applying zero voltage to a phase can be easily accomplished in an asymmetric half bridge converter as shown in Fig. 71. In this mode, the upper switch (T1) is open and the current is flowing through the switch T2 and diode D1.

As discussed in Chapter III, if the ratio of the dc-bus voltage to the shaft speed is big enough, applying positive and negative dc-bus voltage will cause a flat-top phase current (Fig. 72.a). Using benefits of zero-voltage mode, applying zero and negative voltage can also keep the flat-top current shape (Fig. 72.b). This control will reduce the switching frequency of the converter, which will reduce switching losses of the converter and acoustic noise of the machine. For that reason the former current control method is usually called hard-chopping and the latter is called soft-chopping. Phase current and dc-bus current waveforms of a 1-hp SRG at 1000 r/min and 120 V, for hard-chopping and soft-chopping modes are shown in Figures 68 and 73, respectively.

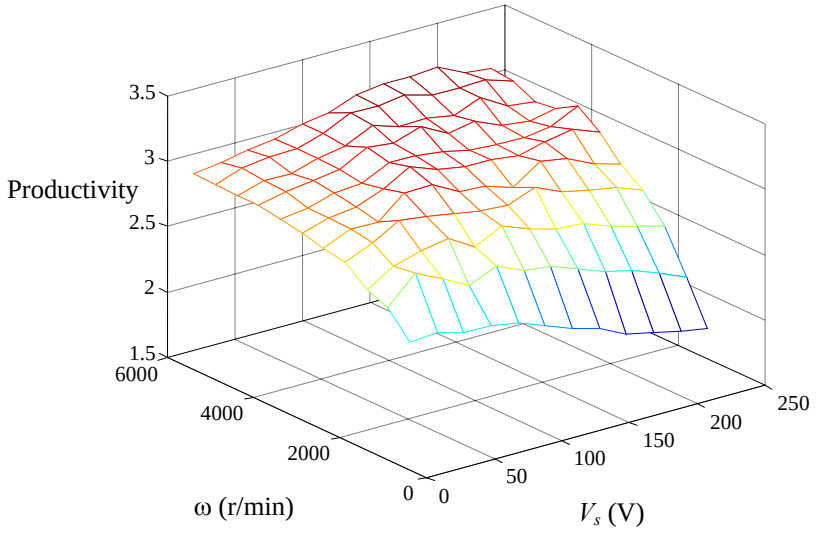

Fig. 69. Productivity of the 1-hp SRG versus speed and dc-bus voltage for the optimal turn-on and turn-off angles for maximum output power.

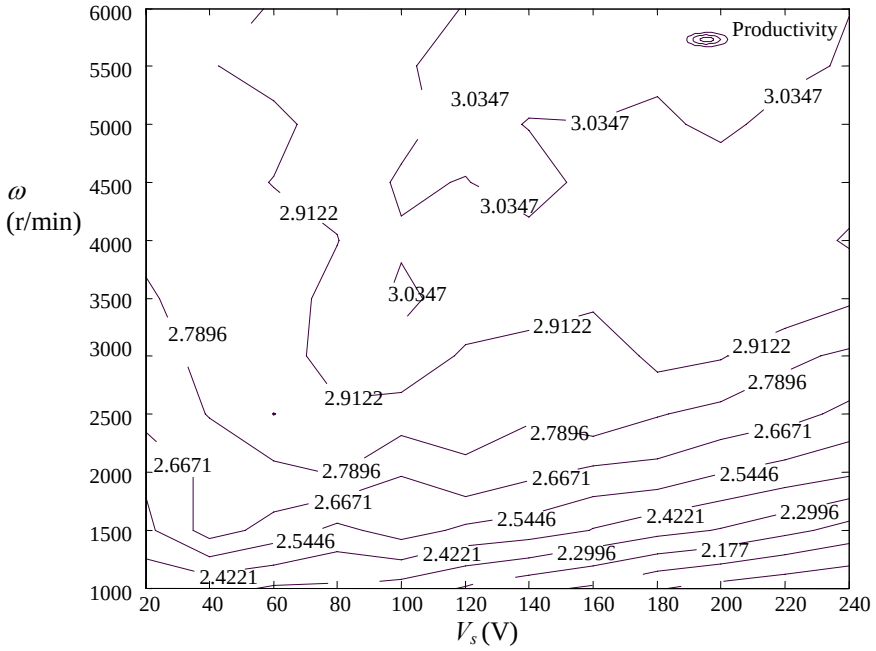

Fig. 70. Contour map of the productivity of the 1-hp SRG versus speed and dc-bus voltage for the optimal turn-on and turn-off angles for maximum output power.

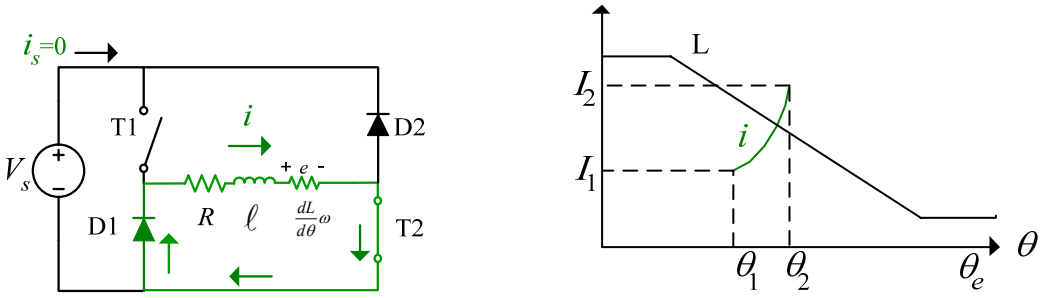

(a) Zero-voltage mode of operation. (b) Phase current in this mode.

Fig. 71. Phase current increases during zero-voltage period.

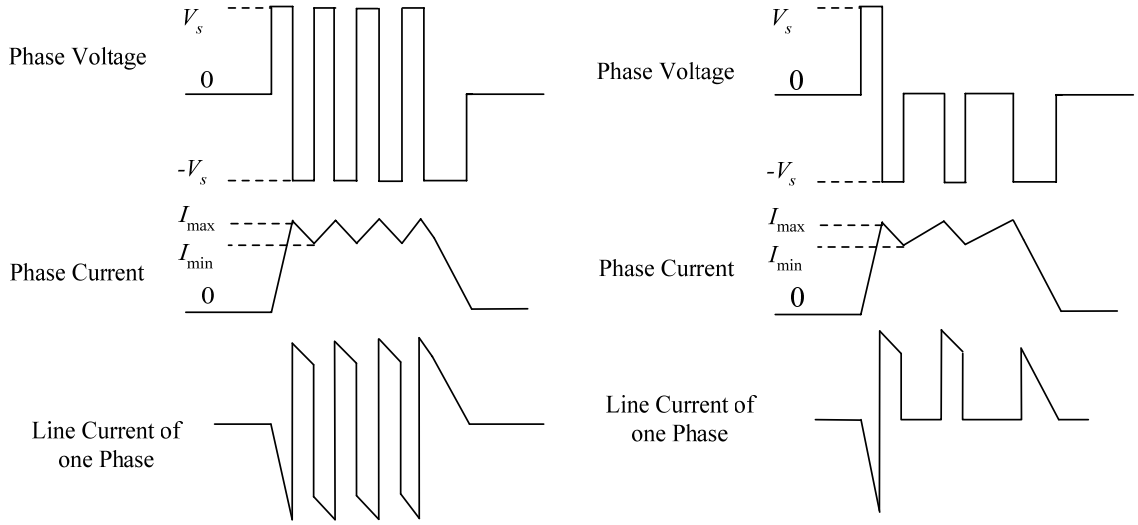

(a) Hard-chopping current control mode. (b) Soft-chopping current control mode.

Fig. 72. Comparison of the hard-chopping and the soft-chopping current control modes.

The current ripple is defined as

$$\% \, r = \frac{(i_o - I_L)_{rms}}{I_L} \cdot 100 \qquad (4.6)$$

Obviously, the smaller dc bus current ripple, the smaller capacitor size is. Implementing the soft-chopping control method instead of the hard-chopping control method, current ripple

is dropped from 58% to 43% at almost the same power level. For further analysis of the effectiveness of this method, soft-chopping and hard-chopping control algorithms are compared at different phase flat top current levels. These results are shown in Fig. 74. The data are measured at shaft speed of 1000 r/min, dc-bus voltage of 120 V, turn-on angle of 5°, and turn-off angle of 25°. It can be easily concluded from figures that by using soft-chopping method, one can achieve up to 25% reduction in dc bus current ripple compared to using hard-chopping method (Fig. 74.a), while the output power is almost at the same level (Fig. 74.b).

In one-step switching, the phase voltage is composed of just the turn-on (θ_{on}) and the turn-off (θ_{off}) angles (Fig. 75.a). Insertion of a zero-voltage period to one-step switching can reduce the current ripple. This switching method is referred as two-step switching against the one-step switching method. In this switching scheme that has been shown in

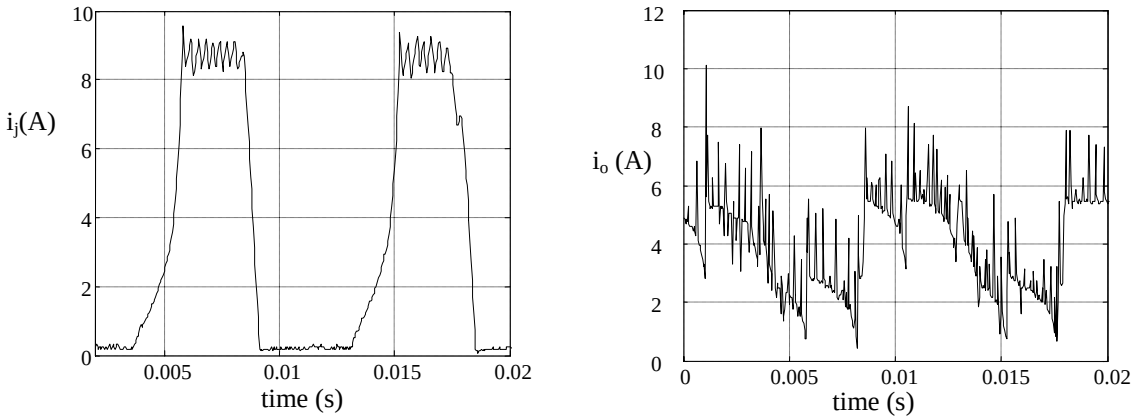

(a) Phase current (b) Output current of the SRG Drive

Fig. 73. The phase and output current of the 1-hp SRG at 1000 r/min and 120 V with the soft-chopping current control.

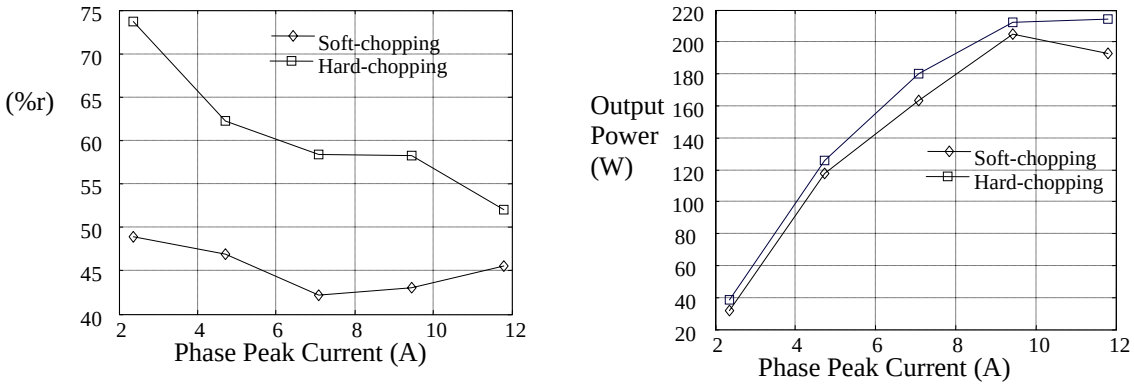

(a) dc-bus current ripple. (b) Output power.

Fig. 74. Comparison of the output power of hard-chopping and soft-chopping test results.

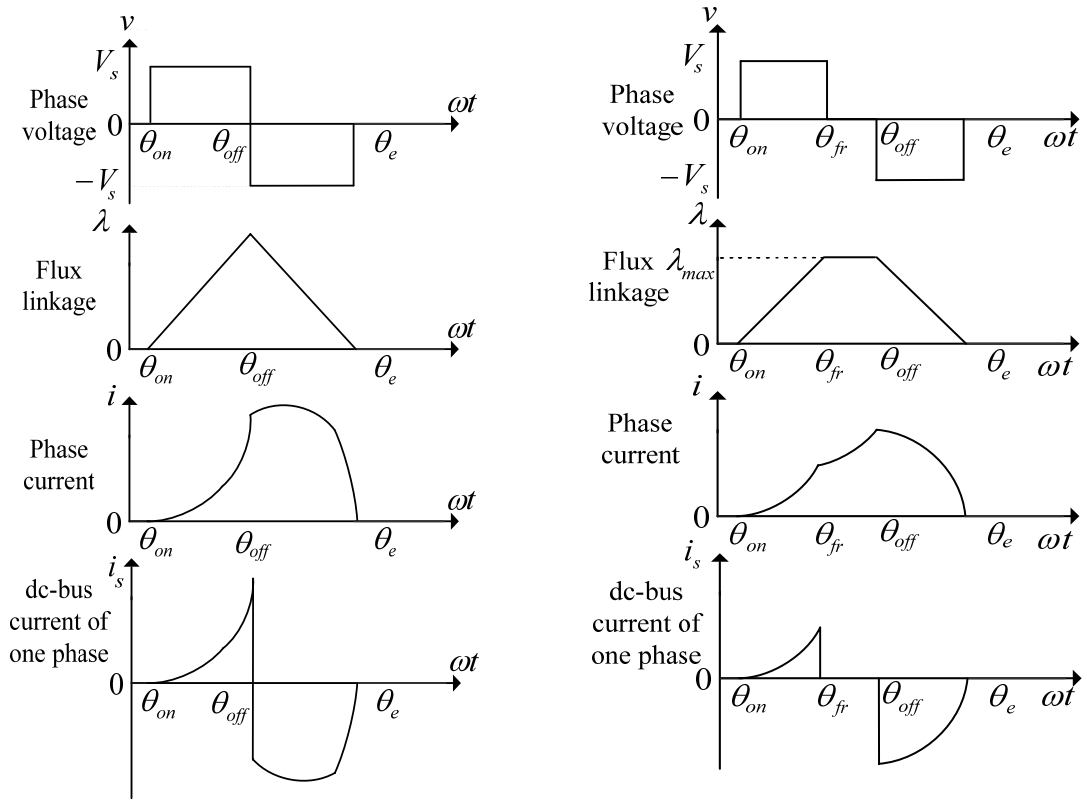

(a) One-step phase switching (b) Two-step phase switching

Fig. 75. Comparison of one-step and two-step phase switching.

Fig. 75.b, from θ_{on} to θ_{fr}, the positive bus voltage is applied to the phase coil and the phase coil sinks current from the dc bus. This current magnetizes the phase and builds up adequate back EMF voltage. From θ_{fr} to θ_{off}, zero voltage is applied to the phase and no current is drawn from the source. However, due to the back EMF voltage of the coil, the current continues to increase. From θ_{off} to θ_{e}, negative dc-bus voltage is applied and the phase coil sources the current to the dc-bus. The phase is demagnetized until the phase current reaches zero at θ_{e}.

This method has been experimentally implemented on the 1-hp SRG test-bed in the lab. The phase current and current of one of the capacitors on the dc-bus, with two-step switching algorithm has been shown in Fig. 76. Data are recorded at 1500 r/min shaft speed, 125 V dc-bus and turn-on angle of -10°, turn-off angle of 12°, and zero-voltage angle of 8°.

The reduction in ripple was experimentally verified. For a range of the zero-voltage angle (θ_{fr}) between 1° to 9°, dc-bus ripple was measured for the fixed turn-on and turn-off angles at -10° and 12°, respectively. Fig. 76 shows the results obtained from this study. It can also be noted from Fig. 77 that for a fixed θ_{on} and θ_{off}, by the variation of θ_{fr}, the ripple factor in the dc-bus can be mitigated. For the given set of conditions to obtain maximum output power, dc bus current ripple is the least for θ_{fr} of approximately 6° from aligned position. Fig. 78 shows the variation of the rms current through one of the phases versus θ_{fr} under the same conditions. Like one-step switching method, a self-tuning algorithm can used to find the optimal θ_{fr} for current ripple minimization.

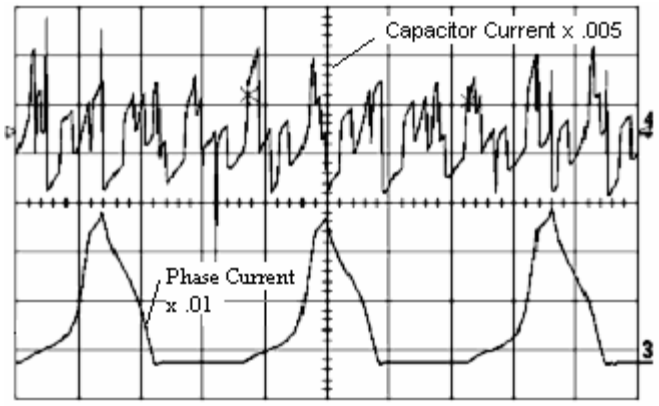

Fig. 76. Phase and capacitor currents on the dc-bus of the two-step switching scheme.

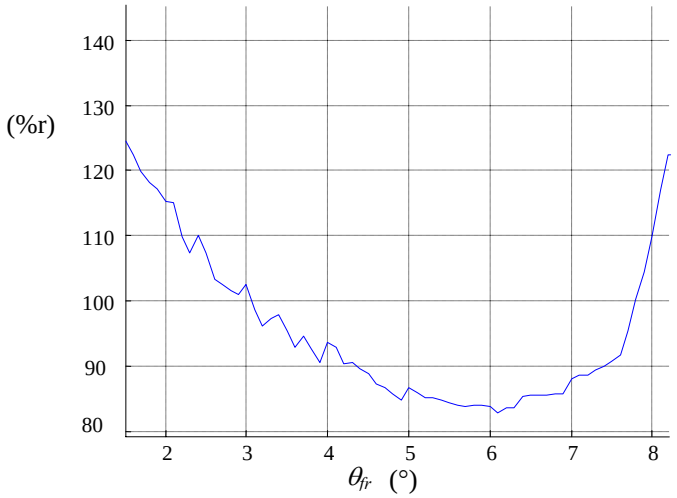

Fig. 77. Variation of the ripple factor with θ_{fr} for the proposed switching scheme.

In addition, Figures 79 and 80 demonstrate the variation of the average and rms values of the dc-bus current versus θ_{fr}. This study was further extended to evaluate the variation of output power of the system with respect to θ_{fr} as shown in Fig. 81. For performing this study, various combinations of θ_{on}, θ_{off} and θ_{fr} were tried and the output electric power was calculated for each combination.

One inherent feature of this switching scheme is that, comparing to one-step switching, for the same magnetization charge two-step switching algorithm produces much higher output power. This can be easily concluded from Fig. 82, where the area under the discharging current of the two-step switching is much bigger than the one-step switching method.

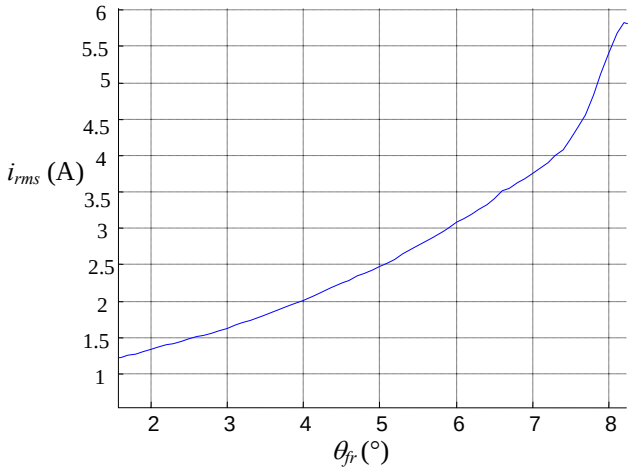

Fig. 78. The phase-current rms-value versus θ_{fr}.

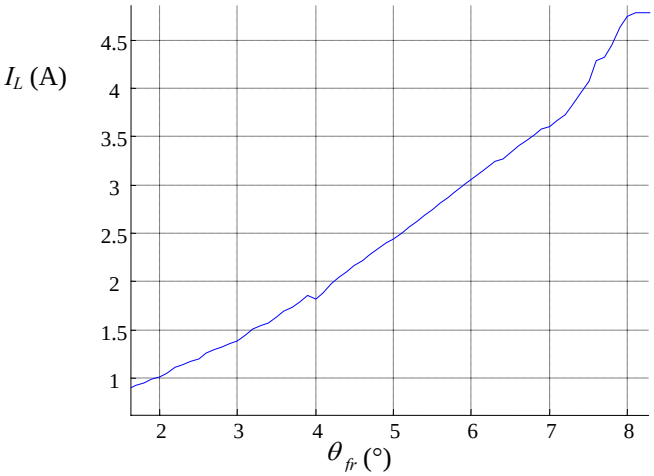

Fig. 79. Average of the dc-bus current versus θ_{fr}.

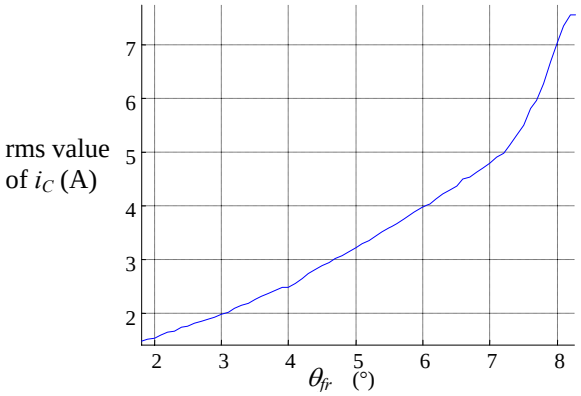

Fig. 80. The dc-bus current rms-value versus θ_{fr}.

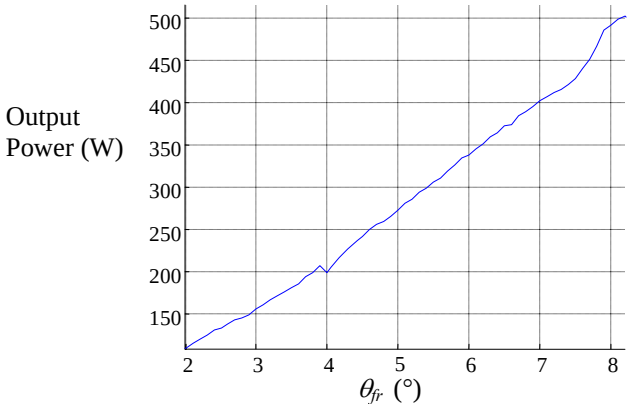

Fig. 81. The output power versus θ_{fr}.

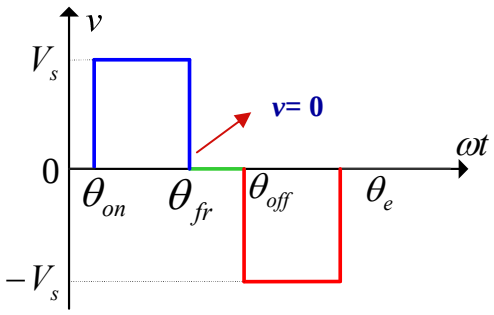

(a) Phase voltage

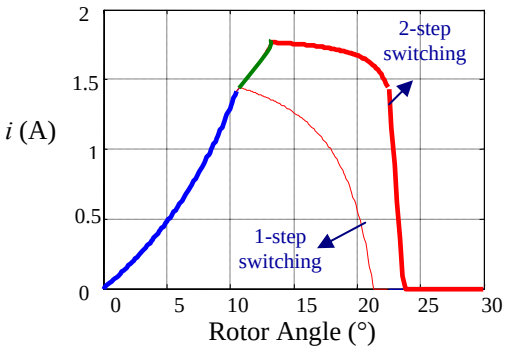

(b) Phase Current

Fig. 82. Comparison of the one-step and two-step phase switching schemes with the same magnetizing current.

D. Conclusion

Real-time control for output power maximization of the generator has been investigated in this chapter. It is essential to consider the characteristics of the prime mover and load for the design of the controller. Because dc-bus voltage changes and shaft speed variations are usually much slower than one electric cycle of the phase switching, the optimal switching angles at each speed and dc-bus voltage can be calculated from either the model of the drive or experimental measurements and stored as a look up table for output power maximization of the generator.

Optimal switching angles of the machine are dependent on the generator parameters. If the model parameters are not exactly matched with the machine parameters or the machine parameters change, the controller may not run the machine at its maximum output power. Therefore, a self-tuning algorithm based on a simple search method has been proposed. This algorithm has been verified and the results demonstrate the effect of this algorithm on reaching the maximum output power.

Maximizing the output power of the SRG drive, may lead to the over sizing of the power electronic converter and its output filter. The effect of switching algorithm on the output current ripple has been studied on this chapter. It has been suggested to apply zero voltage instead of dc-bus voltage for increasing the current on the decreasing slope of the inductor. Applying zero voltage on the phase current doesn’t sink any current from the source, thus it reduces the current ripple on the dc-bus voltage. However, it comes with the expense of loosing a slight fraction of the output power. This algorithm

has been experimentally verified in high-speed and low-speed and results have been analyzed in detail.

CHAPTER V

SUMMARY AND FUTURE RESEARCH

This chapter presents the summary of the work accomplished during the course of this research. Suggestions for the future research work in this area will also be presented.

A. Summary of the Work

In this dissertation, the output power maximization of the switched reluctance generator has been investigated which is the main objective of the design and control of stand alone generators for most of applications. Based on the principles of energy conversion of the machine, design parameters and control variables affecting output power have been identified and the optimal values of the design parameters and control variables that maximize the output power of the generator have been found through analytical approaches and iterative simulations. The results have been verified experimentally. The real-time controller for output power maximization of the generator has been designed. In addition, a novel algorithm for the self-tuning of the controller has been developed and verified with experimental results. The output power maximization can lead to an oversized power converter and output filter, which will reduce the overall power density of drive. Reducing the size of output filter on the dc-bus of converter with

active control of phase currents has been discussed and a novel control algorithm for current ripple minimization of the generator has been proposed and investigated through experiments.

Chapter I addresses briefly the current global status of electric power generation and requirements for electric generators. Then, state of the art of the switched reluctance generator has been presented and advantages and challenges in using the SRG drive for practical application have been discussed. Various publications in literature on application and design of the SRG have been reviewed in this chapter. Research objective and outline of dissertation is also presented.

Chapter II introduces the basics of the SRG drive. The mechanical structure, magnetic characteristic, and principles of power generation are described. The topology of the classic SRM drive converter, which is used in this work, is also presented. The mathematical model of the SRG drive is derived and the basic modes of operations of the SRG drive are also explained.

Chapter III describes the characteristics of the output power of the SRG for the range of design parameters and control variables. Based on principles of energy conversion in the SRG and its voltage terminal equation, design parameters and control variables affecting output power are identified. An analytical method based on the simplified model of the SRG has been used for finding output power in terms of design parameters and control variables. An iterative search method was proposed for finding the maximum output power in range of design parameters and control variables. Due to highly nonlinear characteristics, it is not possible to find a per-unit SRG drive in terms of

its parameters and control variables. Hence, a 1HP 8/6 SRG machine has been used as a case study, and its characteristics have been shown using the proposed iterative search method through simulation and experimental results. However, the results can be generalized as the trend of output power variation in terms of design parameters and control variables in other SRG drives.

In Chapter IV, the real-time control for output power maximization has been explained. For this controller, the optimal firing angles for phase commutation can be found from simulation results or experimental measurements. If the model parameters are not exactly matched with the machine parameters or the parameters of the machine change, the controller won't run the machine at its maximum output power. A self-tuning algorithm which is based on a simple search method has been proposed and the experimental results have been demonstrated. The effect of commutation algorithm on the output current ripple has been presented in this chapter. It has been suggested to apply zero voltage instead of the dc-bus voltage on the decreasing slope of the inductor, which reduces the size of converter and output filter of the SRG drive. This algorithm has been experimentally verified over all the speed range and results have been presented.

B. Contributions of the Research

This research focuses on how to achieve the maximum output power of the SRG for a given size (i.e.: power density maximization) through a systematic approach. It can

serve as a reference for design engineers across many applications. The major contributions of this dissertation can be summarized as follows:

- Having used a systematic approach, shaft speed, dc-bus voltage, switching angles, and phase inductance profile of the machine have been identified as the main design parameters and control variables affecting the output power of the switched reluctance generator.
- An analytical approach has been taken to find the effect of design parameter and control variables on the maximum output power of the generator.
- An iterative search algorithm has been proposed for finding the output power profile of the SRG for the range of design parameters and control variables.
- The iterative search algorithm has been implemented on the simulation model of the SRG and the effect of the following design parameters and control variables have been investigated:
    - ✓ The optimal turn on and turn off phase current commutation angles are obtained;
    - ✓ The effect of shaft speed and dc-bus voltage on the output power is investigated;
    - ✓ The effect of magnetic saturation of iron, inductance modeling, stator and rotor pole width is calculated;

- Simulation results are verified with measurement on the experimental test bed. Using iterative search algorithm, output power on the range of switching angles, shaft speed and dc-bus voltage was measured and compared to simulation results.
- A real-time controller for output power maximization of the switched reluctance machine has been proposed.
- A novel self-tuning algorithm for output power maximization of the generator has been proposed. The advantages of this method are:
    - ✓ The proposed method does not need any information about the machine parameters;
    - ✓ It has high reliability at all operating points;
    - ✓ The proposed self-tuning method requires no additional hardware or huge memory space for implementation;
    - ✓ It can be easily implemented on low cost fixed-point digital signal processors or microcontrollers;
    - ✓ It can be applied to variety of generators with different power ratings and configurations;
    - ✓ The self-tuning method can be generalized for optimization of other objectives such as efficiency or productivity. However, the objective(s) should have only one global optimum on the range of control variables;

- The effect of output power maximization on the dc-bus current ripple has been illustrated and a novel phase switching algorithm for dc-bus current ripple minimization has been proposed. This method has the following benefits:
  - ✓ The proposed control algorithm requires no additional power electronics or hardware;
  - ✓ It is computationally very simple and can be easily implemented on low cost microcontrollers, fixed point digital signal controller, or even ASICs;
  - ✓ It can be easily implemented over all the operating points;
  - ✓ The optimal commutation angles for dc-bus current minimization can be found using self-tuning search method;

C. Future Research Work

This research has defined output power maximization as a key element for utilizing the SRG for more applications. Thus, design parameters and control variables affecting output power of the SRG has been clearly defined, and output power maximization of the SRG drive through design and control has been investigated in details. However, there are certain areas that would require further research for using SRG for more applications.

- In this research the effect of machine geometry on the output power was investigated. This research was limited to the stator and the rotor pole width and can be further extended to the effect of other parameters such as the thickness of the stator or the rotor back iron, the length of air gap, and the iron saturation level.
- The optimal design parameters of the machine such as stator and rotor pole width that was obtained in this research provide a good starting point for designing the machine. However, it is suggested to verify the results with Finite Element Analysis.
- The effect of design parameters and control variables on Power Electronic Converter losses and Iron losses can be investigated.
- The characteristics of the prime mover and load can greatly impact the output power maximization of the generator. Depending on the application, output power maximization should be achieved by considering the overall performance of the system.
- For many applications, there can be other design or control objectives of great concerns as well, such as efficiency or torque ripple minimization the shaft. Trade off between output power maximization and other control objectives should be studied. Moreover, if the load cannot absorb all the converted electric power from the generator, the controller should be able to run based on these control objectives.

- The SRG needs position information with high accuracy for output power maximization. Position sensors are usually fragile and expensive, so developing a position sensorless algorithm is essential for running the SRG drive with maximum output power.

REFERENCES

[1] S. R. MacMinn and J. W. Sember, “Control of a switched-reluctance aircraft starter-generator over a very wide speed range,” in *Proc. Intersociety Energy Conv. Eng. Conf.*, 1989, pp. 631–638.

[2] S. R. MacMinn and W. D. Jones, “A very high speed switched-reluctance starter-generator for aircraft engine applications,” in *Proc. NAECON’89*, May 1989, pp. 1758–1764.

[3] C. A. Ferreira, S. R. Jones, W. S. Heglund, and W. D. Jones, “Detailed design of a 30-kW switched reluctance starter/generator system for a gas turbine engine application,” *IEEE Trans. Ind. Appl.*, vol. 31, pp. 553–561, May/June 1995.

[4] E. Richter and C. A. Ferreira, “Performance evaluation of a 250 kW switched reluctance starter generator,” in *Conf. Rec. IEEE-IAS Ann. Meeting*, 1995, pp. 434–440.

[5] A. V. Radun, C. A. Ferreira, and E. Richter, “Two-channel switched reluctance starter/generator results,” *IEEE Trans. Ind. Appl.*, vol. 34, pp. 1026–1034, Sept./Oct. 1998.

[6] M. A. Mueller, “Design of low speed switched reluctance machines for wind energy converters,” in *Conf. Proc. IEMD’99*, Sept. 1999, pp. 60– 64.

[7] R. Cardenas, W. F. Ray, and G. M. Asher, “Switched reluctance generators for wind energy applications,” in *Proc. IEEE-PESC’95*, 1995, pp. 559–564.

[8] H. Gao, Y. Gao, and M. Ehsani, “Design issues of the switched reluctance motor drive for propulsion and regenerative braking in EV and HEV,” presented at SAE Future Transportation Technology Conf.’01, Costa Mesa, CA, Aug. 2001.

[9] B. Fahimi, “A switched reluctance machine based starter/generator for more electric cars,” in *Conf. Proc. IEMDC’01*, 2001, pp.73– 78.

[10] B. Fahimi, A. Emadi, and R. B. Jr. Sepe, “A switched reluctance machine-based starter/alternator for more electric cars,” *IEEE Trans. Energy Convers.*, vol. 19, pp.116–124, Mar. 2004.

[11] J. M. Miller, A. R. Gale, P. J. McCleer, F. Leonardi, and J. H. Lang, “Starter-alternator for hybrid electric vehicle: Comparison of induction and variable

reluctance machines and drives," in *Conf. Rec. IEEE-IAS Ann. Meeting*, Oct. 1998, vol. 1, pp. 513-523.

[12] Energy Information Administration. (2005, July). International Energy Outlook 2005. U.S. DOE, Washington, DC [Online]. Available: http://www.eia.doe.gov/ieo/index.html

[13] Energy Information Administration. (2004, Mar.). International Energy Annual 2002. U.S. DOE, Washington, DC [Online]. Available: http://www.eia.doe.gov/iea

[14] J. C. Dunkerley, "The role of renewables in the future of electric power generation," presented at the 22nd meeting of the United States-Japan Energy Policy Dialogue, Keidanren Guest House, Japan, Nov. 1998.

[15] T. Gale. (2006). Motors and Generators. Gale Group, Farmington Hills, MI. [Online]. Available: http://galenet.galegroup.com/servlet/BCRC

[16] I. Boldea, "Control of electric generators: A review," in *Proc. IECON'03*, Nov. 2003, pp. 972-980.

[17] A. Emadi, *Handbook of Automotive Power Electronics and Motor Drives*. Boca Raton, FL: CRC Press, 2005, p. 566.

[18] J. M. Miller**, "**Multiple voltage electrical power distribution system for automotive applications," in *Proc. IECEC'96*, Aug. 1996, pp. 1930-1937.

[19] J. M. Miller, *Propulsion Systems for Hybrid Vehicles*. London: The Institution of Electrical Engineers, 2004, pp. 11-12.

[20] T. J. E. Miller, *Switched Reluctance Motors and Their Control*. London: Clarendon Press, 1993, pp. 25-53.

[21] T. J. E. Miller, "Optimal design of switched reluctance motors," *IEEE Trans. Ind. Electron.*, vol. 49, pp. 15 – 27, Feb. 2002.

[22] K. M. Rahman, and S. E. Schulz, **"**Design of high efficiency and high density switched reluctance motor for vehicle propulsion," in *Conf. Rec. IEEE-IAS Annu. Meeting*, Oct. 2001, pp. 2104-2110.

[23] T. J. E. Miller, *Electronic Control of Switched Reluctance Machines*. Boston: Newnes, 2001, pp. 228- 234.

[24] D. A. Torrey, “Switched reluctance generators and their control,” *IEEE Trans. Ind. Electron.*, vol. 49, pp. 3 – 14, Feb. 2002.

[25] A. Radun, “Generating with the switched-reluctance motor,” in *Proc. APEC’94*, 1994, pp. 41–47.

[26] M. Ehsani and B. Fahimi, “Control of switched reluctance generators,” U.S. Patent Pending, Feb. 10, 2002.

[27] M. J. Turner, “Starting of switched reluctance generators,” U.S. Patent 6906490, Jun. 14, 2005.

[28] A. V. Radun, D. W. Jones, and T. M. Jahns, “Switched reluctance generator system with fault recovery capability,” U.S. Patent 5289107, Feb. 22, 1994.

[29] W. S. Heglund, “Output overload and fault tolerant commutation method for a switched reluctance generator and an electric power generating system employing same”, U.S. Patent 5850133, Dec. 15, 1998.

[30] A. V. Radun and Y. Q. Xiang, “Switched reluctance starter/generator system modeling results,” *SAE Tech. Papers*, Doc. 951407.

[31] O. Ichinokura, T. Kikuchi, K. Nakamura, T. Watanabe, and H. Guo, “Dynamic simulation model of switched reluctance generator,” *IEEE Trans. Magn.*, vol. 39, pp. 3253–3255, Sept. 2003.

[32] C. A. Ferreira, S. R. Jones, and W. S. Heglund, “Performance evaluation of a switched reluctance starter/generator system under constant power and capacitive type loads,” in *Proc. APEC '95*, Mar. 1995, pp. 416 – 424.

[33] G. Gallegos-Lopez, K. Rajashekara, and F. J. Reiter, “300-kW switched reluctance generator for hybrid vehicle applications,” *SAE Tech. Papers*, Doc. 2002-01-1087.

[34] I. Husain, A. Radun, and J. Nairus, “Fault analysis and excitation requirements for switched reluctance-generators,” *IEEE Trans. Energy Convers.*, vol. 17, pp. 67–72, Mar. 2002.

[35] T. Sawata, P. Kjaer, C. Cossar, T. J. E. Miller, and Y. Hayashi, “Fault-tolerant operation of single-phase switched reluctance generators,” in *Proc. APEC'97*, Feb. 1997, pp. 553–558.

[36] Y. Sozer and D. A. Torrey, “Closed loop control of excitation parameters for high speed switched-reluctance generators,” *IEEE Trans. Power Electron.*, vol. 19, pp. 355–362, Mar. 2004.

[37] E. Mese, Y. Sozer, J. M. Kokernak, and D. A. Torrey, “Optimal excitation of a high speed switched reluctance generator,” in *Proc. APEC’00*, Feb. 2000, pp. 362 – 368.

[38] S. Dixon and B. Fahimi, “Enhancement of output electric power in switched reluctance generators,” in *Proc. IEMDC'03*, Jun. 2003, pp. 849–856.

[39] G. Suresh, B. Fahimi, K. M. Rahman, and M. Ehsani, “Inductance based position encoding for sensorless SRM drives,” in *Proc. IEEE PESC’99*, 1999, pp. 832-837.

[40] P. Tandon, A. Velayutham Rajarathnam, and M. Ehsani, **“**Self-tuning control of a switched-reluctance motor drive with shaft position sensor,**”** *IEEE Trans. Ind. Appl.*, vol. 33, pp. 1002–1010, Jul./Aug. 1997.

[41] H. Gao, “Sensorless control of the switched reluctance motor drive at standstill and near-zero speed,” Ph.D. Dissertation, Texas A&M University, Dec. 2001.

APPENDIX A

DESCRIPTION OF THE EXPERIMENTAL SETUP

The following are the name plate details of the experimental SRG and the prime mover.

Table A-1. Name plate data of the tested SRG

Power	1 hp
Voltage	120 V
Current	6 A
Base speed	1000 r/min
Number of phases	4
Pole configuration	8/6

Table A-2. Name plate data of the prime mover

Type	Brushed dc
Voltage	180 V
Current	10 A
Rated speed	2500 r/min

APPENDIX B

PARAMETERS OF THE EXPERIMENTAL SRG

Table B-1. Parameters of the tested SRG

Parameter	Value
Stator Outer Diameter	134.56 mm
Stator Inner Diameter	70.21 mm
Rotor Diameter	69.60 mm
Stack Length	80 mm
Stator arc	22.660° (mech)
Rotor arc	23.160° (mech)
Air gap length	0.3 mm
Shaft diameter	13.0 mm
Stator back iron	9 mm
Rotor back iron	12 mm
Number of windings per phase	200

APPENDIX C

INDUCTANCE MODEL OF THE EXPERIMENTAL SRG

The phase inductance equation is given by,

$$L(i,\theta) = L_0(i) + L_1(i)\cos(N_r\theta) + L_2(i)\cos(2N_r\theta) \qquad \text{(C.1)}$$

Where,

$$L_0(i) = \frac{1}{2}\left[\frac{1}{2}\left(L_a(i) + L_u\right) + L_m(i)\right] \qquad \text{(C.2)}$$

$$L_1(i) = \frac{1}{2}\left(L_a(i) - L_u\right) \qquad \text{(C.3)}$$

$$L_2(i) = \frac{1}{2}\left[\frac{1}{2}\left(L_a(i) + L_u\right) - L_m(i)\right] \qquad \text{(C.4)}$$

Where,

$$L_a(i) = L(\theta = 0^\circ) = \sum_{n=0}^{n=k} a_n i^n \qquad \text{(C.5)}$$

$$L_m(i) = L(\theta = \frac{\pi}{2N_r}) = \sum_{n=0}^{n=k} b_n i^n \qquad \text{(C.6)}$$

$$L_u = L(\theta = \frac{\pi}{N_r}) = 0.01054 \qquad \text{(C.7)}$$

The order of the polynomial coefficients a_n and b_n are limited to 5 in the present work. The polynomial coefficients are obtained through curve fitting techniques using the finite element analysis data of the experimental machine as explained [41].

The polynomial coefficients obtained for the experimental motor are given below:

a_0= 0.05993856158583;

a_1= 0.02469722101285;

a_2= -0.01052467701293;

a_3= 0.00147843930117;

a_4= -0.00008869746501;

a_5= 0.00000188511310;

b_0= 0.02685392898869;

b_1= 0.01075602919294;

b_2= -0.00359894844501;

b_3= 0.00044917225179;

b_4= -0.00002591984068;

b_5= 0.00000057738469.

VITA

Peyman Asadi was born in Tehran, Iran. He received his B.S. degree from Iran University of Science and Technology and his M.S. degree from the University of Tehran in in electrical engineering in 1996 and 1999, respectively. In September 2001 he began his graduate studies at Texas A&M University. He can be reached c/o Dr. M. Ehsani, Power Electronics Laboratory, Electrical Engineering Department, Texas A&M University, College Station, Texas 77843-3128.